UNIVERSITÀ DEGLI STUDI DI CATANIA

IN CONVENZIONE

UNIVERSITÀ DEGLI STUDI DI PALERMO

DOTTORATO DI RICERCA IN
SCIENZA DEI MATERIALI E NANOTECNOLOGIE

XXX CICLO

CHIAPPARA CLARA

PUSH-PULL COPOLYMERS IN THIN FILM FOR ELECTRONIC APPLICATION

TUTOR: PROF.BRUNO PIGNATARO
COORDINATORE: PROF.SSA MARIA GRAZIA GRIMALDI

TESI PER IL CONSEGUIMENTO DEL TITOLO DI DOTTORE DI RICERCA

Abstract

In this work, push-pull copolymers have been synthesized by electrochemical and chemical methods in order to fabricate new devices on flexible substrates, for electronic applications in several areas as electrochromism, solar cells and sensors.

Electrochemical synthesis was employed to synthesize copolymers composed of acceptor (A) N,N'-bis(2-octyldodecyl)-2,6-bis(5-(thioph-2-yl)thiophen-2-yl)naphthalene-1,4,5,8-bis(dicarboximide) (NDI2ODT4) and donor (D) ethylenedioxythiophene (EDOT) units on (indium tin oxide/polyethylene terephtalate) ITO/PET substrates, allowing for the fabrication of electrochromic devices, featuring an optical contrast of 29%. In the same way, it was possible to fabricate novel electrochromic devices by combining NDI2ODT4 with the novel system bis-thiophene fulleropyrrolidine (bis-Th2P-C_{60}). Moreover, it was also possible to demonstrate that P(NDI2ODT4), P(bis-Th2P-C_{60}), *co*(NDI2ODT4-bis-Th2P-C_{60}) are good electron acceptor in planar heterojunction(PHJ)-based Organic Solar Cells (OSCs) with poly(3-hexylthiophene-2,5-diyl) (P3HT). Electrochromic devices and OSCs based on bis-Th2P-C_{60} combined with NDI2ODT4, do not show good results. This can be explained by the fact that bis-Th2P-C_{60} imposes a distortion of the main polymeric chain. In addition, the combination of fulleropyrrolidine (A) and thiophene (D) moieties in copolymers has shown to improve the morphology in thin film bulk heterojunctions (BHJs). In particular, the small percentages of a novel tetra-thiophene fulleropyrrolidine (Th4P-C_{60}) copolymer acted as segregation modulators in BHJs based on P3HT mixed with Phenyl-C61-butyric acid methyl ester (PCBM) allowing to improve the state-of-the-art power conversion efficiency of plastic P3HT/PCBM OSCs up to 4.46 %.

Finally, preliminary results are shown on the application of Th4P-C_{60} based systems electrochemically co-deposited with hemin molecules for the recognition of H_2O_2 in plastic electrochemical sensors. This gives interesting perspectives for the application of properly designed D-A copolymers and/or co-deposited systems for the recognition of those drugs developing H_2O_2 during their metabolism.

1. Introduction

Conjugated polymers exhibit several interesting properties that allow them to be applied in several sectors such as electrochromism, solar cells and sensors [1–4] .

Copolymers including electron-withdrawing A and electron-donating D functional groups are of great interest in applied material science because of their exceptional optical and electronic properties [5–8]. Given these reasons, numerous efforts have been directed towards designing, molecular engineering and synthesis of push-pull systems for organic electronics. Among the D systems thiophene rings, such as alkyl- and alkoxy-oligothiophenes or EDOT have been widely used [9–11]. As to A moieties, perylenes, naphthalenes and fullerene derivatives have been employed [12–15].

Those copolymers comprising naphthalenediimide (A) and thiophene (D) derivatives showed excellent air-stability, good processability, low band gap, and large electron mobility[16,17] mainly due to their push-pull character induced by the ordered supramolecular packing [18]. This class of copolymers have been employed together with P3HT in very high fill factor solar cell [19] or for fabricating bottom and top gate organic thin film transistor with high mobility [17] even exceeding 2.5 cm^2/Vs. Also monolayer polymeric field effect transistors as well as vertical transistor with remarkable performance have been realized [20,21].

On the other side systems like EDOT have been employed for the synthesis of π-conjugated copolymers with the possibility to modulate the optical and electrical properties [22–24]. Also, there are few papers dealing with the electrochromic properties of naphthalenediimide-based polymers, with good stability, and high coloration efficiency [25].

Another interesting class of copolymers consists of fullerene cages fixed on π-conjugated polymers [26]. Indeed, there are reports dealing with the combination of fullerene with thiophene for electrochromic devices and photovoltaics. It has been shown the ability of fullerene polymeric derivatives to control the thin film morphology, structure along with the performance of BHJs solar cells [27]. Such a control of morphology can be achieved by introducing small quantities of additives into D-A heterojunctions in order to improve the components miscibility [28–31].

However, to date most of the works show only a slight increase of photovoltaic cell efficiency (PCE) or short circuit current (Jsc), mainly due to the nature of the different units of the copolymer. For example, the presence of insulating blocks hinders the exciton transport to the interface, resulting in an increase of the series resistance and deteriorating the charge carrier transport [31,32].

Finally, push-pull copolymers are of interest due to their superior electrochemical properties with respect to applications in the field of non-enzymatic sensors. In particular the electro-polymerization of D-A conducting monomers has been studied extensively for the construction of biosensors, due to their excellent electrocatalytic properties and rapid electron transfer ability. Also, conducting copolymers permit the transfer of charges to produce electrochemical signals between the electrode and the incorporated biomolecules [33,34]. Moreover, the amperometric electrochemical methods can be used remotely, for minimal sample amounts, without any pre-treatment processing. Although enzymatic sensors allow for high selectivity in their response to the analyte, the most serious problem is their lack of stability, due to the intrinsic nature of the enzyme, the activity of which can be easily affected by various factors such as temperature, pH, etc. In this regard, non-enzymatic sensors are ideal systems for direct oxidation or reduction of analytes that does not need introduction of fragile and costly enzymes. For biosensor applications, the conducting polymers (CPs) are often functionalized with carboxyl, amino, aldehyde or succinimidyl carbonate groups, or conjugated directly with various electronic mediators or bio-recognizable molecules to facilitate immobilization. Interestingly, porphyrins are excellent electron donors for their extensive π-conjugated systems, which increase their electron-donating ability and makes them easier to combine with the electron acceptor. One of the most employed model analytes in electrochemical analysis is H_2O_2 because it is a common by-product of diverse substances under the catalysis of their highly selective oxidases. In fact, the determination of H_2O_2 is very important in the field of industrial, biological, food, pharmaceutical, clinical, and environmental analyses [35].

The main aim of this thesis is to demonstrate the high flexibility in designing and synthesising novel copolymers onto flexible plastic substrates with remarkable properties for applications such as electrochromism, solar cells and sensors.

Accordingly, chemical and electrochemical-based synthetic approaches will be employed for the realization of new classes of co-polymers with peculiar physico-chemical properties. Thus, novel symmetric naphthalenediimidethiophenes, namely N,N'-bis(2-octyldodecyl)-2,6-bis(2-thienyl)naphthalene-1,4,5,8- bis (dicarboximide) (NDI2ODT2) and NDI2ODT4 will be used (Figure 1) to synthesise push-pull conjugated copolymers. Their symmetric structure allows for regioregular electropolymerization. Accordingly, electropolymerized films with new structural and optoelectronic properties along with electrochromic devices at high coloration efficiency will be realized.

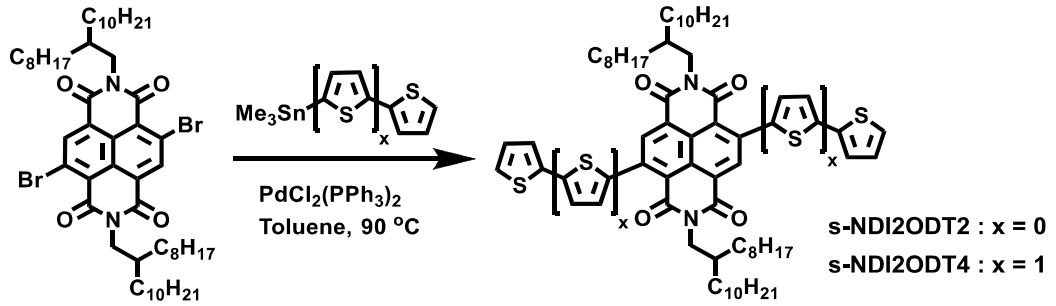

Figure 1. Description of chemical structure and synthesis of NDI2ODT2 and NDI2ODT4. Adapted from[36].

Also, the possibility to combine fulleropyrrolidine thiophenes with the above systems will be investigated by electrochemical synthetic approaches to develop both electrochromic and photovoltaic devices on flexible substrates.

By employing even different class of D-A copolymers, the thesis will aim also to demonstrate that such systems are able to improve the opto-electronic performance of functional thin film heterojunctions also by modulating their morphology. This will be performed by designing and synthesising new copolymers containing C_{60} units and oligothiophenes of different length and using them as additives in polythiophene– fullerene based organic solar cells.

Finally, new push-pull systems will be designed and synthesised to develop a new non-enzymatic electrochemical sensor with higher stability and sensitivity by *co*-fulleropyrrolidine thiophene-hemin conjugate for the electrochemical determination of H_2O_2 as a model analyte for biomolecule recognition in aqueous media.

In order to facilitate the reading of this thesis, the work is structured in three parts. The first part is subdivided into three chapters. The first chapter presents the semiconductors polymers that recently thanks to their electronic structure have been effective in applications such as electrochromism, solar cells and sensors as push-pull systems, fullerene and fullerenic derivatives. In the second chapter, both electrochemical and chemical methods of polymerization are illustrated. The third chapter describes applications for functional devices by employing push-pull copolymeric systems.

The second part of the thesis includes the synthesis of the novel materials and copolymers, and the description of the techniques used for the characterization of the systems and the experimental procedure.

The third part includes the results and discussion and is conveniently divided into three chapters depending on the different possible applications. The first chapter reports the

results concerning the synthesis of electrodeposited push-pull systems for electrochromic devices. The second chapter deals with push-pull copolymers for organic solar cells. The third chapter presents preliminary results on the electrodeposited copolymers combined with hemin for the realization of electrochemical sensors.

References

[1] H. Sirringhaus, *Adv. Mater.* **2005**, *17*, 2411.

[2] J. Smith, W. Zhang, R. Sougrat, K. Zhao, R. Li, D. Cha, A. Amassian, M. Heeney, I. McCulloch, T. D. Anthopoulos, *Adv. Mater.* **2012**, *24*, 2441.

[3] H. Chen, Y. Guo, G. Yu, Y. Zhao, J. Zhang, D. Gao, H. Liu, Y. Liu, *Adv. Mater.* **2012**, *24*, 4618.

[4] Z. He, C. Zhong, S. Su, M. Xu, H. Wu, Y. Cao, *Nat. Photonics* **2012**, *6*, 593.

[5] E. Bartollini, M. Seri, S. Tortorella, A. Facchetti, T. J. Marks, A. Marrocchi, L. Vaccaro, *RSC Adv.* **2013**, *3*, 9288.

[6] A. Marrocchi, D. Lanari, A. Facchetti, L. Vaccaro, *Energy Environ. Sci.* **2012**, *5*, 8457.

[7] K. Okamoto, J. Zhang, J. B. Housekeeper, S. R. Marder, C. K. Luscombe, *Macromolecules* **2013**, *46*, 8059.

[8] M. Shao, J. Keum, J. Chen, Y. He, W. Chen, J. F. Browning, J. Jakowski, B. G. Sumpter, I. N. Ivanov, Y.-Z. Ma, C. M. Rouleau, S. C. Smith, D. B. Geohegan, K. Hong, K. Xiao, *Nat. Commun.* **2014**, *5*, DOI 10.1038/ncomms4180.

[9] J. Roncali, *Macromol. Rapid Commun.* **2007**, *28*, 1761.

[10] P. M. Beaujuge, S. Ellinger, J. R. Reynolds, *Nat. Mater.* **2008**, *7*, 795.

[11] C. B. Nielsen, A. Angerhofer, K. A. Abboud, J. R. Reynolds, *J. Am. Chem. Soc.* **2008**, *130*, 9734.

[12] Y. Ie, T. Sakurai, S. Jinnai, M. Karakawa, K. Okuda, S. Mori, Y. Aso, *Chem. Commun.* **2013**, *49*, 8386.

[13] I. V. Sazanovich, M. A. H. Alamiry, J. Best, R. D. Bennett, O. V. Bouganov, E. S. Davies, V. P. Grivin, A. J. H. M. Meijer, V. F. Plyusnin, K. L. Ronayne, A. H. Shelton, S. A. Tikhomirov, M. Towrie, J. A. Weinstein, *Inorg. Chem.* **2008**, *47*, 10432.

[14] L. J. Rozanski, E. Castaldelli, F. L. M. Sam, C. A. Mills, G. Jean-François Demets, S. R. P. Silva, *J. Mater. Chem. C* **2013**, *1*, 3347.

[15] S. Fabiano, H. Wang, C. Piliego, C. Jaye, D. A. Fischer, Z. Chen, B. Pignataro, A. Facchetti, Y.-L. Loo, M. A. Loi, *Adv. Funct. Mater.* **2011**, *21*, 4479.

[16] Y. Kim, J. Hong, J. H. Oh, C. Yang, *Chem. Mater.* **2013**, *25*, 3251.

[17] A. Facchetti, *Chem. Mater* **2011**, *23*, 733.

[18] R. Kim, P. S. K. Amegadze, I. Kang, H.-J. Yun, Y.-Y. Noh, S.-K. Kwon, Y.-H. Kim, *Adv. Funct. Mater.* **2013**, *23*, 5719.

[19] S. Fabiano, Z. Chen, S. Vahedi, A. Facchetti, B. Pignataro, M. A. Loi, *J. Mater. Chem.* **2011**, *21*, 5891.

[20] H. Krüger, S. Janietz, D. Sainova, D. Dobreva, N. Koch, A. Vollmer, *Adv. Funct. Mater.* **2007**, *17*, 3715.

[21] M. Greenman, A. J. Ben-Sasson, Z. Chen, A. Facchetti, N. Tessler, *Appl. Phys. Lett.* **2013**, *103*, DOI 10.1063/1.4818585.

[22] J. Roncali, P. Blanchard, P. Frère, *J. Mater. Chem.* **2005**, *15*, 1589.

[23] Gregory A. Sotzing, and Christopher A. Thomas, J. R. Reynolds*, P. J. Steel, **1998**, DOI 10.1021/MA971290F.

[24] S. Akoudad, J. Roncali, *Chem. Commun.* **1998**, *0*, 2081.

[25] M. Sassi, M. M. Salamone, R. Ruffo, C. M. Mari, G. A. Pagani, L. Beverina, *Adv. Mater.* **2012**, *24*, 2004.

[26] T. Yamazaki, Y.Murata, K. Komatsu, K. Furukawa, M. Morita, N. Maruyama, and T.Yamao, S. Fujita, *Org. Lett.* **2004**, *6*, 4865

[27] C. G. de Almeida, S. G. Reis, A. M. de Almeida, C. G. Diniz, V. L. da Silva, M. Le Hyaric, *Chem. Biol. Drug Des.* **2011**, *78*, 876.

[28] J. Peet, J. Y. Kim, N. E. Coates, W. L. Ma, D. Moses, A. J. Heeger, G. C. Bazan, *Nat. Mater.* **2007**, *6*, 497.

[29] S. Cataldo, C. Sartorio, F. Giannazzo, A. Scandurra, B. Pignataro, *Nanoscale* **2014**, *6*, 3566.

[30] E. Bicciocchi, M. Haeussler, E. Rizzardo, A. D. Scully, K. P. Ghiggino, *J. Polym. Sci. Part A Polym. Chem.* **2015**, *53*, 888.

[31] M. Raïssi, H. Erothu, E. Ibarboure, H. Cramail, L. Vignau, E. Cloutet, R. C. Hiorns, *J. Mater. Chem. A* **2015**, *3*, 18207.

[32] C. Yang, J. K. Lee, A. J. Heeger, F. Wudl, *J. Mater. Chem.* **2009**, *19*, 5416.

[33] K.-D. Seo, S.-D. Oh, S.-H. Choi, S.-H. Oh, J.-C. Woo, S.-H. Kim, **n.d.**, DOI 10.4028/www.scientific.net/KEM.342-343.869.

[34] A. Rahman, P. Kumar, D. Park, Y. Shim, **2008**, 118.

[35] A. A. Karyakin, O. V. Gitelmacher, E. E. Karyakina, *Anal. Chem.* **1995**, *67*, 2419.

[36] V. Figà, C. Chiappara, F. Ferrante, M. P. Casaletto, F. Principato, S. Cataldo, Z. Chen, H. Usta, A. Facchetti, B. Pignataro, *J. Mater. Chem. C* **2015**, *3*, 5985.

2. State of the art

2.1. Organic semiconductors

Nowadays, a great number of different monomers are known to form conducting polymers. Among the possible substituents that can be considered, substituted derivatives of the hydrocarbons and heterocycles can be taken into account, but also new compounds, e.g. EDOT [1,2] that has lately become a reference in the field of conducting materials (Figure 2.1).

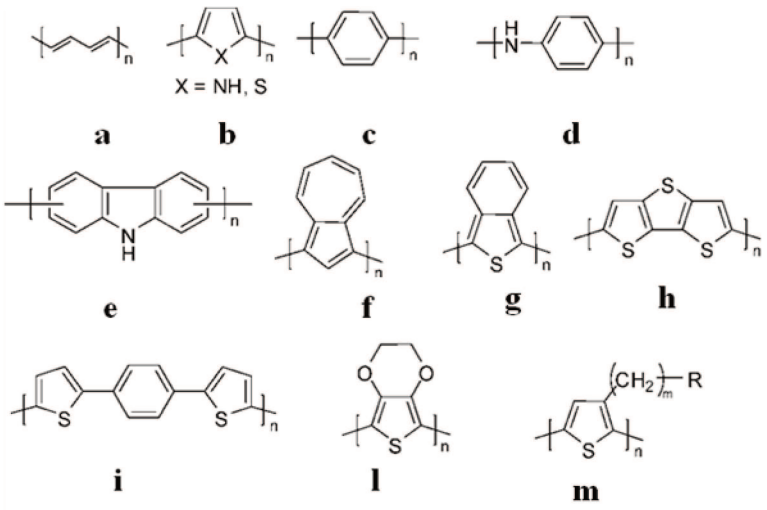

Figure 2.1. Selected building units of conducting polymers: (a), polyacetylene (PA); (b), polypyrrole (PPy), polythiophene (PTh); (c), poly-p-phenylene (PPP); (d), polyaniline (PANI); (e), polycarbazole; (f), polyazulene; (g), poly(isothionaphthalene); (h), poly(dithienothiophene); (i), poly(dithienylbenzene); (l), poly(ethylenedioxythiophene) ; (m), poly(3-alkylthiophene). Adapted from [2].

The electrical conductivity and the optical properties of the conjugated polymers are strictly dependent on the presence of the π orbitals, which, if in high numbers, produce virtually continuous bands of valence and conductance. The valence band is composed of the orbitals π (bonding) and the conduction band by π * orbitals (of antibonding). The two bands are separated by a band gap (Eg), which decreases by increasing the number of double conjugated bonds, as reported in the following (Figure 2.2.). By reducing the distance between valence (highest occupied molecular orbital (HOMO)) and conduction

(lowest unoccupied molecular orbital (LUMO)) orbitals, the conjugated polymer can obtain good conductivity.

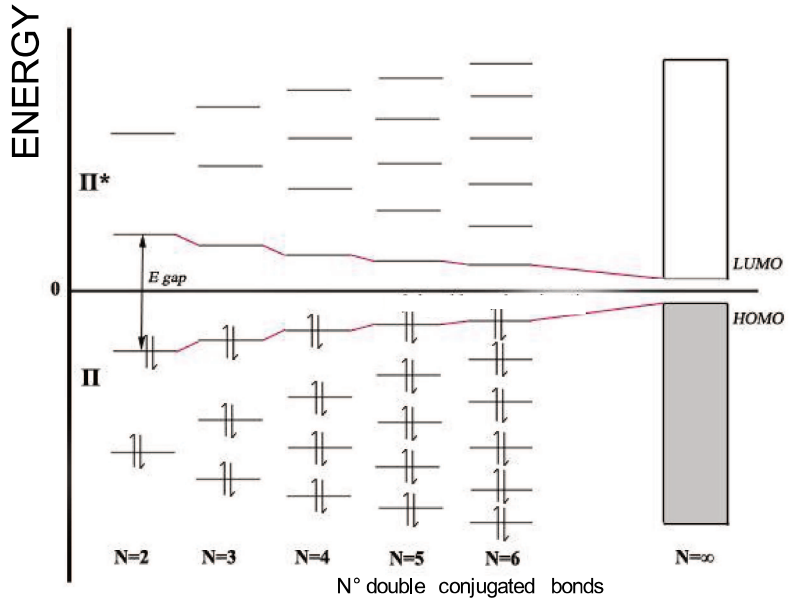

Figure 2.2. Variation in the distribution of energy levels for electrons in conjugated polymers, as a function of the number of double bonds (N).[1]

2.1.1 Naphthalene Diimide-Thiophene Structures

Molecular structures containing fused aromatic rings decorated with tetracarboxylicdiimide moieties, like perylene or naphthalene derivatives, can be considered extremely strong electron acceptors [3]. Examples of these structures are reported in Figure 2.3.

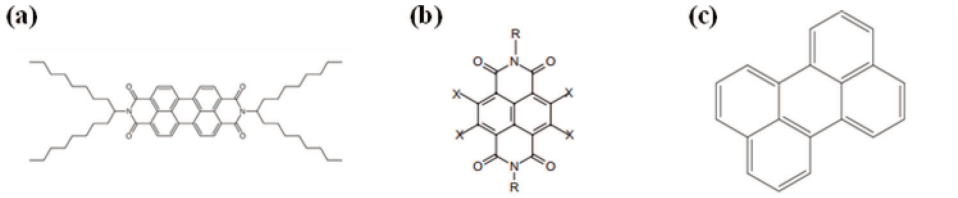

Figure 2.3: Structure of tetracarboxylic diimide a), perylene b), naphthalene derivatives c). Adapted from [3].

The above described molecular systems are characterized by strong π–π overlap because of short intermolecular distances, permitting to achieve outstanding charge transport properties. Such fused aromatic ring systems suffer from poor solubility in organic

[1] Image reproduced from http://wps.prenhall.com/wps/media/objects/4680/4793217/ch21_04.htm

solvents. It is possible to improve solubility in non-polar organic solvents by introducing into the naphthalene core, substituents like aromatic units, e.g., thiophene rings. These systems can also show significant intermolecular interactions as a function of the side-chain molecular structure [4,5]. In this regard, Kruger et al. [6] showed a synthetic approach to obtain a new set based on 1,4,5,8-naphthalenetetracarboxylic dianhydride, which constitutes the central unit, with thiophene substituents of varying chain length attached to the naphthalene core by imidization. The result of this concept is a molecule which integrates acceptor and donor properties. This example represents a hybrid supramolecular push-pull system structure. Given their ordered supramolecular crystalline structure, new push-pull polymers based on derivatives of naphthalenediimide A and thiophene D derivatives (Figure 2.4), have very interesting properties such as high air stability, good workability, low band gap, high electron mobility [7].

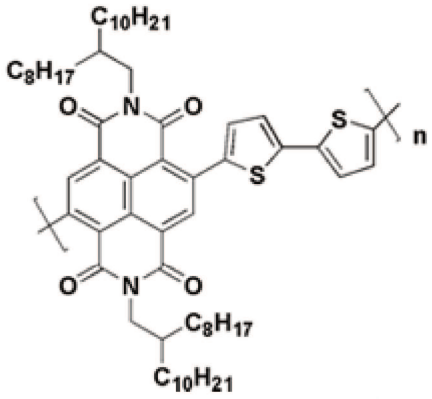

Figure 2.4. Structure of P(NDI2OD-T2). Adapted from [7].

2.1.2. Fullerene

Fullerenes can be defined as a family of large all-carbon cage molecules consisting of fused pentagons and hexagons forming a curved structure. The smallest stable, and the most abundant, fullerene obtained by synthetic preparation method is the I_h-symmetrical buckminsterfullerene C_{60} [8] (Figure 2.5). Each carbon atom in a fullerene-C_{60} system is bonded to three others and is sp^2 hybridized. C_{60} structure behaves like an electron-deficient alkene, and is able to react readily with electron-rich species. The estimated values of electron affinity (EA) (2.7 eV) and ionization potential (IP) (7.8 eV) of C_{60} indicate that it can contribute to the electron transfer reaction, showing a quite rich electrochemistry that makes them quite remarkable candidates for electroanalytical

applications [9]. The next stable homologue is C_{70} followed by higher fullerenes C_{74}, C_{76}, C_{78}, C_{80}, C_{82}, C_{84}, and so on [10,11].

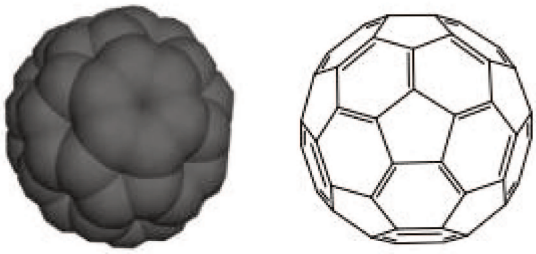

Figure 2.5. Schematic representation of C_{60}. Adapted from [8].

The electrochemistry of the fullerenes, e.g. C_{60}, is able to arouse interest because it can provide information about the energetics and kinetics of electron-transfer processes. Thus, reduction of C_{60} in solvents where it is moderately soluble (toluene, o-dichlorobenzene(o-DCB)) [12] gives rise to reduction waves showing the successive addition of electrons to the molecule (Figure 2.6).

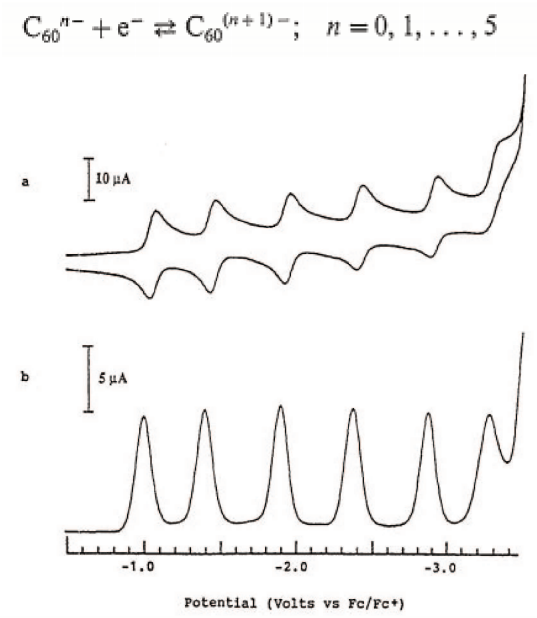

Figure 2.6. Reduction of C_{60} in acetonitrile (CH_3CN)/toluene (1:5.4 by volume) at -10°C using (a) cyclic voltammetry, 100 mV/s scan rate, and b) differential pulse voltammetry, 50 mV pulse, 50 ms pulse width, 3000 ms period, 25 mV/s scan rate. Adapted from [12].

2.1.3. C_{60} *functionalization and chemistry*

The pyramidalization of fullerene carbon atoms is a source of strain affecting its reactivity; the relief of strain is primarily responsible for fullerene reactivity. In general, fullerenes are

insoluble or sparingly soluble in most common organic solvents [13], making it very difficult to handle. It is well-known that this problem can be in part solved by chemical functionalization. In particular, chemical modifications of C_{60} is constituted by single or multiple attacks on the cage, typically taking place at the 6:6 bonds. In the case of single-additions, the reactions can be classified into categories based on the nature of the obtained structure. As a function of the shape built on a 6:6 ring, it is possible to subdivide junction of the C_{60} as follows: (a) open structure, (b) three-membered ring, (c) four-membered ring, (d) five-membered ring and (e) six-membered ring as reported in literature (Figure 2.7) [14].

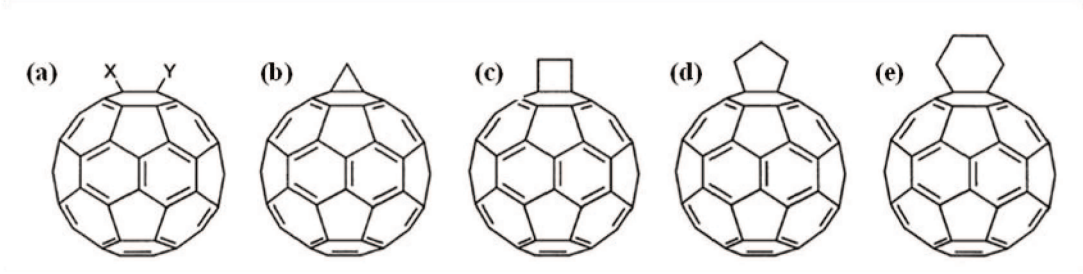

Figure 2.7. Geometrical shapes built onto a 6,6 ring junction of C_{60}: (a) open; (b) three-membered ring; (c) four-membered ring; (d) five-membered ring and (e) six-membered ring. Adapted from [14].

Furthermore, C_{60} can undergo electron deficient polyolefin reactions. The [6,6] bonds show a remarkable double bond character and are shorter than the [5,6] bonds and, thus, can be employed to functionalize C_{60} by nucleophilic additions, radical additions, as well as cycloadditions [15]. Functionalization of C_{60} has been carried out by different kinds of reactions, which consist of cyclopropanation (the Bingel reaction), [4+2] cycloaddition (the Diels-Alder reaction) and [3+2] cycloaddition (the Prato reaction), [2+2] cycloaddition (Figure 2.8) [15].

In particular, the 1,3-dipolar cycloaddition of azomethine ylides to C_{60} has been largely used among the possible cycloadditions reactions, because of its easiness in preparation and the large number of methods to generate the reactive intermediates derived from a wide series of starting materials [16]. This particular kind of reaction was developed by Prato and Maggini up to now, it is considered one of the most convenient route to obtain functionalized fullerene. Figure 2.9 presents an example of this reaction. It involves the generation of azomethine ylide via decarboxylation of the ammonium salt resulting from the condensation of a α-amino acid with an aldehyde. The azomethineylide then reacts selectively with a 6:6 bond of the fullerene to produce the fulleropyrrolidine.

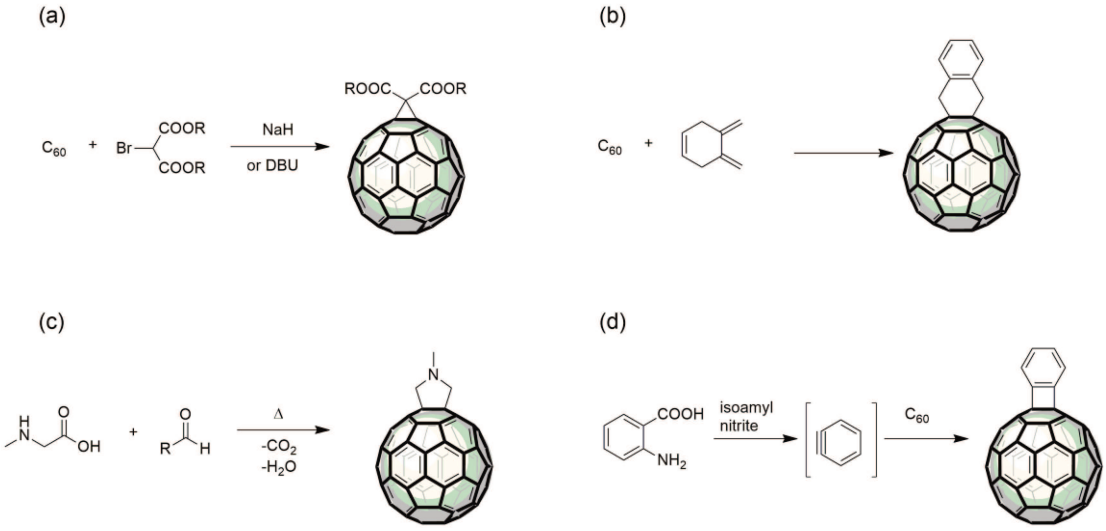

Figure 2.8. (a) The Bingel reaction; (b) the Diels-Alder reaction; (c) the Prato reaction; and (d) the Cycloaddition reaction. Adapted from [15].

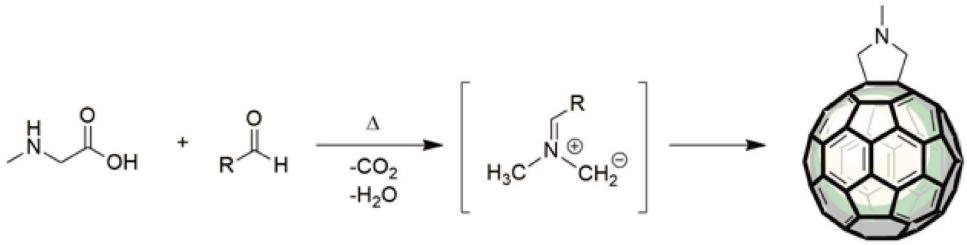

Figure 2.9. Scheme of the Prato reaction in which an aldehyde and N-methyl glycine (sarcosine) are employed to obtain functionalized fullerene by 1,3-dipolar cycloaddition. Adapted from [16].

Besides, by using an additional reaction step in which the corresponding fulleropyrrolidines react with halogenated compounds, it is possible to introduce a third chain to the system, in order to obtain fulleropyrrolidinium salts which have enhanced electron-accepting properties with respect to both the parent pyrrolidine derivatives and C_{60} [17].

Electrochemical properties of fulleropyrrolidine derivatives can be enhanced by attaching thiophene moieties to the pyrrolidine ring. The resulting species show good solubility in polar solvents and may be used as the starting monomer for obtaining, by electrochemical oxidation, of the thiophene moiety, thin films of a fullerene-containing conducting polymer. Figure 2.10 reports an example of a thiophene D–fullerene conjugate A. This molecule was obtained according to standard procedures, reported in [16].

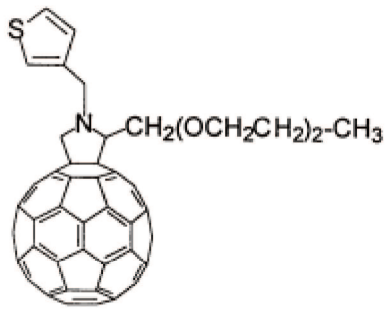

Figure 2.10. Thiophene-fullerene conjugate. Adapted from [16].

2.2 Copolymerization methods

The preparation of the conductive polymers takes place through typical polymerization reactions, such as condensation and addition polymerization [18]. Electrochemical and chemical synthesis the two main techniques for conducting polymers synthesis.

2.2.1 Electrochemical synthesis

The interest of electrochemists in conducting polymers is based on several reasons. From the viewpoint of molecular electrochemistry, the most relevant aspect concerns the mechanism of electropolymerization involving initially the formation of oligomers followed by nucleation and growth steps, leading to polymeric materials. Mechanistic details are important for optimizing the conditions of electropolymerization and play a decisive role in determining the quality of the fabricated materials.

In the electrochemical polymerization, the monomer dissolved in an appropriate solvent containing the dopant (support electrolyte) is oxidized (or reduced) on the surface of the electrode by applying an anode (or cathode) potential. Figure 2.11 shows the proposed mechanism for electropolymerization of thiophene and, in general, of heterocycles.

The electropolymerization mechanism is carried out by the following steps:

- initial phase comprising the oxidation of the monomer resulting in the formation of the radical cation.

As the electronic transfer reaction occurs faster than the monomer diffusion process from the bulk of the solution, near the surface of the electrode there is a constant a high concentration of radicals.

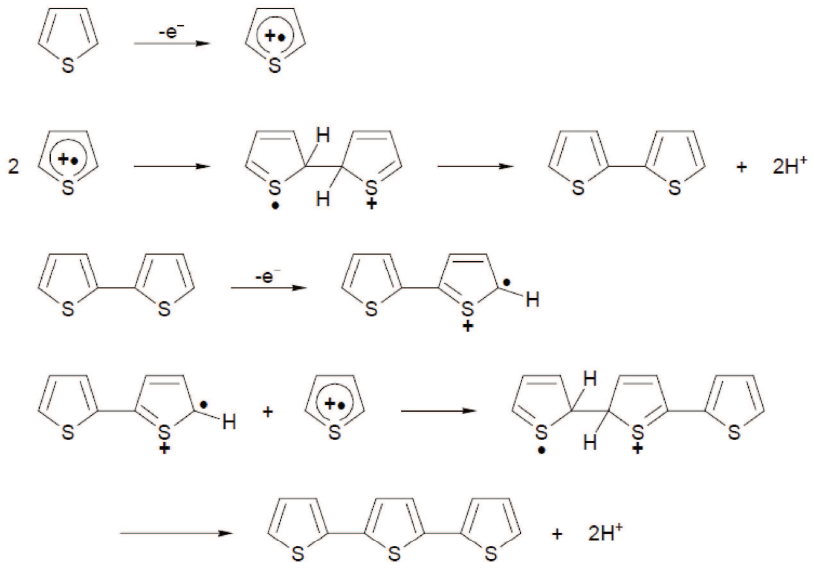

Figure 2.11. Electropolymerization of thiophene. Adapted from [19].

- propagation by coupling between two cationic radicals to give a dimeric cation which, due to the loss of two protons and subsequent re-aromatization, will result in dithiophene.
- termination of the process for exhaustion of reactive radicals or by precipitation of the oligomer on the electrode surface due to scarce solubility in the chosen solvent system [20].

The choice of a suitable solvent system is of crucial importance in the design of the electro-polymerization experiment because on the one hand, it must provide an adequate solubility of the monomer, while at the same time, it does not have to solubilize the growing oligomeric chains. The solvent also exerts a strong effect on the structure and properties of the polymeric film. It has been observed that the solvent used in the electropolymerization must be aprotic, it must have a high dielectric constant to ensure the conductivity of the ions in the electrolytic medium and possess good electrochemical resistance to the potentials required for polymerization [19].

As mentioned above, electro-polymerization occurs in the presence of a supporting electrolyte providing the anions necessary to balance the charge determined by the formation of cationic radicals. Such anions must be inert both from a chemical and electrochemical point of view, and they must be soluble in the solvent used for the synthesis and must have a high ionic mobility in solution. The nature of the electrode material is also of great importance because the chemical-physical properties of the deposition surface can affect both the nature and the strength of the interactions

responsible for the adhesion of the film to it. Polythiophene generally can be efficiently grown on noble metals (Pt, Au) on optically transparent electrodes (ITO glasses) [21], but can also be deposited on graphite electrodes, glassy carbon (GC) or steel. A central point of electrochemical research is the analysis of the “doping” process. When a potential greater than the equilibrium potential is applied, the dopant anion migrates from the solution to the delocalized charge sites on the CP, resulting in anionic doping. This anionic doping is termed "p-type doping". If on the contrary, a potential lower than potential equilibrium is applied to the CP, a cation migrates from the solution to the polymer or anion moves from the polymer to the solution.

In the electrochemical polymerization, deposition and doping of the polymer occur simultaneously. Anion (or cation) is incorporated into the polymer matrix to ensure electron neutrality of the film. Doping agents may be small anions or cations or larger polymer species. The conductivity of conjugated polymers can be influenced by the "doping level" measured as the percentage of dopant ions or embedded molecules per unit of monomer and depends on the type of CP or dopant. It can be expressed as a molar fraction or as a percentage [22].

In contrast to conventional doping processes in semiconductor materials, electrochemical synthesis leads to additional local distortions in the chain during the charging of the polymer. The first step of the doping process consists in the formation of polarons, for which there is a gain of relaxation energy E_{rel}. This energy is released by structural relaxation after ionization, for which a vertical Franck-Condon-like ionization energy $E_{1P\text{-}v}$ has to be taken into account [23] (Figure 2.12 a). E_{rel} corresponds to the bonding energy of the polaron (Figure 2.12b).

The structural relaxation determines a local distortion of the chain in the vicinity of the charge, whereby the twisted benzoid-like structure of the affected segments transforms into a quinoid-like structure in which the single bonds between the monomeric units shorten and assume double bonding character (Figure 2.13a). Removing the second electron from the polymer segment results, not in two polarons but a bipolaron, which is predicted to be energetically more favored than the polaron (Figure 2.13b).

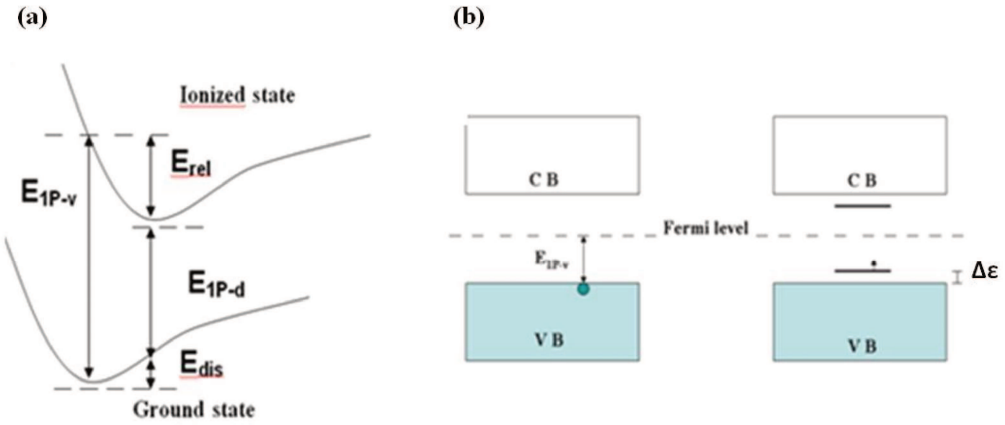

Figure 2.12. Illustration of a polymer chain band structure in a) a vertical ionization process and b) formation of new energy levels due to the polaron. Adapted from [2].

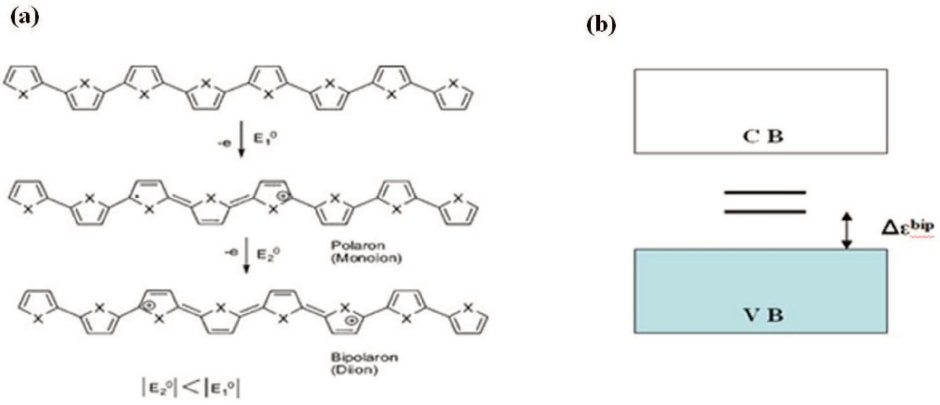

Figure 2.13. Formation of the bipolaron state in PPy or PTh upon oxidation: During charging of the polymer chain, the ionized states are stabilized by a local geometrical distortion from a benzoid-like to a quinoid-like structure a) and formation of new energy levels due to the bipolaron b). Adapted from [2].

2.2.2. Chemical synthesis

Chemical synthesis can be achieved by condensation and addition reactions, showing a reaction mechanism different from that followed in electrochemical synthesis. In fact, after the initial generation of the radical ion, instead of the radical-radical coupling (the main stage in propagation in the electrochemical reaction), a radical and monomer coupling is produced. This is due to the fact that, in the bulk of the reaction environment, where radical initiators are produced, the concentration of monomer is in excess, unlike to what happens in the electrochemical process. An example of chemical polymerization is shown in Figure 2.14, where the polythiophene growth mechanism is reported [2].

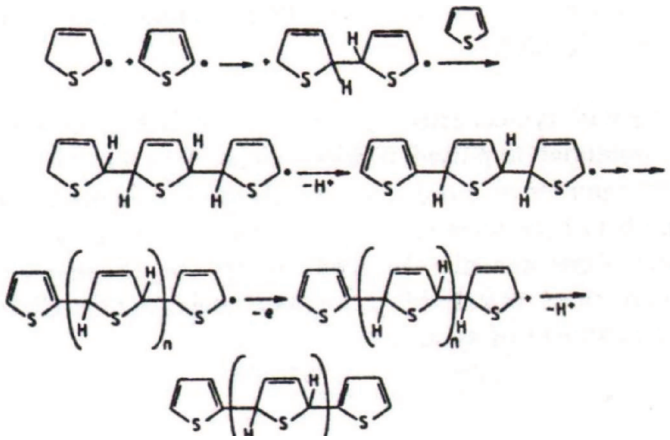

Figure 2.14. Chemical thiophene polymerization mechanism. Adapted from [24].

Whereas chemical polymerization approach takes a few hours, the electrochemical approach is featured with high rapidity, necessitates a smaller amount of solvents, permits to the *in-situ* characterization both the growth process and the polymer from its electrochemical responses. With this technique, it is possible to deposit the polymer directly on the electrode surface, so constituting a versatile and convenient strategy to obtain an electrode surface having new electronic, optical, electrocatalytic properties which finally results in remarkable technological potentialities. It is also possible to control the film thickness on the electrode according to deposition charge.

2.3 Applications

Given the redox, electrical, optical, mechanical, modulating doping properties of conjugated polymeric polymers, it is evident the great potential of these materials in the field of technology.

2.3.1. Electrochromic devices

Electrochromism is a phenomenon of color variation induced in a material through reversible electrochemical processes: in other words, there are changes in the visible spectral zone associated with the reversible doping and de-doping processes [25] (Figure 2.15). The doping and de-doping processes corresponding at the simultaneous injection or extraction of small ions (H^+ or Li^+) or electrons by means of a voltage pulse in the CPs, cause an alteration in the size of the bandgap and in turn a color variation, as shown in Figure 2.15 [26].

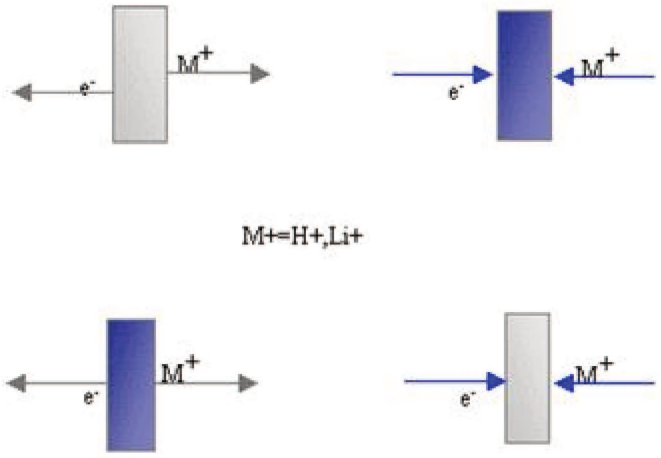

Figure 2.15: Representation of the electrochromism phenomenon: color change as a result of the doping and de-doping processes. Adapted from [26].

An ideal electrochromic material is characterized by a high electrochromic contrast, a parameter which is often reported as a percentage change in the material transmittance (ΔT%) at the wavelength of the maximum absorption (λ_{max}). In this regard, coloration efficiency is a parameter used to compare performances among different electrochromic materials and devices. Colouration efficiency (CE) is defined by the following equation (2.1) [27,28]:

$$\Delta OD/Q = \ln[T_{bleached}(\lambda)/T_{coloured}(\lambda)]/Q \,, \qquad (2.1)$$

where Q is the electronic charge injected into the electrochromic material per unit area, $T_{bleached}$ is the transmittance in the bleached state, and $T_{coloured}$ is the transmittance of the colored state. Then, the coloration efficiency gives the change in optical density (or contrast ratio) achieved by the injection of unit charge over a unit area and is typically given in units of cm^2 per Coulomb.

Electrochromic materials can be used for the construction of intelligent windows to regulate the flow of light and heat of incoming and outgoing buildings. They can also be used (in addition to smart sunglasses) in displays for laptops, information signs (airports, railways, advertising, etc .) and anti-glare mirrors for cars. An example of smart windows in the airplane is shown in Figure 2.16.

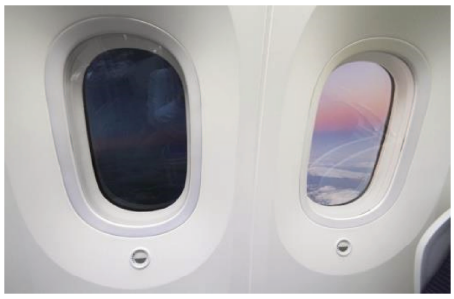

Figure 2.16: Example of smart windows in an airplane.

In Figure 2.17 a typical electrochromic window coating is reported. This object consists of an active electrochromic electrode layer, a counter electrode layer, an electrolyte layer separating the two electrodes, two transparent conducting layers which serve as electrical leads, and the supporting substrates. The two electrode layers often consist of transition metal oxides. Certainly, the design of the electrolyte layer is important for all three types of Electrochromic devices (ECDs). In particular, the electrolyte should have high ionic conductivity to achieve rapid response and low voltage operation, and it must be chemically stable to repeated cycling over a prescribed voltage range. Accordingly, solid or gel electrolytes are more desirable than liquid electrolytes for ECD fabrication. This device structure is referred to as “battery type” and is the most common geometry for ECDs [27]. Nowadays, the progress in science and technology aims at the fabrication of a new class of systems for energy storage or optics based on all polymeric (due to its lower costs) and flexible (due to its easy handling) devices, the so-called "cheap and bendy" devices.
The electrolyte is a fundamental part of electrochromic devices. Polymeric solid electrolytes can be used without loss of the electrochromic parameters since the polymer-electrolyte-counter electrode interface is satisfactory. These desirable conditions could be reached studying new electrode-electrolyte preparation methods and perhaps a simultaneous film-electrolyte preparation [28]. These devices operate as follows: applying an electrical potential difference to the more transparent transducer force ions to migrate through the conductive ion layer, from the counter electrode to the electrochromic layer. Consequently, a reversible electrochemical reaction produces a particular coloration. By reversing the potential, the ions migrate in the opposite direction, leading to the discoloration of the glass. These films can be customized in a wide range of colors. These devices can be controlled by electronic switches, in order to control window color change as well as other functions such as color change interval, speed as a function of temperature, absorbed power, duration, and color.

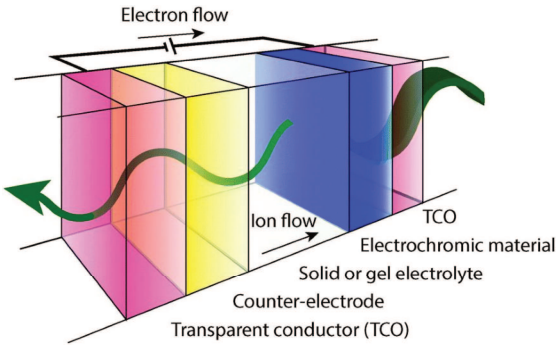

Figure 2.17. The principle of operation of an electrochromic device for the design of intelligent windows. Adapted from [29].

Many polybithiophenes with alternating aromatic units have been synthesized and characterized[30]. Chen et al. and Würthner et al. combined perylenes with electropolymerizable thiophene monomers and oligomers [31,32].These research groups attached electron-rich oligothiophenes at the bay positions of electron-poor perylenebisimides. Würthner et al. pointed out that the films are much more electroactive in the p-doping than in the n-doping process. A very recent publication by Würthner and Bäuerle reports on the synthesis of dendritic oligothiophene-perylenebisimide hybrids and their electropolymerization toward donor-acceptor networks, Figure 2.18 [33].

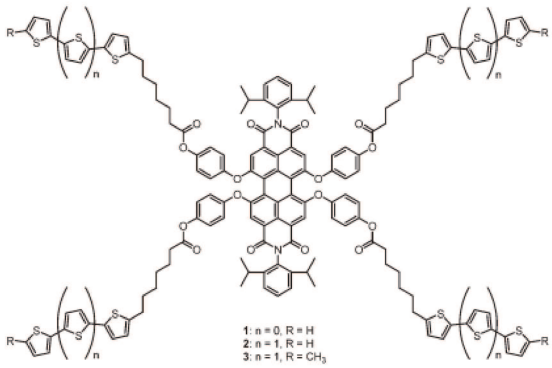

Figure 2.18. Structure of oligothiophene-functionalized perylenebisimide. Adapted from [33].

Copolymers based on 1- (2-ethylsilyl) -2,5-di-thiophen-2-yl-2,3-dihydro-1H-pyrrolo (SNS-HE) and EDOT showed multicromism within a wide spectrum of visible spectrum (Figure 2.19). Such copolymers revealed shorter response times (about 0.5 s) and ΔT about 36%. A new electrochromic solid-state device based on (SNS-HE-EDOT) electrhocromic device showed an ΔT of 26.6% [34].

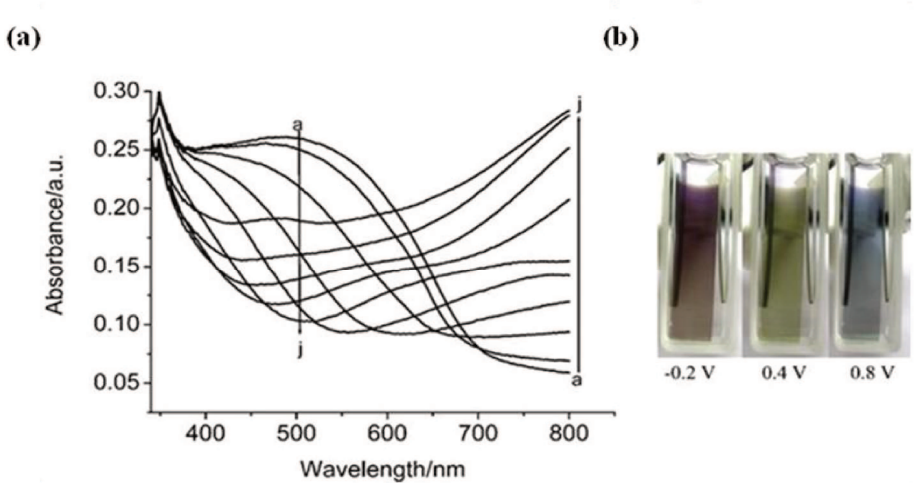

Figure 2.19: Spectroelectrochemistry of poly(SNS-HE-EDOT) film on an ITO coated glass slide in monomer-free 0.1 M $LiClO_4$/MeCN electrolyte solution at applied potentials (a) −0.2 V at (j) 1.6V vs Ag wire. The color change of electrodeposited polymers on ITO/glass by varying the polarization voltage: red at -0.2V: green 0.4V and blue 0.8V respectively. Adapted from [34].

There are few applications of fullerene or thiophene fullerene derivatives in literature reports. For example, Yamazaki and co-workers described the electropolymerization of ethylenedioxy-substituted terthiophene-fullerene molecules reported in Figure 2.20. One main advantage of using EDOT monomers is that the 3-position of the thiophene is blocked, resulting in exclusive electropolymerization of the 2-position, leading to regiochemically defined structures. The fullerene molecules were attached to the terthiophene unit by a triple bond, which apparently did not affect the electropolymerization process [35].

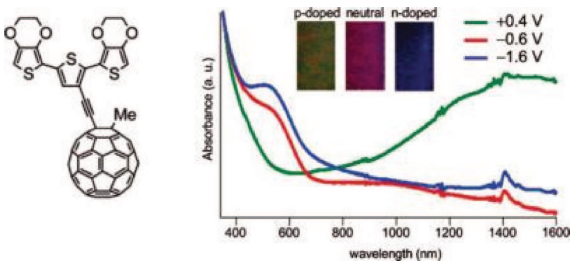

Figure 2.20: Electronic absorption spectra of the derived fullerene (C_{60}) on ITO/ glass electrode at three different potentials in CH_3CN. Adapted from [35].

2.3.2. Organic Solar cells

The limited supply of traditional fossil fuels (oil, natural gas, coal, etc.) is a clear indication of the urgency to look for alternative energy sources. Nowadays, photovoltaics plays the most important role in seeking for alternative and ecocompatible energy sources. The global power of energy resources can be estimated to be as high as 20 TW. The solar power delivered to the Earth is ~10^5 TW. The direct conversion of solar energy into electricity is due to the photovoltaic effect which was first discovered by the French physicist Alexander-Edmond Becquerel in 1839 on inorganic materials [36]. In the 1900s, this effect was observed also for organic compounds thanks to pioneering studies conducted on anthracene [37].

Solar cells are defined as devices which are capable to convert solar energy into electricity. Solar cells are mainly based on inorganic semiconducting materials in particular on crystalline and amorphous silicon. Silicon solar cells have been known for more than half a century – they reach power conversion efficiencies as high as 20% and show a service life which is more than 25 years (Fig. 2.21). The cost of silicon itself is low. However, silicon solar cells are not widely used thus far. The reason is that silicon photovoltaic technology is very complex, resulting in high cost of silicon solar cells. For this reason, new technologies are needed to fabricate solar cells at low cost and low-temperature, by employing solution-based thin films preparations. In particular, OSCs are being extensively studied worldwide since they can be easily produced with very low cost, permitting to inexpensively produce electricity from solar energy [38]. Remarkably, with respect to silicon solar cells, OSCs have another important advantage, i.e. flexibility. In fact, whereas classical electronics is dominated by the use of rigid and brittle structures, which is determined by the physical properties of inorganic materials, organic semiconductors allow for the synthesis of thin films on flexible substrates, such as plastic, paper just to cite the most important ones. Such cells can be easily integrated into clothing, facial coatings, packaging, etc. Their flexibility permit to roll them up into compact cylinders, which are easy to transport and can be unrolled when needed. They can be used as compact and portable 100 mW-scale power source, that can supply energy to mobile devices or also recharge their batteries.

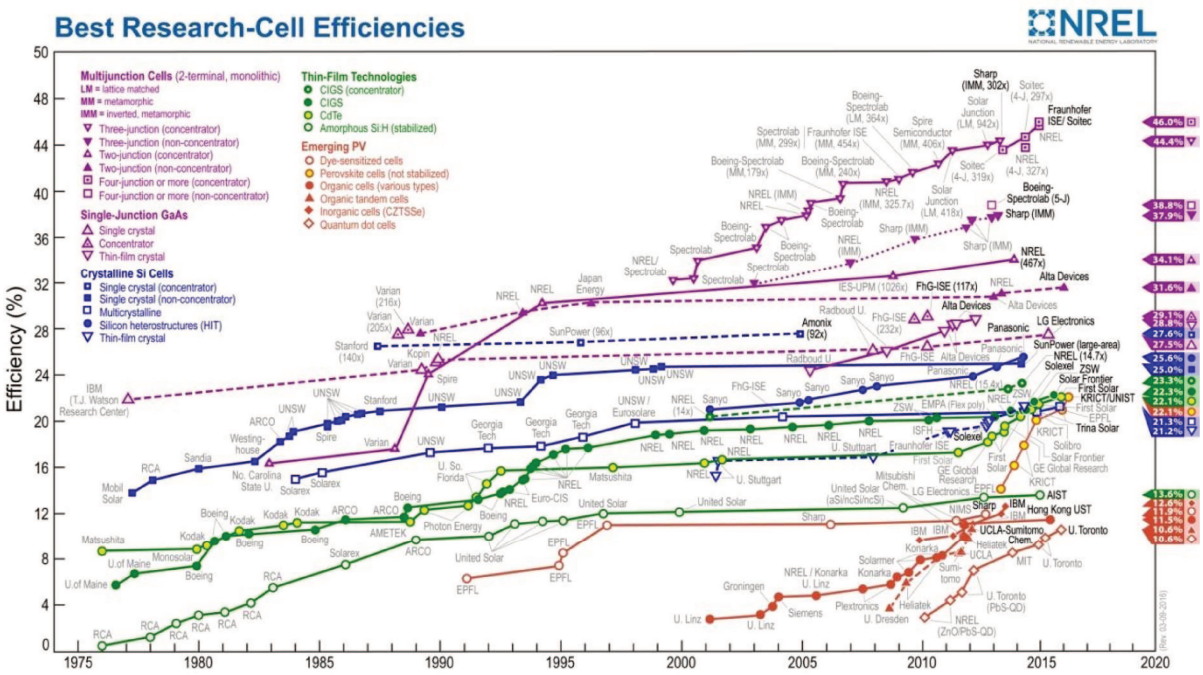

Figure 2.21. NREL- chart on record cell efficiencies.

The architecture of the device plays a crucial role in the efficiency of solar cells. In the inorganic cells, charge carriers, which are generated within the material, separate from the electrical field and move to their respective electrodes. On the other hand, in OSCs charge carriers are linked to each other in the form of excitons (hole-electron pair generated by the interaction of the semiconductor with the light radiation), which dissociate at an interface, see Figure 2.22 [39].

In a conventional p-n junction device, the junction that creates the charge separation is represented by the contacts between the metal electrodes and the organic layer. The potential difference between the electrodes may be enough to provide the electric field necessary to break the photo-generated excitement and separate charge carriers to their respective contacts. Unfortunately, these devices suffer from many disadvantages that make overall efficiency very low: the high disexcitation rate by exciton emission, the low diffusion of excitons towards the electrode and the quality of the junctions which is not effective in generating charge separation.

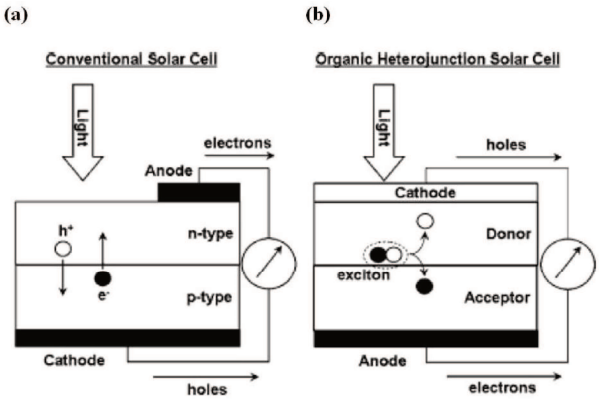

Figure 2.22. Scheme of a conventional p-n junction (a) photovoltaic cell and of a heterogeneous organic cell (b). Adapted from [39].

A device architecture that can significantly improve cell efficiency is PHJ solar cell. The latter is composed of two layers consisting of an electron donor material and an electron acceptor material placed between a semitransparent anode (ITO) and a metallic cathode (e.g. Ag, Al, Mg or Ca).

The photovoltaic process within an OSCs device includes four steps: light absorption through exciton generation; exciton movement towards the donor/acceptor interface; exciton separation at the donor/acceptor interface; charge-carrier transfer to the electrodes.

Each step of the depends by the choice of the donor-acceptor couple in the active layer[40,41] (Figure 2.23).

The choice of donor and acceptor materials in the active layer is critical for the efficient operation of the OSCs device. In fact, the donor material should absorb photons by creating excitons, while the acceptor material must be able to dissociate exciton by extracting an electron from the LUMO and transferring them to the cathode. At the same time, the HOMO must have energy values in order to allow a rapid transfer of the holes to the anode. In this case, the D/A junction favors the dissociation of the exciton into electron pairs. Electrodes must be selected in such a way as to ensure maximum charge transfer efficiency and slow down all possible de-energization and recombination processes of the hole/electron pairs [42].

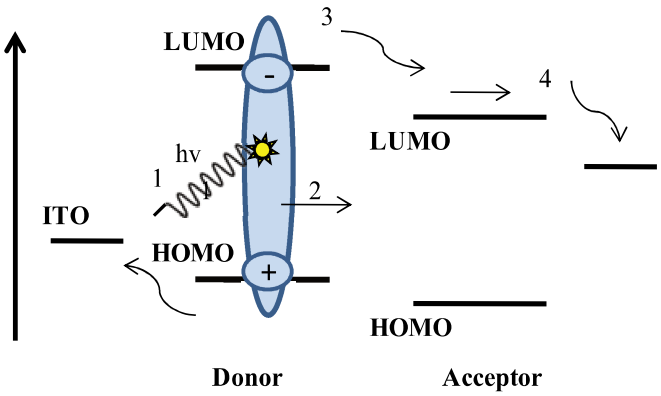

Figure 2.23. The general scheme of the photovoltaic process in an organic-based device.

One of the limiting factors of this type of cell is the modest extension of the D/A junction interface where the hole-electron pairs are created. Bulk-heterojunction cells are able to solve this issue, by increasing the contact surface between the two types of materials, as represented in. The active layer consists of the mixture of two materials with homogeneous domain sizes which are comparable to the diffusion length of the exciton (Figure 2.24). Thus, wherever exciton is photogenerated, this finds an interface which can dissociate it. Consequently, it is possible to increase the hole-electron pairs formation[43]. Finally, if there is a continuous path that can carry the charge to the respective electrodic contact, then a current will be recorded.

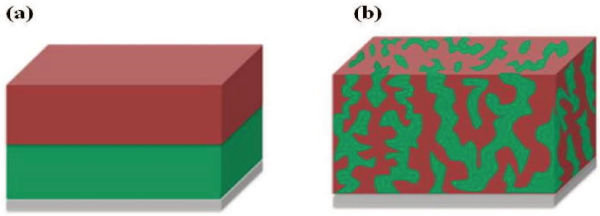

Figure 2.24. PHJ layer between D (red) and A (green) materials (a) BHJ layer (b) whit an inter-dispersed D and A phase made by mixing respectively.

- *Photovoltaics parameters*

According to the previously explained mechanisms, it is possible to describe the photovoltaic properties of OSCs in terms of open circuit voltage (V_{OC}), short-circuit current density and Fill Factor (FF), which can be determined from the current-voltage curve (J-V). The photovoltaic cell efficiency can be represented by the combination of these terms as expressed in Equation (2.2):

$$PCE=V_{oc}J_{sc}FF/P_{in} \qquad (2.2)$$

where P_{in} is the power of incident light [44].

The J-V voltage curve of an OPV solar cell in dark conditions is shown in Figure 2.25 (a). For a dark device, the J-V curves pass through the interception of the axes. When the cell is put under the light, the J-V curve runs as shown in Figure 2.25 (b).

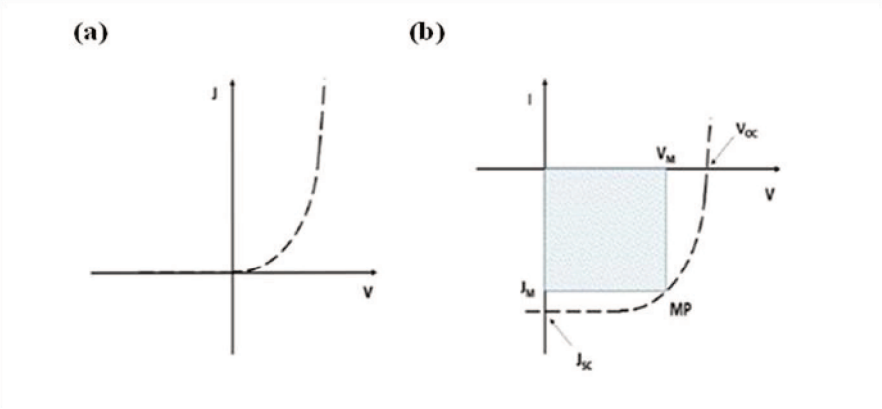

Figure 2.25. J-V curves of an OPV solar cell under (a) dark and (b) illuminated conditions. Adapted from [44].

The J-V curve permits to obtain the parameters to describe the efficience of the device. The short-circuit current, Jsc, is the maximum current that can flow into the device under lighting when no polarization is applied. This parameter provides information on the efficiency of processes such as charge separation and charging in the cell. When a polarization is applied and no current flows through the cell the device is in open circuit state and the applied voltage is the open circuit voltage (V_{OC}), which is the maximum voltage obtainable from the device. This parameter is proportional to the difference between HOMO and LUMO. The FF is given by the maximum power quantity, Voc x Jsc product (blue rectangle in Figure 2.25 (b)).

- *p-type materials*

Polythiophenes are one of the major families of conjugated polymers for applications in organic solar cells. Among polythiophenes, P3HT is the most used in OSCs with the reported efficiency of a P3HT:PCBM solar cell of ca. 4-5%. However, the efficiency of the P3HT-based devices is limited by the relatively large bandgap (1.9 eV) of this polymer.

A different strategy consists in using of polythiophene-based push-pull copolymers. In these type of polymers, an electron-rich comonomer (e.g. fluorene, carbazole, dibenzosilole, benzodithiophene, etc.) is coupled with a second electron-deficient

comonomer (e.g. benzodiathiazole, diketopyrrolopyrrole, etc.). The application of this new class of conjugated polymers into devices has led to a remarkable increase in the efficiency of the device. The efficiency of 10.3% and 11.5% have been reported for single junction and tandem devices respectively [45,46]. Some examples of low band gap polymers are reported in Figure 2.26.

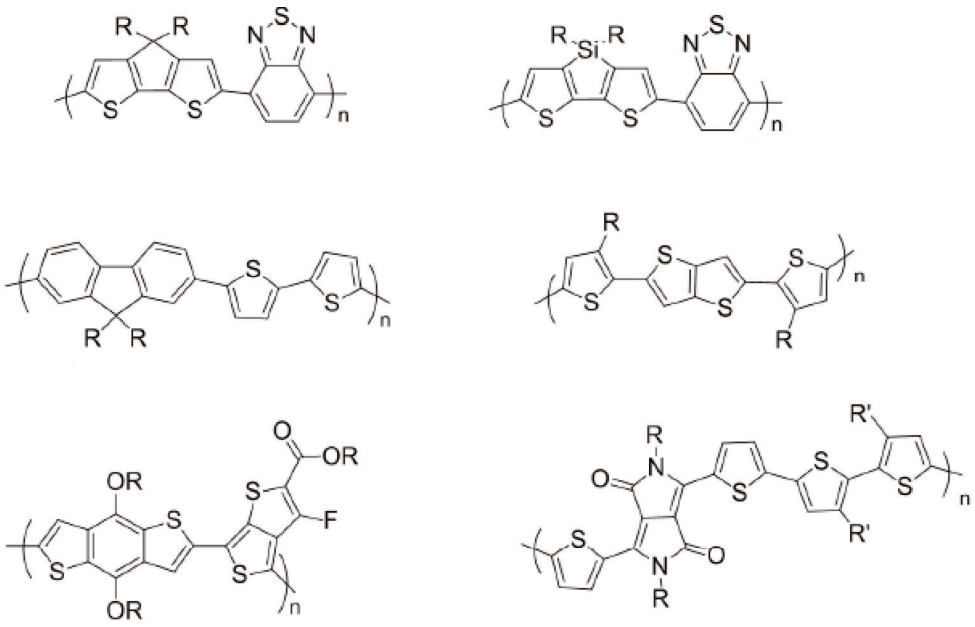

Figure 2.26. Low band-gap semiconducting polymers. R=alkyl chain. Adapted from [45,46].

- *n-type materials*

Among the different n-type materials, fullerene derivatives have a particular relevance. The most used acceptor materials for organic solar cells, indeed, are the fullerene derivatives and in particular PCBM, given its solubility in most organic solvents. While most of the applications are historically covered by fullerene derivatives, other small molecules have been developed to fulfill the role of the acceptor in organic electronic devices.

Double-cable (D-C) polymers have found applications in electro-optical devices due to their electronic properties. The concept of double-cable polymers for organic optoelectronic devices was first introduced by Cravino and Sariciftci in 2002 [47]. These polymers are constituted of a π-conjugated polymer, as main chain polymer, to which n-type materials, C_{60} for instance, are covalently linked. Among their advantages, it is possible to remark the possibility of the large donor-acceptor interfacial area, good

tunability of the components, as well as good stability upon phase separation and clustering.

Electropolymerization of aromatic monomers is one of the most used strategies to obtain C_{60}-containing D-C. As an example, electropolymerization giving a double cable polymer in which C_{60} was used as an n-type material with terthiophene - as the main-chain monomer is shown in Figure 2.27 [48].

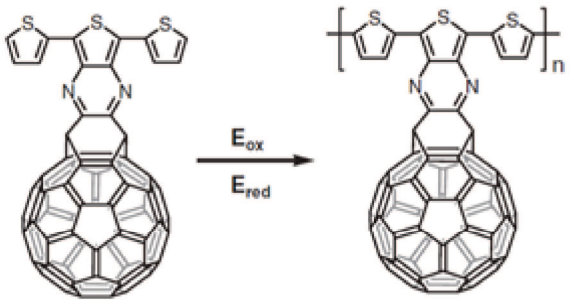

Figure 2.27. Electropolymerization D-C polymer: bisfulleroid, as electron-acceptor and terthiophene as donor material. Adapted from [48]

Kaunisto et al. proposed a synthesis of a series of tailored fulleropyrrolidine derivatives with thiophene substituents to be used as electron acceptor materials in inverted organic BHJ solar cells (Figure 2.28). They found a strong correlation between the molecular structure of the acceptor and its capability to form a photovoltaic BHJ film with the used electron donor material P3HT with 2.0% PCE. [49].

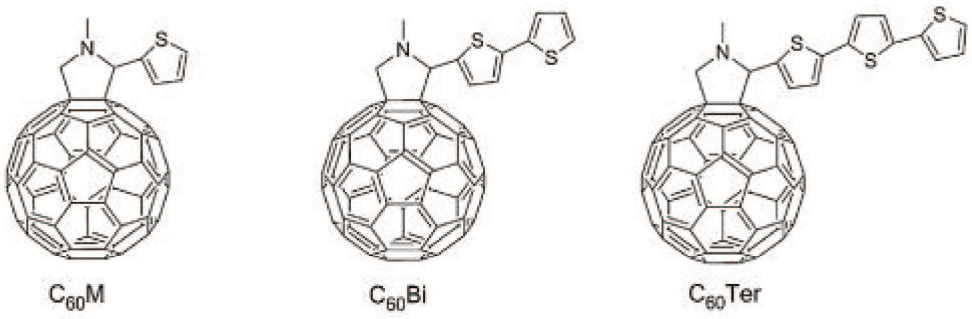

Figure 2.28. Chemical structures of the tailored fulleropyrrolidine derivatives synthesized and tested in inverted BHJ OPVs with P3HT as a donor. Adapted from [49].

- *Morphology control in BHJ OSCs by additives*

The photovoltaic performance of a BHJ device is controlled by multiple factors including intrinsic electronic properties of the compounds, their miscibility, and solubility. In particular, morphology plays a key role in the photovoltaic process. Accordingly, an ideal

morphology would entail structure ordering at various length scales, i.e. from local molecular ordering to global phase-separated domains or networks. However, solution processing of the BHJ layer from a blend solution of donor material and acceptor material in a single solvent typically does not permit to control resulting morphology, leading to a device with poor performances. Therefore, various approaches as different as thermal and solvent vapour annealing [50–53], additives including small molecules [54,55], polymers [56–60], inorganic nanocrystals [61], high boiling solvents have been employed in order to gain control film organization at the previously reported length scales. In particular, processing with the solvent additive in addition to the primary host solvent – an approach developed in the mid-2000s [62–64] – has been widely employed as a convenient approach, given its compatibility with large-scale processing [65,66].

Block copolymers have also been used as additives to reduce micron-scale phase separation in polymer blends P3HT:PCBM solar cells even upon extended thermal annealing (Figure 2.29). In particular, when the gradient copolymer was included in the blend at 1 wt%, the size and density of PCBM needle-shaped aggregates were markedly reduced [67]. Nevertheless, although this stabilized film morphology led to a stable PCE of the corresponding bulk heterojunction solar cells even upon extended thermal annealing the short-circuit current and FF were reduced when the gradient copolymer was present, leading to a lower PCE value [67].

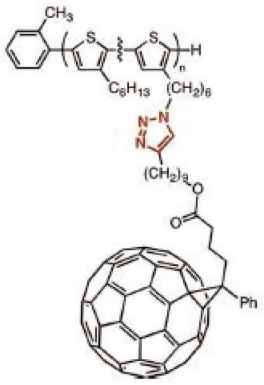

Figure 2:29. Fullerene-functionalized copolymer. Adapted from [67].

Recently a new multi-block copolymer based on ([1,4]-fullerene)-*alt*-[1,4-dimethylene-2,5-bis(cyclohexylmethyl ether)phenylene] and 3-hexylthiophene (Figure 2.30) were deposited on ITO/glass substrates *via* spin-coating and used as additives in P3HT:PCBM BHJ. It was shown that the introduction of 0.4% of the additive in P3HT:PCBM BHJ

device induced a favorable morphology with interpreting network and increased of P3HT crystallinity. Moreover, the effect of the additive in P3HT: PCBM BHJ resulted in a slight increase in efficiency from 3.6 to 4.2% [68].

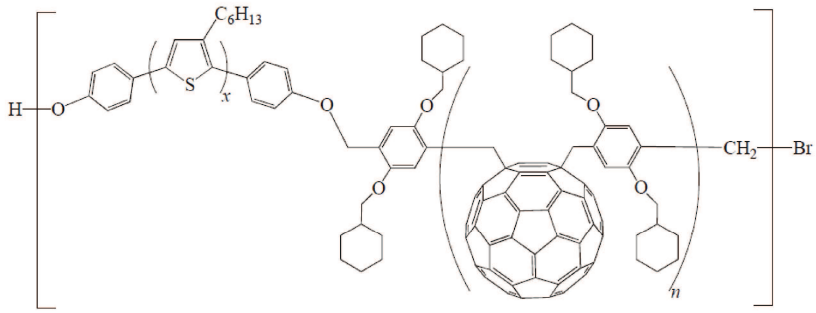

Figura 2.30. Multi-block copolymer, P3HT-b-PFDP. Adapted from [68].

- *Stability of OSCs*

OSCs degrade during illumination. In particular, the phenomena of chemical and physical degradation takes place in an OSCs under illumination and also in the dark. Exposure to air leads to two different kinds of degradation, i.e. intrinsic degradation which is caused by the thermal diffusion of species within the device and an extrinsic degradation, which is due to air intrusion in the device [69]. Several approaches have been proposed to improve device stability. A general approach is to use metal oxides as buffer layer, and silver as the upper anode. Also, glass or encapsulation membranes have been employed as coating layers to reduce the amount of oxygen and water impurities in the devices. These optimizations allow defining a protocol of device-packaging which would improve the stability of OSCs under ambient conditions.

2.3.3. Electrochemical sensors

An electrochemical biosensor is a self-contained integrated device, which is capable of providing specific quantitative or semi-quantitative analytical information using a biological recognition element (biochemical receptor) which is retained in direct spatial contact with an electrochemical transduction element. For this reason, the biospecific reagent is immobilized on a suitable electrode, capable of giving an electrochemical response related to the action of the biochemical receptor [11,71].

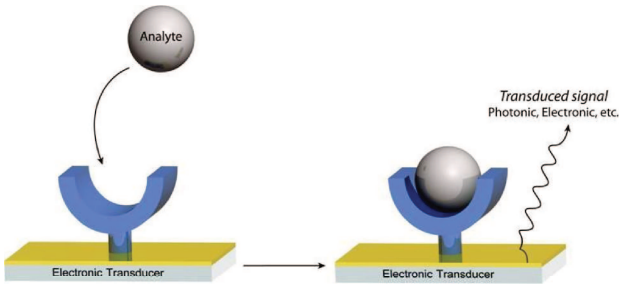

Figure 2.31. Scheme of molecular recognition and signal transduction.

One of the key properties of a sensor is selectivity, that is, the ability to recognize and, therefore, respond to a specific chemical substance. Biochemical recognition processes are characterized by high selectivity, so the development of biosensors is of great interest. The transducer serves to transfer the signal from the output of the receptor domain (that is, the modification of some chemical-physical property of the receptor) almost always to the electrical domain (i.e., an electrical signal). Often it is called a detector, or sensor or electrode, even though the transducer term is more appropriate (Figure 2.31).

- *Enzymatic electrochemical biosensors*

The use of enzyme as a bio-recognition element can provide highly selective detection of the target analyte due to the high specificity of enzymes towards the analyte. An enzyme specific for the analyte of interest is immobilized on the nanomaterial modified-electrode. The amperometric detection is based on the bio-electrocatalytic reaction between the target analyte and electrode, which results in an electrical signal (current) that can be used for quantitative detection of the analyte.

Enzymes are catalysts of biological reactions. They are proteins that enhance biochemical reactions. More generally, oxidases are enzymes that transform their own substrates (glucose, lactate, glutamate, cholesterol, and other endogenous metabolites) in some products and hydrogen peroxide(H_2O_2) [72].

The amperometric signal can be obtained through either direct or mediated electron transfer based electrochemical reactions (Figure 2.32). Unlike other types of biosensors, which are not widely commercialized, the enzymatic electrochemical biosensors have been successfully commercialized, thanks to the invention of glucose biosensors, which are widely used in personal diabetes monitors [73].

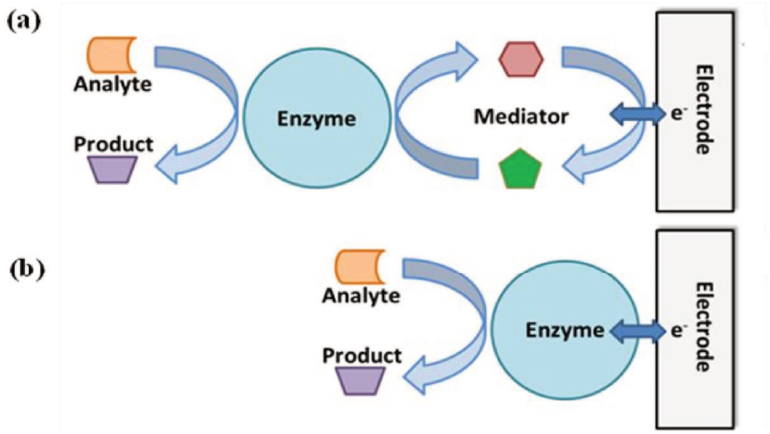

Figure 2.32. Schematic illustration of enzymatic biosensor based on (A) mediated electron transfer and (B) direct electron transfer.

In all cases, the enzyme acts by fixing the metabolite in its active site (e.g., glucose or lactate), by using a molecule of oxygen, by transforming the metabolite into a redox product (e.g., gluconic acid or pyruvate), and by releasing the reaction product and hydrogen peroxide. Once the hydrogen peroxide comes into contact with the electrodes at the transducer interface, it is transformed into the water by the release of two electrons. The counting of these electrons (by measuring the current) constitutes the detection of the metabolite. At the end of each cycle, only one hydrogen peroxide molecule is produced for each metabolite. Thus, counting the hydrogen peroxide molecules returns the number of metabolites that have been transformed. To count the hydrogen peroxide molecules, we can see the possible redox reactions on the hydrogen peroxide.
There are two main ones:

1. An oxidation: $2H_2O_2 \rightarrow O_2 + 2H_2O + 4e^-$ (2.3)
2. And a reduction: $H_2O_2 + 2H^+ + 2e^- \rightarrow 2H_2O$ (2.4)

This mode of operation is typical of the first generation electrochemical biosensors, which operate indirectly, the enzyme reacts with the substrate (in this case glucose), producing secondary chemical species (H_2O_2) that is capable of interact with the electrode. The electrode, therefore, interacts with this secondary product (oxidizing or reducing it, as appropriate) by measuring the current, which is correlated with the concentration of the product and hence at the concentration of substrate. This system has two limits: on one side product production efficiency may not always be optimal, so the sensitivity of this methodology is not the best. On the other hand, more generally limiting, the fact that the

electrode process, especially if of the amperometric type, measuring the current that accompanies the reduction or oxidation of the product is not very selective, because there may also be other chemical species that can interact. Simultaneously with the product and the electrode is not able to discriminate since it is not specific to it but is a generic electronic conductor. This results in a decrease, lower selectivity of the receptor. For example, in the case of glucose biosensors, in biological analyzes, there is very often the presence of ascorbic acid or uric acid, which can be oxidized. For this reason, it was thought to develop second-generation biosensors, which require a different interaction of the electrode with the receptor system. It makes the enzyme "conductive" by introducing mediators, redox (Ox / Red) groups capable of spreading within the enzymatic envelope, to reduce the leap between centers to the heart of the enzyme.

- *Non-enzymatic electrochemical sensors*

Non-enzymatic electrochemical sensors have been advocated among various biosensors in recent years as ideal systems for direct oxidation or reduction of analytes. Although they can avoid the intrinsic defects of enzymes, these sensors vary considerably depending on electrode materials because the slow kinetic process can not lead to discernible faradaic current.

Therefore, many efforts have been centered on the research of new electrocatalytic materials to improve the kinetic process of electron transfer.

The performance and sensitivity of electrochemical biosensors can be greatly improved by the integration of nanomaterials into their construction. In addition, the use of nanomaterials can help to address some of the key challenges in the development of biosensors, such as the sensitive interaction of an analyte with biosensor surface, efficient transduction of the biorecognition event, and reduced response times.

Fullerene was reported to be used as a mediator in the development of biosensors for detecting various biomolecules, such as glucose, urea, proteins [74,75].

An effective mediator for highly sensitive biosensor should possess two qualities, hydrophilic in nature and having some active functional groups so that it can conjugate with targeted biomolecules and make a liaise between the recognition site and the electrode surface to promote the transfer of electrons produced due to the biochemical reactions at recognition site. However, it is known that pristine fullerene is hydrophobic in nature and also insoluble in polar solvents which make it difficult to process. This difficulty can be overcomed once it is functionalized with some suitable functional groups, e.g., carboxyl,

hydroxyl, amine groups, etc. A bulk of research works and investigations implies that in order to incorporate fullerene derivatives or modified fullerene into biosensors, they need to possess a functional group that can be easily reacted with biomolecules [76].

The functional fullerene has also been used in a non-enzymatic electrochemical biosensor. Recently interesting results showed that the ZnPp−C_{60} demonstrated in Figure 2.33 could be a novel material for construction of a non-enzymatic electrochemical sensor for H_2O_2 and nitrite [77].

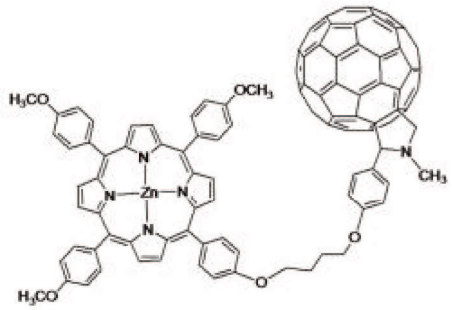

Fig. 2.33. Chemical structure of the ZnPp−C_{60}. Adapted from [77].

The electrocatalytic reduction of H_2O_2 showed a wide linear range from 0.035 to 3.40 mM, with a high sensitivity of 215.6 μA mM^{-1} and a limit of detection (LOD) as low as 0.81 μM. Moreover, the TOAB/ZnPp−C_{60}/GCE showed excellent stability and reproducibility, and good testing recoveries for analysis of the nitrite levels of river water and rainwater.

Recently have been realized new functional material, 3-amino-5-mercapto-1,2,4-triazole functionalized fullerene-C_{60} based gold nanocomposite [78] (Figure 2.34). Thus, the highly stable and low onset potential non-enzymatic sensor exhibited high electrocatalytic activity and effective electron transfer from the electrocatalyst to the substrate electrode in a linear concentration range spanning over 0.025–0.8 mM and a higher sensitivity response of 1.2 A mM^{-1} cm^{-2} with good reproducibility, long-term stability, anti-interference ability and chloride poisoning resistance.

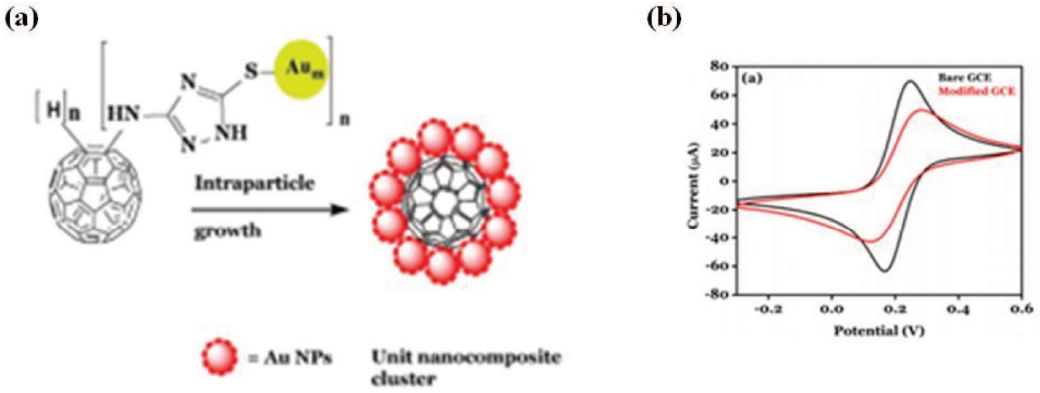

Figure 2.34. Schematic illustration of the formation of nanocomposite (a) and cyclovoltammetry(CV) of bare and modified GC electrodes with scan rate 100 mVs^{-1} in 0.1 M KCl. Adapted from [78].

Thiophenes represent another class of materials widely used for the preparation of polymer nanocomposites geared for preparation of electrochemically modified electrodes for biosensors. Recently, Peteu et al have suggested that new hemin-P(EDOT) systems electrodeposited on boron-doped diamond (BDD) microelectrode were promising for quantificationnn of peroxynitrite (Fig. 2.35) [79]. The electrochemical response to peroxynitrite was studied by voltammetry and time-based amperometry. The measured detection limit was 10 ± 0.5 nM (S/N = 3), the sensitivity was 4.5 ± 0.5 nA nM−1 and the response time was 3.5 ± 1 s.

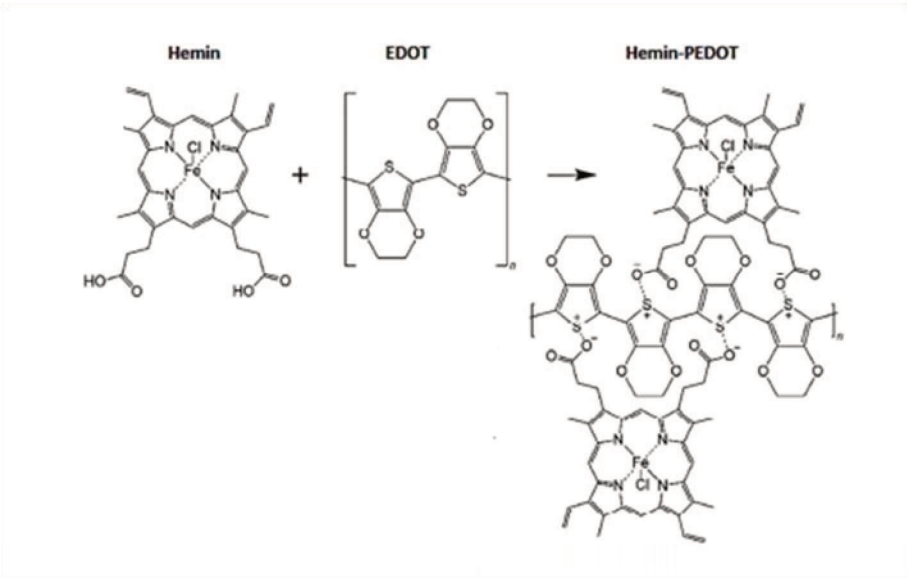

Figure 2.35. The hemin-P(EDOT) film is formed by the electropolymerization of EDOT with hemin. Adapted from [79].

References

[1] G. Heywang, F. Jonas, *Adv. Mater.* **1992**, *4*, 116.

[2] J. Heinze, B. A. Frontana-Uribe, S. Ludwigs, *Chem. Rev.* **2010**, *110*, 4724.

[3] H.E. Katz, J. Johnson, and A. J. Lovinger, W. Li, *J. Am. Chem. Soc.*, **2000**, 122, 77887.

[4] E. Mena-Osteritz, *Adv. Mater.* **2002**, *14*, 609.

[5] A. Facchetti, M.-H. Yoon, C. L. Stern, G. R. Hutchison, and M. A. Ratner, T. J. Marks*, *J. Am. Chem. Soc.* **2004**, 126, 13840.

[6] H. Krüger, S. Janietz, D. Sainova, D. Dobreva, N. Koch, A. Vollmer, *Adv. Funct. Mater.* **2007**, *17*, 3715.

[7] H. Yan, Z. Chen, Y. Zheng, C. Newman, J. R. Quinn, F. Dötz, M. Kastler, A. Facchetti, *Nature* **2009**, *457*, 679.

[8] D. Bagchi, *Bio-Nanotechnology : A Revolution in Food, Biomedical, and Health Sciences*, Wiley-Blackwell, **2013**.

[9] D. Jariwala, V. K. Sangwan, L. J. Lauhon, T. J. Marks, M. C. Hersam, *Chem. Soc. Rev.* **2013**, *42*, 2824.

[10] M. S. Dresselhaus, G. Dresslhaus, *Annu. Rev. Mater. Sci.* **1995**, *25*, 487.

[11] A. W. Jensen, S. R. Wilson, D. I. Schuster, *Bioorg. Med. Chem.* **1996**, *4*, C_{60}7.

[12] D. Dubois, K. M. Kadish, S. Flanagan, L. J. Wilson, *J. Am. Chem. Soc.* **1991**, *113*, 7773.

[13] W. A. Scrivens, J. M. Tour, *J. Chem. Soc. Chem. Commun.* **1993**, *0*, 1207.

[14] M. Prato, *J. Mater. Chem.* **1997**, *7*, 1097.

[15] A. Hirsch, *Phys. status solidi* **2006**, *243*, 3209.

[16] M. Maggini, G. Scorrano, M. Prato, *J. Am. Chem. Soc.* **1993**, *115*, 9798.

[17] T. Da Ros, M. Prato, M. Carano, P. Ceroni, and F. Paolucci, S. Roffia, *J. Am. Chem. Soc.* **1998**, *120*, 11645.

[18] P. Chandrasekhar, in *Conduct. Polym. Fundam. Appl.*, Springer US, Boston, MA, **1999**, pp. 3–22.

[19] J. Heinze, in *Electrochem. IV*, Springer-Verlag, Berlin/Heidelberg, **1990**, pp. 1–47.

[20] L. D. S. Lapitan, B. J. V. Tongol, S.-L. Yau, *Langmuir* **2010**, *26*, 10771.

[21] C. Hamann, *Cryst. Res. Technol.* **1988**, *23*, 384.

[22] A. F. Diaz, K. K. Kanazawa, G. P. Gardini, *J. Chem. Soc. Chem. Commun.* **1979**, *0*, 635.

[23] J. M. Luis, D. M. Bishop, B. Kirtman, *J. Chem. Phys.* **2004**, *120*, 813.

[24] P. Zarras, J. Irvin, in *Encycl. Polym. Sci. Technol.*, John Wiley & Sons, Inc., Hoboken, NJ, USA, **2003**.

[25] C. Zhang, C. Hua, G. Wang, M. Ouyang, C. Ma, *J. Electroanal. Chem.* **2010**, *645*, 50.

[26] O. Turkarslan, M. Ak, C. Tanyeli, I. M. Akhmedov, L. Toppare, *J. Polym. Sci. Part A Polym. Chem.* **2007**, *45*, 4496.

[27] G. A. Niklasson, C. G. Granqvist, A. Azens, G. Gustavsson, R. Karmhag, C. G. Granqvist, Y. Nishikitani, H. Watanabe, C. G. Granqvist, K. K. Wong, A. G. Rinzler, *J. Mater. Chem.* **2007**, *17*, 127.

[28] K. Ziemelis, *Nature* **1998**, *393*, 619.

[29] E. L. Runnerstrom, A. Llordés, S. D. Lounis, D. J. Milliron, *Chem. Commun.* **2014**, *50*, 10555.

[30] A. M. Fraind, J. D. Tovar, *J. Phys. Chem. B* **2010**, *114*, 3104.

[31] S. Chen, Y. Liu, W. Qiu, X. Sun, and Y. Ma, D. Zhu, *Chem. Mater.*, **2005**, *17*, 2208.

[32] C.-C. You, C. R. Saha-Möller, F. Würthner, Y. Geerts, K. Müllen, A. J. Bard, V. S. K. Balagurusamy, P. A. Heiney, I. Schnell, A. Rapp, H.-W. Spiess, S. D. Hudson, H. Duan, *Chem. Commun.* **2004**, *41*, 2030.

[33] M. K. R. Fischer, T. E. Kaiser, F. Würthner, P. Bäuerle, D. L. Officer, C. O. Too, G. G. Wallace, L. de Cola, R. M. Williams, F. Würthner, E. H. A. Beckers, S. C. J. Meskers, R. A. J. Janssen, *J. Mater. Chem.* **2009**, *19*, 1129.

[34] P. Camurlu, C. Gültekin, Z. Bicil, *Electrochim. Acta* **2012**, *61*, 50.

[35] T. Yamazaki, Y.Murata, K. Komatsu, K. Furukawa, M. Morita, N. Maruyama, and T.Yamao, S. Fujita, *Org. Lett.* **2004**, *6*, 4865

[36] Becquerel A E, *Comptes Rendus L'Academie des Sci.* **1839**, 145.

[37] A. Pochettino and A. Sella, *Acad. Lincei Rend* **1906**, 355.

[38] S. E. Shaheen, D. S. Ginley, G. E. Jabbour, *MRS Bull.* **2005**, *30*, 10.

[39] C. Sah, R. Noyce, W. Shockley, *Proc. IRE* **1957**, *45*, 1228.

[40] J.-L. Brédas, J. E. Norton, J. Cornil, V. Coropceanu, *Acc. Chem. Res.* **2009**, *42*, 1691.

[41] T. M. Clarke, J. R. Durrant, *Chem. Rev.* **2010**, *110*, 6736.

[42] A. J. Pearson, T. Wang, D. G. Lidzey, *Reports Prog. Phys.* **2013**, C_{60}, 22501.

[43] R. F. Service, *Science.* **2004**, *306*, 2034.

[44] H. Hoppe, N. S. Sariciftci, *J. Mater. Res.* **2004**, *19*, 1924.

[45] B. Tieke, A. R. Rabindranath, K. Zhang, Y. Zhu, *Beilstein J. Org. Chem.* **2010**, *6*, 830.

[46] S. Fabiano, Z. Chen, S. Vahedi, A. Facchetti, B. Pignataro, M. A. Loi, *J. Mater. Chem.* **2011**, *21*, 5891.

[47] A. Cravino, N. S. Sariciftci, M. Barcu, B. Cuadra, A. K. Rai, P. Cheng, L. T. Scott, N. S. Sariciftci, C. J. Brabec, N. S. Sariciftci, *J. Mater. Chem.* **2002**, *12*, 1931.

[48] G. Sonmez, C. K. F. Shen, Y. Rubin, F. Wudl, *Adv. Mater.* **2005**, *17*, 897.

[49] K. M. Kaunisto, N. K. Subbaiyan, C. B. K.C., V. I. Chukharev, H. M. Hakola, T. K. Vuorinen, V. M. Manninen, N. V. Tkachenko, H. J. Lemmetyinen, F. D'Souza, *Synth. Met.* **2014**, *195*, 193.

[50] G. Li, V. Shrotriya, J. Huang, Y. Yao, T. Moriarty, K. Emery, Y. Yang, *Nat. Mater.* **2005**, *4*, 864.

[51] Y. Kim, S. Cook, S. M. Tuladhar, S. A. Choulis, J. Nelson, J. R. Durrant, D. D. C. Bradley, M. Giles, I. McCulloch, C.-S. Ha, M. Ree, *Nat. Mater.* **2006**, *5*, 197.

[52] G. Li, Y. Yao, H. Yang, V. Shrotriya, G. Yang, Y. Yang, *Adv. Funct. Mater.* **2007**, *17*, 1636.

[53] C. S. Kim, L. L. Tinker, B. F. DiSalle, E. D. Gomez, S. Lee, S. Bernhard, Y.-L. Loo, *Adv. Mater.* **2009**, *21*, 3110.

[54] S.-H. Chan, C.-S. Lai, H.-L. Chen, C. Ting, C.-P. Chen, *Macromolecules* **2011**, *44*, 8886.

[55] K. R. Graham, P. M. Wieruszewski, R. Stalder, M. J. Hartel, J. Mei, F. So, J. R. Reynolds, *Adv. Funct. Mater.* **2012**, *22*, 4801.

[56] J.-F. Lin, W.-C. Yen, C.-Y. Chang, Y.-F. Chen, W.-F. Su, *J. Mater. Chem. A* **2013**, *1*, 665.

[57] S.-Y. Chang, H.-C. Liao, Y.-T. Shao, Y.-M. Sung, S.-H. Hsu, C.-C. Ho, W.-F. Su, Y.-F. Chen, *J. Mater. Chem. A* **2013**, *1*, 2447.

[58] H.-C. Liao, C.-S. Tsao, T.-H. Lin, M.-H. Jao, C.-M. Chuang, S.-Y. Chang, Y.-C. Huang, Y.-T. Shao, C.-Y. Chen, C.-J. Su, U.-S. Jeng, Y.-F. Chen, W.-F. Su, *ACS Nano* **2012**, *6*, 1657.

[59] J.-H. Tsai, Y.-C. Lai, T. Higashihara, C.-J. Lin, M. Ueda, W.-C. Chen, *Macromolecules* **2010**, *43*, 6085.

[60] C. Yang, J. K. Lee, A. J. Heeger, F. Wudl, *J. Mater. Chem.* **2009**, *19*, 5416.

[61] J. Peet, J. Y. Kim, N. E. Coates, W. L. Ma, D. Moses, A. J. Heeger, G. C. Bazan, *Nat. Mater.* **2007**, *6*, 497.

[62] Y.-M. Chang, L. Wang, *J. Phys. Chem. C* **2008**, *112*, 17716.

[63] Y. Yao, J. Hou, Z. Xu, G. Li, Y. Yang, *Adv. Funct. Mater.* **2008**, *18*, 1783.

[64] C. Yang, E. Zhou, S. Miyanishi, K. Hashimoto, K. Tajima, *ACS Appl. Mater. Interfaces* **2011**, *3*, 4053.

[65] Y. Kim, G. Kim, J. Lee, K. Lee, *Sol. Energy Mater. Sol. Cells* **2012**, *105*, 272.

[66] J. K. Lee, W. L. Ma, C. J. Brabec, J. Yuen, J. S. Moon, J. Y. Kim, K. Lee, G. C. Bazan, A. J. Heeger, *J. Am. Chem. Soc.* **2008**, *130*, 3619.

[67] E. F. Palermo, S. B. Darling, A. J. McNeil, *J. Mater. Chem. C* **2014**, *2*, 3401.

[68] M. Raïssi, H. Erothu, E. Ibarboure, H. Cramail, L. Vignau, E. Cloutet, R. C. Hiorns, *J. Mater. Chem. A* **2015**, *3*, 18207.

[69] A. J. Heeger, *Chem. Soc. Rev.* **2010**, *39*, 2354.

[70] E. By, A. P. F. Turner, G. S. Wilson, **n.d.**

[71] S. Bosi, T. Da Ros, G. Spalluto, M. Prato, *Eur. J. Med. Chem.* **2003**, *38*, 913.

[72] S. Carrara, in *Bio/CMOS Interfaces and Co-Design*, Springer New York, New York, NY, **2013**, pp. 135–155.

[73] S. Zhang, G. Wright, Y. Yang, *Biosens. Bioelectron.* **2000**, *15*, 273.

[74] J. Davis, D. Huw Vaughan, M. F. Cardosi, *Enzyme Microb. Technol.* **1995**, *17*, 1030.

[75] Z. Chen, L. Ma, Y. Liu, C. Chen, *Theranostics* **2012**, *2*, 238.

[76] J. R. Baena, M. Gallego, M. Valcárcel, *TrAC Trends Anal. Chem.* **2002**, *21*, 187.

[77] K. E. Toghill, R. G. Compton, *Int. J. Electrochem. Sci* **2010**, *5*, 1246.

[78] S. Sutradhar, A. Patnaik, *Sensors Actuators B Chem.* **2017**, *241*, 681.

[79] S. F. Peteu, B. W. Whitman, J. J. Galligan, G. M. Swain, *Analyst* **2016**, *141*, 1796.

3. Materials and methods

3.1. Synthesis and characterization of NDIT systems[2]

The synthesis of symmetric, NDI2ODT2 and NDI2ODT4, was carried out under argon by reacting a mixture of 2-(trimethylstannyl)thiophene and 5-(trimethylstannyl)-2,2'-dithiophene, respectively, with NDI2OD-Br_2 and $Pd(PPh3)_2Cl_2$ in anhydrous toluene. After cooling to room temperature, the reaction mixtures have been diluted with chloroform and then washed with water, dried over anhydrous sodium sulfate, and concentrated on rotary evaporator. The residues were subjected to column chromatography on silica gel using a mixture of chloroform: hexane as eluent. This procedure leads to an orange NDI2ODT2 or a purple NDI2ODT4 solid as the resulting product (Figure 3.1).

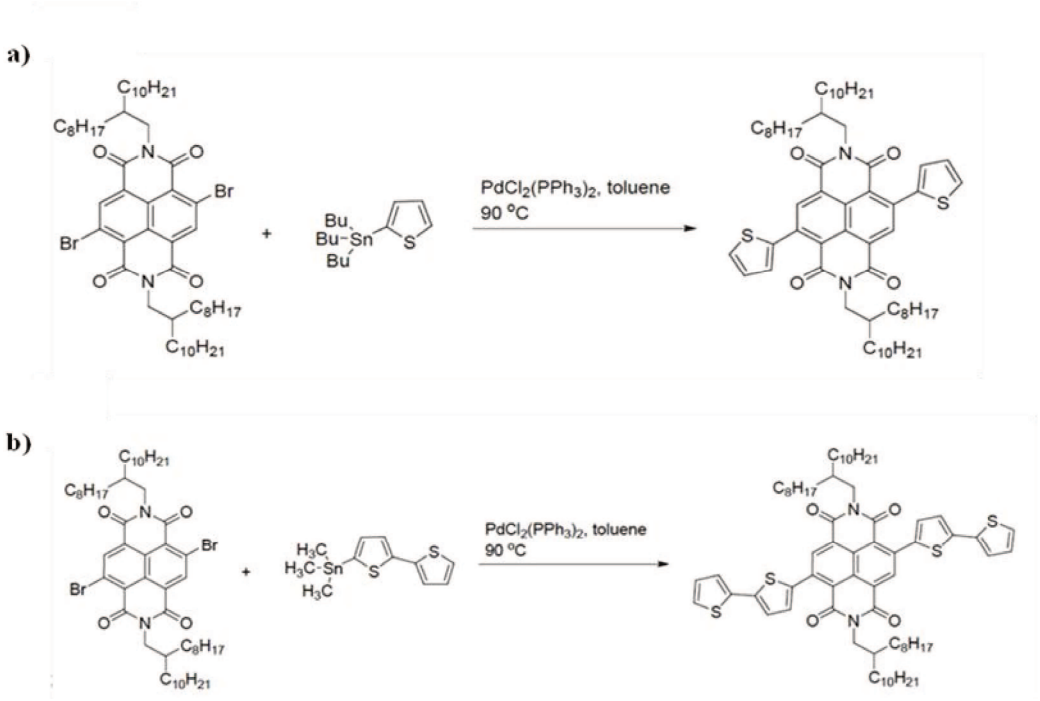

Figure 3.1. Synthesis of a) NDI2ODT2 and b) NDI2ODT4. Adapted from [1].

Figure 3.2 represents a UV-visible spectrum for NDI2ODT2 and NDI2ODT4 acquired in CH_3CN: dichloromethane (CH_2Cl_2) solution. It can be seen from the Figure 3.2 that a maximum absorption for NDI2ODT2 and NDI2ODT4 was reached at 250 nm and 300 nm respectively.

[2] Chemical synthesis of NDI2ODT2 and NDI2ODT4 was provided by the group of Prof A. Facchetti (Northwestern University, USA)

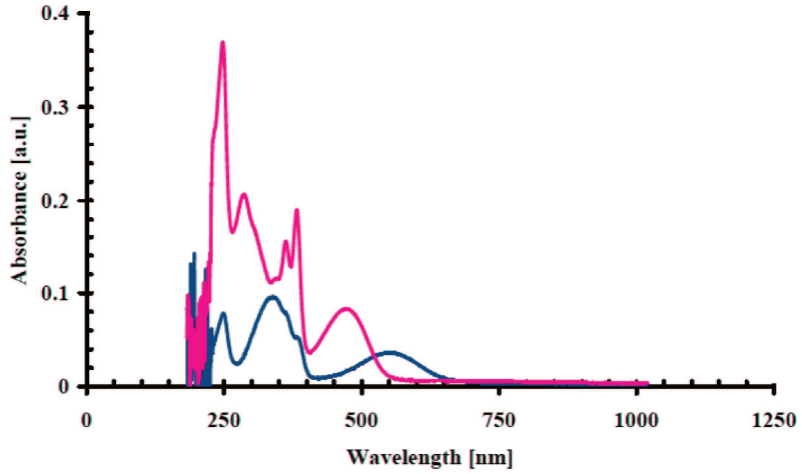

Figure 3.2. Absorption spectra of NDI2ODT2 (magenta line) and NDI2ODT4 (blue line) recorded in CH_2Cl_2:CH_3CN (3:2; v:v) Adapted from [1].

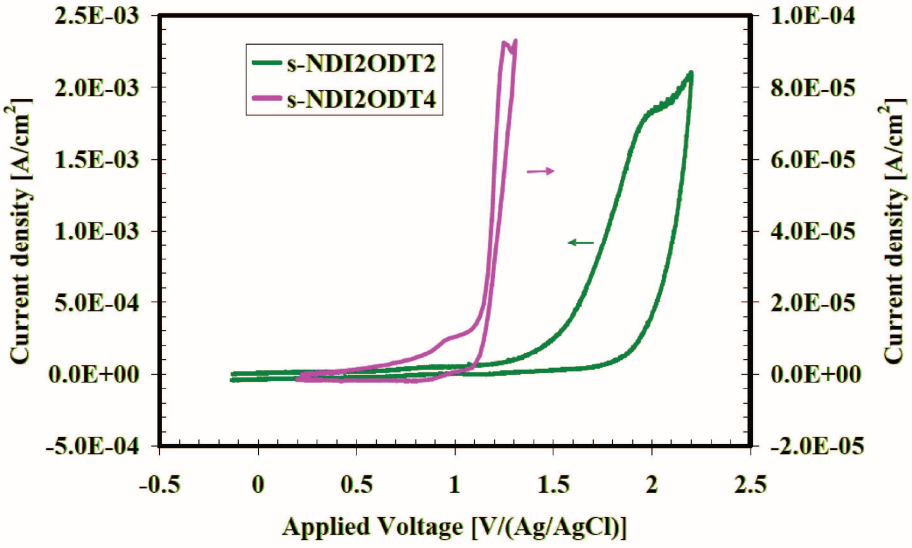

Figure 3.3. Cyclic voltammograms of NDI2ODT2 (green curve) and NDI2ODT4 (magenta curve) recorded in CH_2Cl_2:CH_3CN (3:2; v:v) and 0.1M $LiClO_4$. Scan rate: 50 mVs^{-1}. Adapted from [1].

In order to conduct electrochemical studies CV measurements (Figure 3.3) were performed in CH_3CN:CH_2Cl_2 solution (2:3; v:v) containing 10^{-2} M of $LiClO_4$ and 10^{-4} M of the monomers. The cyclovoltammetry in Figure 3.3 shows that oxidation onset potentials situated at +1.6V and + 0.9V for NDI2ODT2 and NDI2ODT4 respectively and oxidation peaks located at +1.8V and +1.0 V for NDI2ODT2 and NDI2ODT4, respectively. These findings suggest that the presence of a greater number of electron-rich thiophene units facilitate oxidation. Moreover, a cathodic peak at -1.1V was observed only for the

NDI2ODT4 system suggesting that zero suppression of the current occurs in s-NDI2ODT2.

3.2. Synthesis and characterization of new bis-Th2P-C_{60}[3]

A solution of C_{60} (500 mg, 0.69 mmol) in o-dichlorobenzene (o-DCB) (50 mL) was sonicated for 20 minutes before adding 2,2′-bithiophene-5-carboxaldehyde (336 mg, 1.73 mmol) and sarcosine (460 mg, 5.17 mmol). The resulting solution was stirred at 130 °C for 18 h. After solvent removing by a rotary evaporator, the obtained dark residue was dissolved in chloroform, adsorbed onto silica by removing chloroform under vacuum and loaded onto the top of a chromatography column. The monoadduct was recovered mixture of hexane/toluene (2:1 and 1:1), whereas a mixture of toluene/hexane 2:1 was used to recover the fraction of bisadducts of interest. Then, the isolated bisadducts were dissolved in chloroform and precipitated with an excess of methanol first and then with hexane. The bisadducts were obtained as a dark solid (180 mg; 22%). The synthesis is shown in Figure 3.4.

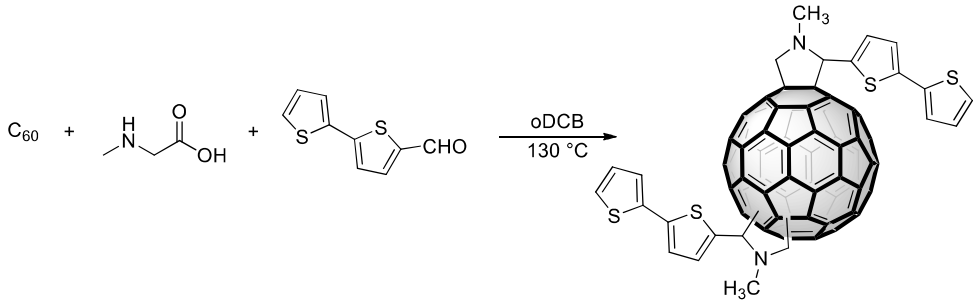

Figure 3.4. Synthesis of the new bis-Th2P-C_{60} monomer.

^{1}H NMR spectrum is shown in Figure 3.5.a. Given the possibility of different addition patterns of the addends on fullerene C_{60} that results in the formation of multiple regioisomeric bisadducts.

^{1}H NMR spectrum results complex with many signals overlapped. Therefore, the exact assignment of the different signals is very difficult. However, it is possible to define three major regions in the NMR spectrum. In the first region between 7.12-6.79 ppm, there is resonance of the aromatic protons. In the 5,46-3,36 ppm region, there is the resonance of

[3] Chemical synthesis and characterization of all fullerene-based derivatives and polymers in 3.2-3.3 was provided by Group of Prof. F. Giacalone

the fulleropyrrolidine ring protons, while at ca. 2.78 ppm are present the methylene protons. NMR signals correspond to those obtained for the similar molecules in the literature [2].

The analysis of bis-Th2P-C_{60} by means of FT-IR spectroscopy in Figure 3.5.b showed the IR bands at 527 and 691 cm^{-1}, associated with the fulleropyrrolidine monomer [3]. It is possible to identify three regions in the IR spectrum: bands a C_{60}0-900 cm^{-1}arerelated to the C–S stretching vibrations, the region 1400–1600 cm^{-1} shows the most intense bands related to the stretching of C=C bonds and 3200-2700 $cm^{-1}$are related to various types of C–H stretching vibrations.(KBr) ν/cm^{-1} = 3104, 3066, 2947, 2919, 2840, 2778, 1460, 1424, 1331, 1234, 1181, 1034, 840, 800,755, 691, 525, 480.

The UV-vis spectrum of bis-Th2P-C_{60} recorded in chloroform reported in the inset of Figure 3.5.c. Two major bands are clearly discernible at 246 and 313 nm. The bands can be ascribed to the presence of the C_{60} group in the monomer.

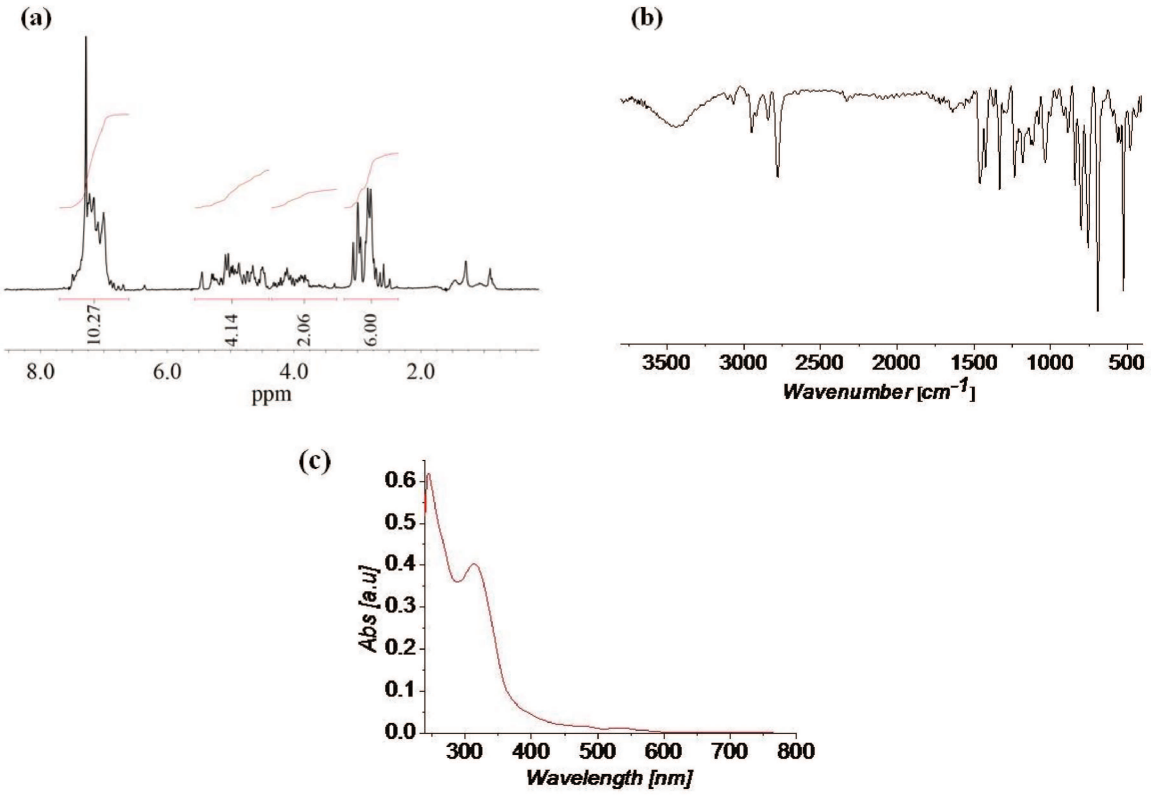

Figure 3.5. a.^{1}H NMR in $CDCl_3$ b. FT-IR (KBr) c.Uv-vis spectra in chloroform of bis-Th2P-C_{60}.

3.3. Synthesis and characterization of Th4P-C_{60} monomer and copolymers

The fulleropyrrolidine-thiophene **3** (Th4P-C_{60}) monomer was obtained by the reaction between C_{60}, aldehyde **1**, and amine **2**. In particular, a solution of C_{60} (C_{60}0 mg, 0.96 mmol), amine **1** (442.83 mg, 1.44 mmol), and 2,2'-bithiophene-5-carboxaldehyde **2** (285.46 mg, 1.44 mmol) in 34 mL of o-DCB was stirred at 160 °C for 4 h.Then, the solvent was evaporated under vacuum and the obtained residue was taken up with chloroform and centrifuged to remove most of the unreacted C_{60}. The recovered supernatant was further diluted with chloroform, adsorbed onto silica gel and loaded to the top of a chromatography column (hexane/toluene from 8:1 to 7:1 v/v to recover unreacted C_{60}, hexane/toluene from 6:1 to 5:1 v/v to recover compound3). The recovered compound was then solubilized in a small amount of chloroform, precipitated with methanol and then centrifuged. Finally, the obtained residue was washed with hexane and centrifuged. It was possible to obtain the desired product with a good yield (51%) and, remarkably, a high stereo selectivity towards the trans isomer. The product is a mixture of **trans/cis** isomers (**trans/cis** molar ratio = 86:14). ^{1}H NMR (300 MHz, $CDCl_3$, δ): 7.42 (d, J = 3.7 Hz, 2H), 7.29 – 7.26 (m, 4H), 7.19 (d, J = 3.6 Hz, 1.7H, trans isomer), 7.15 (d, J = 3.0 Hz, 0.3H, cis isomer), 7.06 (dd, J = 5.1, 3.6 Hz, 2H), 6.49 (s, 1.7H, trans isomer), 5.86 (s, 0.3H, cis isomer), 3.46 – 3.34 (m, 0.3H, cis isomer), 3.33 – 3.23(m, 0.85H, trans isomer), 2.88 – 2.80 (m, 0.85H, **trans** isomer), 2.13 – 1.71 (m, 2H), 1.57 – 1.28 (m, 10H), 0.91 (t, J = 6.8 Hz, 3H) ppm.^{13}C NMR (75 MHz, $CDCl_3$, δ):154.93, 153.09, 147.41, 146.26, 146.24, 146.18, 146.03, 145.98, 145.56, 145.53, 145.38, 145.33, 145.16, 144.56, 144.52, 143.06, 142.68, 142.53, 142.20, 142.15, 141.93, 141.83, 141.C_{60}, 139.99, 139.89, 139.77, 139.04, 137.23, 137.09, 136.42, 130.08, 127.92, 124.72, 124.01, 122.88, C_{60}.53, 73.15, 47.01, 31.97, 29.67, 29.34, 28.36, 27.20, 22.77, 14.23 ppm. IR: (KBr) ν= 3066, 2949, 2921, 2851, 1463, 1426, 1370, 1045, 841, 798, 757, 691, 575, 552, 527 cm^{-1}. UV−vis: ($CHCl_3$) λ_{max} (ε) = 254 (107264), 322 (62736), 428 nm (3491).

Finally, $FeCl_3$-mediated oxidative polymerization of fulleropyrrolidine **3** and different amounts of 3,4'-dihexyl-2,2'-bithiophene4permitted to obtain the copolymers (**5a-c**) containing oligothiophene moieties with different lengths and fullerene units in 58-60% yield (Figure 3.6).

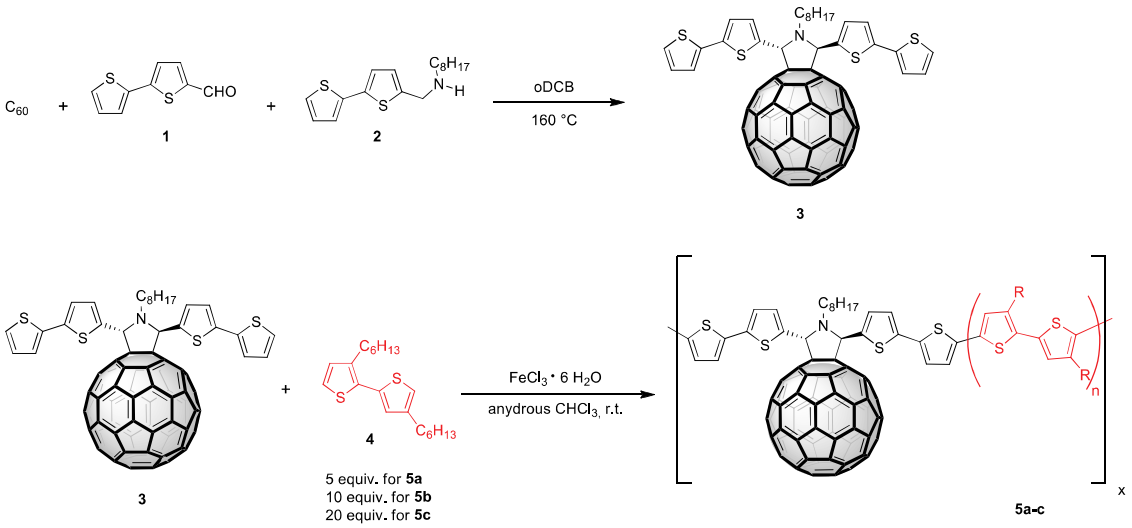

Figure 3.6. Synthesis of copolymers **5a-c**. The subscript n refers to 5, 10, 15 units for **5a**, **5b**, **5c**, respectively.

As was done with bis-Th2P-C_{60} the above-described, Th4P-C_{60} monomer and copolymers were also characterized by 1H NMR, FT- IR, and Uv-visible.

-^{1}H NMR

^{1}H NMR spectrum of C_{60}-ThPh **3** is shown in Figure 3.7a, whereas the ^{1}H NMR spectra of copolymers **5a-c** are overlapped in Figure 3.7b. It is of remarkable importance to point out that the synthesis of compound **3** could afford both cis and trans isomers. However, by comparing the peaks of NMR spectrum in Figure 3.7a centered at 6.49 and 5.86 ppm, belonging to the trans and cis isomers, respectively, it can be concluded that the reaction permits to achieve, with a high stereoselectivity, the trans isomer with a trans/cis molar ratio of 86:14. The C_{60}monoadduct/bithienyl moieties mean molar ratio of the copolymers 5a-c was determined considering the portion of the spectra between 2.7 and 3.5 ppm (magnified in Figure 3.7b) where it is possible to find the resonance peaks of the protons of the methylene linked to the nitrogen atom of the fulleropyrrolidine derivatives (cis/trans isomers) and the α-methylene protons of the hexyl chain present in the polythiophenic moiety. For the calculation of the C_{60}monoadduct/bithienyl moieties mean molar ratio, the different contributions deriving from the fulleropyrrolidine monomer and those from the bithienyl moieties were discriminated, considering the overlapping at 2.84 ppm of the signals due to the methylenic group of the bithiophene alkyl chain with proton $H_{b'}$ of the trans isomer of compound **3** (compare Figures 3.7a and 3.7b). In this way, it was possible to determine at C_{60}monoadduct/bithienyl moieties mean molar ratio of 1:4.5, 1:8.5 and 1:18.2 for copolymers **5a-c**, respectively. Moreover, it was possible to give an estimation

of the regioregularity values of the different copolymers **5a-c**, determined as the relative ratio of Head-to-Tail (HT) couplings to non-HT couplings, by making a comparison of the integrated areas of the peaks centered at 2.82 and 2.60 ppm which are ascribed to α-methylene protons of the hexyl chains in HT and Head-to-Head (HH) linkages, respectively [4]. It was possible to calculate regioregularity values reaching values of 84, 86 and 89% for copolymers **5a-c**, respectively.

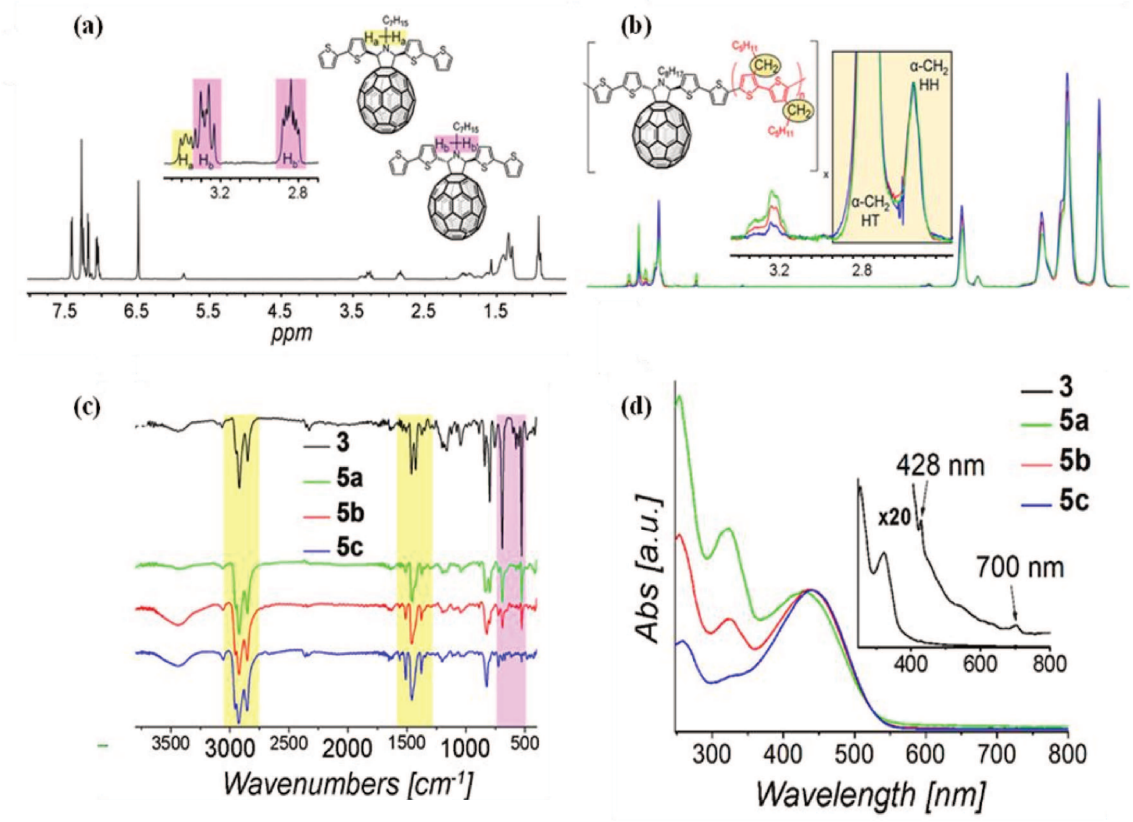

Figure 3.7.[1]H NMR in $CDCl_3$ of a) compound **3** and b) copolymers **5a** (green), **5b** (red), and **5c** (blue). c) FT-IR (KBr) of compound **3** and copolymers **5a-c**. d) Uv-vis spectra in chloroform of compound **3** and copolymers **5a-c**.

- FT-IR spectroscopy

FT- IR spectra in Figure 3.7 c acquired for copolymers **5a-c** show that the IR bands at 527 and 691 cm^{-1}, associated with the fulleropyrrolidine monomer decrease their relative intensity in comparison to the bands associated with the polythiophenic moiety, passing from copolymer **5a** to **5c**. These results are in accordance with the trend obtained by the NMR analysis.

- UV-vis spectroscopy

Uv-vis of compound **3** recorded in chloroform is reported in the inset of Figure 3.7d. It is possible to distinguish two major bands at 254 and 322 nm. Moreover, a sharp band at 428 nm and a broader band at 700 nm, which is typical of fullerene C_{60}-monoadducts at [6,6] junction [8], are also clearly identified. The UV-vis spectra of copolymers 5a-c show the same transitions of compound 3 at 254 and 322 nm. Accordingly, the intensities values of these bands are directly proportional to the content of the C_{60} derivative in the copolymers (Figure 3.7d). It is interesting to note that in the UV-vis spectra of copolymers 5a-c, it is possible to observe a third band that increases with the C_{60} conjugated thiophene chains from 428 to 442 nm and overlaps with that at 428 nm.

3.4 Electrochemical thin films deposition and characterization

The characterization of electrochemical properties and electrodeposition of push-pull system was performed by CV and cronoamperometry.

Voltammetric techniques are a group of electro-analytical methodologies based on the evaluation of the current flowing on a working electrode immersed in a solution containing electroactive species depending on the potential applied to it. These are, therefore, methods of interest for the study of conductive polymers in which polymerization occurs precisely through redox phenomena. The schematic configuration of a voltammetric experiment is given in Figure 3.8.

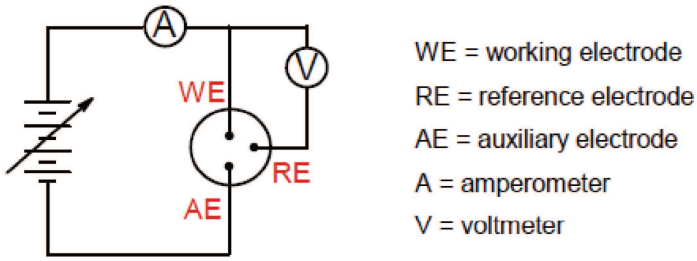

Figure 3.8. Schematic configuration of a voltammetric experiment.

In the cell, three electrodes are present. The electrode to which the reaction takes place is called the working electrode. The second electrode is the reference electrode, whose

potential is maintained constant during the experiment. The latter is the auxiliary electrode that simply serves to conduct the current to the working electrode through the solution.
The operating conditions adopted are such as to allow the electrolyte to be transported to the electrode only by diffusion: after the discharge process the solution near the electrode becomes less concentrated in an electroactive species than the rest of the solution and this gradient recalls spontaneously another analyte from the solution to the electrode. This phenomenon follows a physical law according to which the diffusion rate is directly proportional to the concentration gradient of the species that diffuses (Fick's Law). Some examples of potential scans and corresponding currents are given in Figure 3.9. Depending on voltammetry techniques, quantitative analysis or qualitative analysis, it can provide thermodynamic and kinetic information.

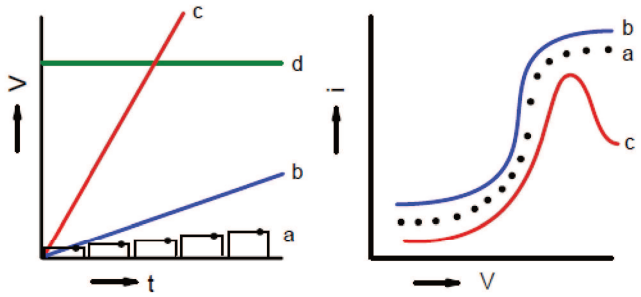

Figure 3.9. voltammetry with current sampling a), stationary voltammetry b), linear scanning voltammetry c) and chronoamperometry.

In voltammetry, both linear and cyclic, the electrode potential is varied over time in a linear way $E=E_i \pm vt$;
where v and the scanning speed, that is, the speed at which the potential of the working electrode is varied (always with respect to the potential of the reference).
In linear voltammetry, as shown in Figure 3.10a, there is a potential scan from an initial value at which no electrochemical process occurs, to the final result, which potential may remain fixed at that value or may return abruptly to the initial value.
In CV, the trend of the potential applied to the working electrode according to time, so as to induce the reduction and then oxidation (or *vice versa*) of the electroactive species, is represented by a characteristic triangular diagram (Figure 3.10a). Potential, from values in which no faradic current flows, is varied to reach the discharge potential; When passed this point, the scan polarity is inverted leaving the module unchanged. The working electrode is

thus exploited at first as an anode and, by inverting polarity, as a cathode (or vice versa, if you want to first reduce the electroactive species).

The result obtained is a current/voltage curve called the voltammogram (Figure 3.10b), whose morphology is due to the nature of the oxidation-reduction reactions on the electrode of the electro-active species present in solution, and therefore characteristic of each species.

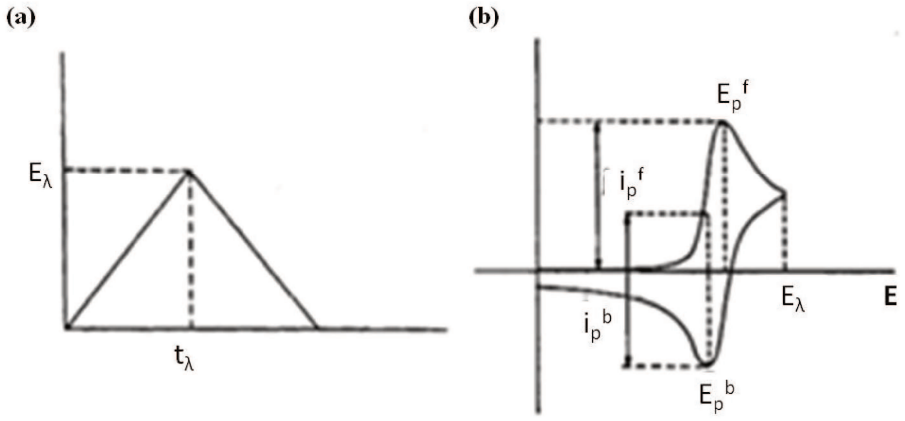

Figure 3.10. A triangular wave of potential in terms of a) time and b) voltammogram.

As can be seen in Figure 3.10b, which represents a typical voltammogram, once the potential applied is sufficient for the faradic process to occur, the current increases rapidly, passes for a maximum (corresponding to E_p^f) and subsequently decreases.

In the case where the electro-chemistry reaction is electrically reversible, by reversing the direction of the potential scanning, a return peak with a corresponding opposite signal current (relative to the potential E_p^b) is observed. In the case where the degree of reversibility is lower the return peak becomes less high, it moves away from the forward one and, in the case of complete irreversibility, tends to disappear.

For a non-subject reversible charge transfer and collateral chemical reactions, the peak current is given by the equation of Randles [5,6] and Sevcik [4] equation 3.1:

$$i_p = (2.69 \cdot 10^8) n^{3/2} A D^{1/2} v^{1/2} C^b \qquad (3.1)$$

where:

- A: area of the electrode surface;

- n: number of electrons exchanged in the redox process;
- D: diffusion coefficient of the electroactive species;
- v: potential scan speed;
- Cb: bulk concentration of the solution of the species concerned.

This report establishes that the peak current is directly proportional to the concentration of electro-active species in the bulk of the solution, an important quantitative information for analytical purposes.

Cyclic voltammetry also allows to distinguish electrodes in which the charge transfer is reversible from irreversible processes by means of an important parameter which is the scan rate and allows to verify whether the irreversibility is due to the electronic transfer process or rather to reactions collateral that consume the electro-active species. Such side-effects may be due to adsorption phenomena. There is the talk of non-specific adsorption when long-range electrostatic forces interfere with the distribution of ions near the electrode surface. Instead, it speaks of specific adsorption, when strong interactions between the species in solution and the electrode material occur.

Cyclic voltammetry of the compounds was recorded with the Potentiostat/Galvanostat (MetrohmAutolab PGSTAT 128N) in a three-electrode cell using (GC diameter = 3 mm, Bio-Logic SAS) as a working electrode, platinum as a counter electrode, and Ag/AgCl 3.5MKCl (Hanna Instruments) reference electrode respectively.

Electrodepositions were carried out under the following experimental three electrodes set-up which includes: a working electrode (ITO/PET 1.5*1.5 cm^2) where the reaction of interest takes place, a reference electrode whose potential was maintained constant by Ag/AgCl and a counter electrode(graphite), known as an auxiliary electrode, which is intended to ensure the current flow through the electrochemical cell.

Prior to each electrolysis, the ITO/PET electrodes were cleaned with methanol, acetone and propanol each for 10 minutes using an ultrasonic bath and subsequently subjected to UV-ozone cleaning for 30 minutes. All experiments were performed under nitrogen flow at a pressure of 0.5 bar and at room temperature.

- CV of NDI2ODT4-EDOT

Cyclic voltammetry of NDI2ODT4 and EDOT was carried out dissolving the monomers at 10^{-4} M concentration in an CH_3CN:CH_2Cl_2 solution (2:3; v:v) containing 10^{-2} M of $LiClO_4$

as support electrolyte. Following these experimental conditions, homopolymers and copolymer were synthesized.

Chronoamperometry is the simplest of the electro-analytical techniques at the interphase. To the working electrode immersed in a quiescent solution, thermostated and containing a support electrolyte (and therefore also in the diffusion mode), a potential is applied to which no faradic process occurs and, at a moment defined as zero, a step of such a potential to reach the discharge value that is then maintained for the duration of the analysis. It is, therefore, a potentiostatic technique. The current flow rate in response to the application of the discharge potential is recorded for a predetermined time interval during which the current chronoamperometric decay described by Cottrell law is observed in the current/time diagram [7] (equation 3.2):

$$i(t) = nFAD_0^{1/2} C_b \pi^{-1/2} t^{-1/2} \qquad (3.2)$$

where:

- n: number of exchanged electrons;
- F: constant of Faraday;
- A: area of the electronic surface;
- D0: diffusion coefficient of the active species;
- Cb: bulk concentration of the solution of the species concerned.

From the equation governing this technique, as is the case for voltammetry, a ratio of current with respect to the concentration of analyte in the body of the solution is shown, but unlike voltammetry the current trend also depends on the time of application of the potential of the solution, which is the ultimate responsible of the typical chronoamperometric decay.

- Chronoamperometry of NDI2ODT4- bis-Th2P-C_{60}

Electrodepositions of NDI2ODT4, bis-Th2P-C_{60} were performed by galvanostatic methods whose potential was maintained at 1.5 V constant. The three electrodes were immersed in an appropriate electrolytic solution comprising a solvent mixture chlorobenzene (C_6H_5Cl:CH_3CN (2:1 v:v)) and monomers at concentrations ranging from $2 \cdot 10^{-4}$ to $4 \cdot 10^{-4}$ M for the deposition of homopolymers and copolymer respectively. In the experiments, 0.1 M of tetrabutylammonium perchlorate ($TBAClO_4$) was added as support electrolyte.

After electrodeposition of the polymer, the modified working electrodes were washed with the solvents mixture employed in the synthesis in order to remove excess cations deriving from the electrolytic support and the monomer which is present in the solution used for the synthesis.

3.5. Experimental conditions thin films characterization

- XPS

Both electrodeposited polymers on ITO/PET substrates were investigated by XPS using a ULVAC-PHI PHI 5000 Versa Probe II Scanning XPS Microprobe™, source Al Kα (1486.6 eV), 128 channels hemispherical analyzer, FAT mode.

- Optical characterization

Uv-vis absorption and Fluorescence spectra were recorded on thin films electrodeposited and spin-coated onto ITO/PET substrates (Aldrich, surface resistivity 60 Ω sq^{-1}), using a Specord S 600 (Analytik Jena, Jena, Germany) and Fluoromax-4 (HORIBA JobinIvon, Edison, USA) spectrofluorometer equipped with a 150 W xenon arc lamp as the excitation source, respectively.

- DFT Computational modeling

The structural and electronic properties of the electrodeposited copolymer in this work have been performed by means of Density Functional Theory. The singlet-singlet adiabatic electronic transitions have been investigated by means of the time-dependent density functional approach (TDDFT) by using the Coulomb- Attenuating Method applied to the B3LYP exchange-correlation functional (CAM-B3LYP) joined with the correlation consistent polarized valence double zeta basis set (cc-pvzd). The calculation has been performed on the electronic ground state geometries, fully optimized at the same level of theory. All calculations have been performed by employing the Gaussian 09 package.

- Morphology characterization

Atomic Force Microscope (AFM) analysis has been performed using a Multimode 5 microscope joined with a Nanoscope V controller (Veeco, Germany) and a Bruker Dimension Icon. All images have been acquired by using commercial etched-silicon

probes (RTESP type tips; Bruker, Germany) and rastering 512 x 512 points per image, using a constant scan rate lesser than 1 line/s.
Electron Microscopy (SEM) studies have been performed using an FEI FEG-ESEM (mod. QUANTA 200) at different voltages and magnifications. Gold has been sputtered onto the samples before the morphological analysis.

- Electrical characterization

The electrical measurements have been performed by a Keithley 4200-SCS Parameter Analyzer, configured in the voltage sweep mode. The metal contact with the organic thin layers electrodeposited on ITO/PET substrate was realized with circular orifices through Polytetrafluoroethylene (PTFE) substrate filled with mercury (Hg). The Hg contact area was 0.05 cm2. The Hg potential was connected to the force connector of the Parameter Analyzer whereas the ITO was held to the ground potential.

- Electrochromic characterization

Electrochromic properties of electrodeposited polymers have been investigated by the simultaneous use of electrochemical techniques and optical techniques. The effect of the state of oxidation of thin films on their optical properties was investigated by recording the absorption spectra under different polarization voltages and using a two-electrode cell equipped with quartz windows. Modulation of optical properties was highlighted by subtending the films at a potential square wave and simultaneously recording the time-dependent transmission. These measurements have made it possible to calculate important parameters such as optical contrast and response times. Films deposited on ITO/PET transparent electrodes of 0.9 × 2.5 cm^2 size were used. All measurements were corrected for the absorption of the electrolyte solution and conducted at ambient conditions.

3.6. Electrochromic and solar cells device construction

- Electrochromic Device fabrication

Solid state electrochromic devices have been fabricated in a common sandwich configuration. Copolymers thin films electrodeposited on ITO/PET have been separated from ITO/PET counter electrodes by means of a transparent gel electrolyte. Support electrolyte and poly(methyl methacrylate) (PMMA; Mw:120,000 Sigma Aldrich) (0.7 g) have been dissolved in CH_3CN (7 g); propylene carbonate (2 g) has been added as a plasticizer. The obtained gel electrolyte has been spread onto the polymeric film and finally, the counter electrode has been added to the top.

- PET/ITO/electrodeposited polymer/P3HT/Al PHJ OSCs

To realize the Al/P3HT/electrodeposited polymer/ITO/PET PHJ OSCs, the electrodeposited polymers on ITO/PET (active area $2.5 \cdot 2.5 cm^2$) were transferred to a gloveboxes system (MBraun, Germany) in N_2 atmosphere (<0.1 ppm O_2 and H_2O) in order to deposit the layers of P3HT and Al in inert conditions. P3HT was solubilized in C_6H_5Cl (15 mg /mL) and deposited by spin coating at 1500 rpm with 500 rpm acceleration for 45 seconds. Al electrode, about 100 nm, was deposited by thermal evaporation at a speed of 15 $Å \cdot s^{-1}$.

- PET/ITO/P(EDOT): PSS- *i*-PrOH/electrodeposited polymer/P3HT/ PHJ OSCs

The realization of the ITO/P(EDOT):polystyrene sulfonate-isopropyl alcohol(PSS-*i*-PrOH) /electrodeposited polymer/P3HT/Al device was carried out as follows. The ITO/PET substrates were subjected to a cleaning treatment consisting of ultrasonic bath in different solvents, methanol, acetone and propanol for 20 minutes each, followed by surface cleaning by UV-ozone cleaner (Procleaner Plus, Bioforce) for 20 minutes. In each device, the first layer is realized by spin-coating of a solution containing P(EDOT):PSS (Sigma-Aldrich, 1.3 wt% dispersion in H_2O) and i-PrOH (50 wt%), deposited at 1500 rpm (with an acceleration of 500 rpm for 60 seconds) and then treated thermally at 100 ° C for 10 minutes to improve its crystallinity and thus its conductivity. The second layer is realized by the electrodeposition of polymer film on the P(EDOT):PSS electron transport layer (ETL). Finally, the P3HT and Al layers were deposited as described above.

- PET/ITO/P(EDOT): PSS/copolymer/ P3HT:PCBM /LiF/Al BHJ OSCs

OSCs were prepared by spin coating the copolymers on ITO/PET substrates cleaned sequentially by sonication in methanol, acetone, and isopropanol for 20 min each and exposed to UV-ozone cleaner (Procleaner Plus, Bioforce) for 60 min. The hole-transport material (~ 40 nm) (P(EDOT):PSS, Aldrich, 1.3 wt % dispersion in H_2O, conductive grade) was spin-coated 4000 rpm and dried at 100 °C for 10 min on a hot plate under air. The substrates were transferred in a gloveboxes system (MBraun, Germany) filled with N_2 (< 0.1 ppm of O_2 and H_2O), where heterojunctions were deposited. In particular, a blend solution (30 mg mL^{-1}) of P3HT:PCBM (1:0.8) in o-DCB with different copolymers was stirred, filtered through a 0.45μm filter, and subsequently spin-coated at 1500 rpm (~ 110 nm) on the ITO/P(EDOT):PSS layer. In the gloveboxes, 1 nm LiF layer and 100 nm Al were thermally evaporated to complete the fabrication of the devices. Thermal processes for device annealing and aging processes have been performed within the gloveboxes.

Electrical measurements

Devices have been characterized using a halogen lamp as a source of illumination with a radiant power of 100 mW /cm^2. The J-V curves were acquired in a glovebox system (MBraun, Germany) filled with N_2 (<0.1 ppm of O_2 and H_2O), by using a Keithley 2400 source meter.

References

[1] V. Figà, C. Chiappara, F. Ferrante, M. P. Casaletto, F. Principato, S. Cataldo, Z. Chen, H. Usta, A. Facchetti, B. Pignataro, *J. Mater. Chem. C* **2015**, *3*, 5985.

[2] S.-G. Liu, C. Martineau, J.-M. Raimundo, J. Roncali, L. Echegoyen, **2001**, 0, 913-914.

[3] B. Barszcz, B. Laskowska, A. Graja, E. Y. Park, T.-D. Kim, K.-S. Lee, *Chem. Phys. Lett.* **2009**, *479*, 224.

[4] A. Ševčík, *Collect. Czechoslov. Chem. Commun.* **1948**, *13*, 349.

[5] J. E. B. Randles, *Trans. Faraday Soc.* **1948**, *44*, 327.

[6] J. E. B. Randles, *Trans. Faraday Soc.* **1948**, *44*, 322.

[7] A. J. Bard, L. R. Faulkner, *Electrochemical Methods : Fundamentals and Applications*, Wiley, **2001**.

4. Results and Discussion

4.1. Push-pull copolymers and electrochromic devices

4.1.1. Electrodeposition of push-pull system

Before electropolymerization, it was necessary to carry out preliminary experiments in order to know the onset oxidation potential (Eox) along with the co-polymerization availability of the monomers. For the reasons mentioned in Chapter 3.1 it was possible to conclude that NDI2ODT2 did not electropolymerize under several conditions studied, whereas, NDI2ODT4 alone or in the presence of EDOT efficiently formed a solid thin film on the electrode. To do so, linear sweep potential (LSV) was performed to obtain the oxidation initiation of the NDI2ODT4 and EDOT monomers, while oxidation and reduction cyclovoltammetry were acquired for NDI2ODT4 and bis-Th2P-C_{60} monomers, which allowed us to obtain information on both oxidation potential onset and behavior of electrochemical monomers.

Figure 4.1 represents studies of the onset oxidation potential of the monomers by LSV by dissolving 10^{-4} M NDI2ODT4 and 10^{-4} M EDOT in a CH_2Cl_2:CH_3CN (3:2; v:v) electrolyte solution and containing 10^{-2} M $LiClO_4$ at 50 mV·s^{-1}.

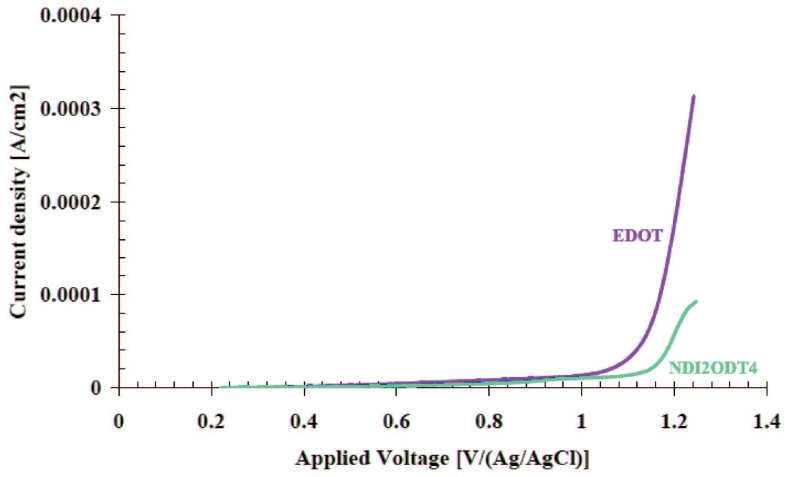

Figure 4.1. LSV of 10^{-4}M NDI2ODT4 and 10^{-4} M EDOT, recorded in CH_2Cl_2:CH_3CN (3:2; v:v) containing 10^{-2} M $LiClO_4$ at 50 mV·s^{-1}. Adapted from [1].

Onset oxidation potential processes derived from LSV shown in Figure 4.1 for both the monomer systems resulted in potentials greater than 1.1V vs Ag/AgCl. The contiguousness of NDI2ODT4 and EDOT oxidation potential onsets suggests the possibility of their copolymerization [2].

In order to optimize polymerization conditions three NDI2ODT4:EDOT molar ratios have been used with the aim to obtain the following copolymers on ITO/PET by cyclovoltammetry: **copol[1]** (10:1), **copol[2]** (1:1), **copol[3]** (1:10) (Scheme 4.1).

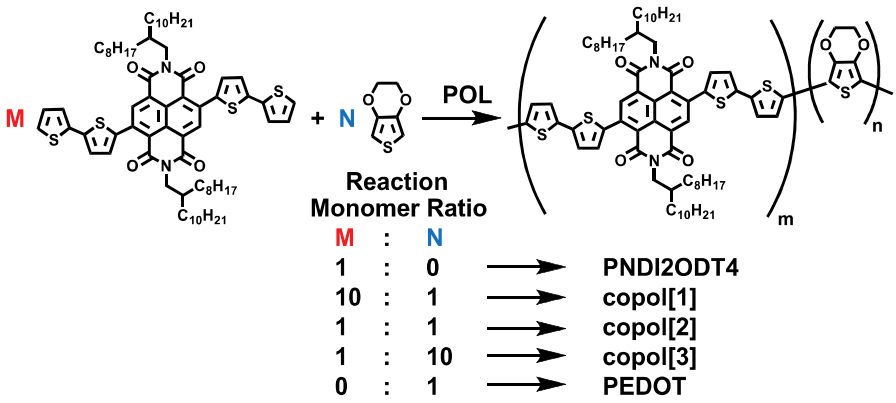

Scheme 4.1. Chemical structure of the NDI2OT4:EDOT electropolymerized copolymers. M and N are the monomer loading ratios, while m and n are the number of incorporated NDI2OT4 and EDOT units in the polymeric structure, respectively. Adapted from [1].

Figures 4.2-4.4 shows CV respectively for NDI2ODT4, EDOT and NDI2ODT4-EDOT (1:1) registered in CH_3CN:CH_2Cl_2 solution (2:3; v:v) containing 10^{-2} M of $LiClO_4$ and 10^{-4} M of the monomer at a potential scan rate of 50 mV/s. For all the systems, the electrode potential has been increased from the open circuit value to +1.3V and reversed to the open circuit value for several cycles.

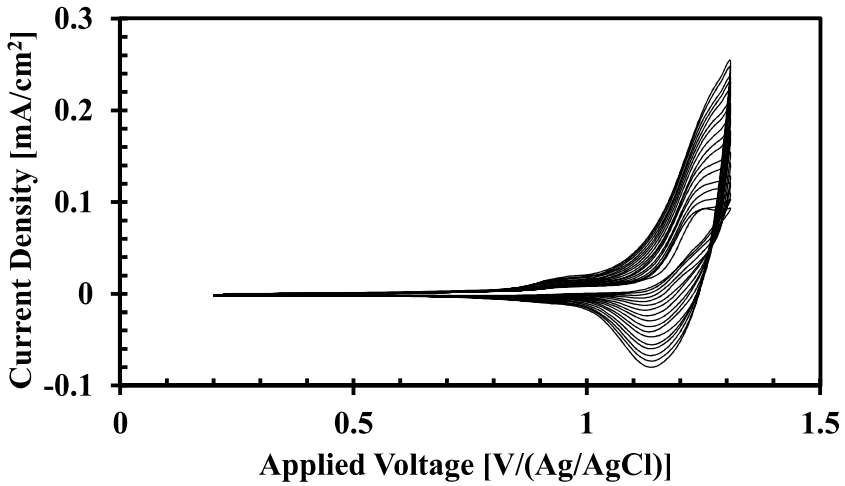

Figure 4.2. Cyclic voltammetry of a 10^{-4} M CH_3CN:CH_2Cl_2 solution (2:3; v:v) of NDI2ODT4 containing 10^{-2} M of $LiClO_4$. Adapted from[1].

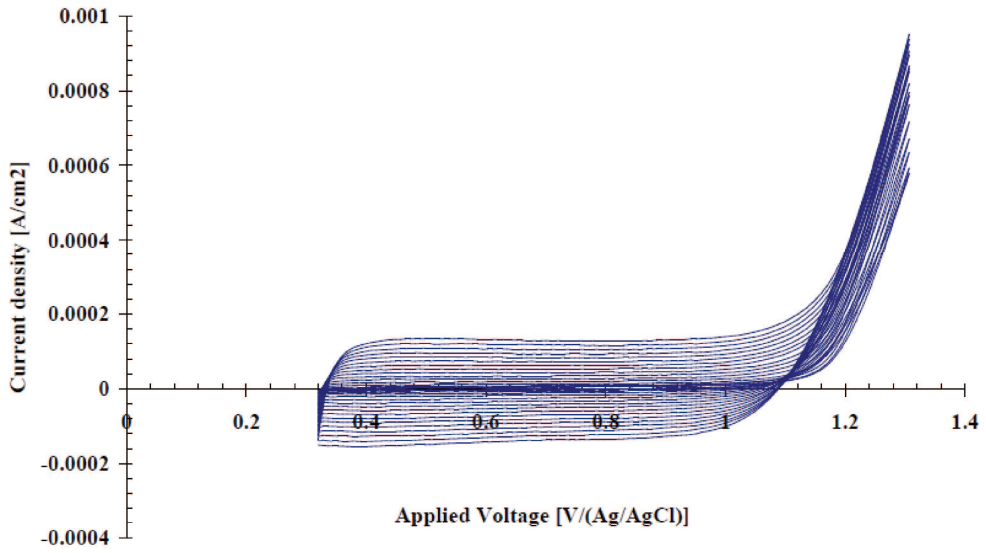

Figure 4.3.Cyclic voltammetry of a 10^{-4} M CH_3CN:CH_2Cl_2 solution (2:3; v:v) of EDOT containing 10^{-2} M of $LiClO_4$. Adapted from [1].

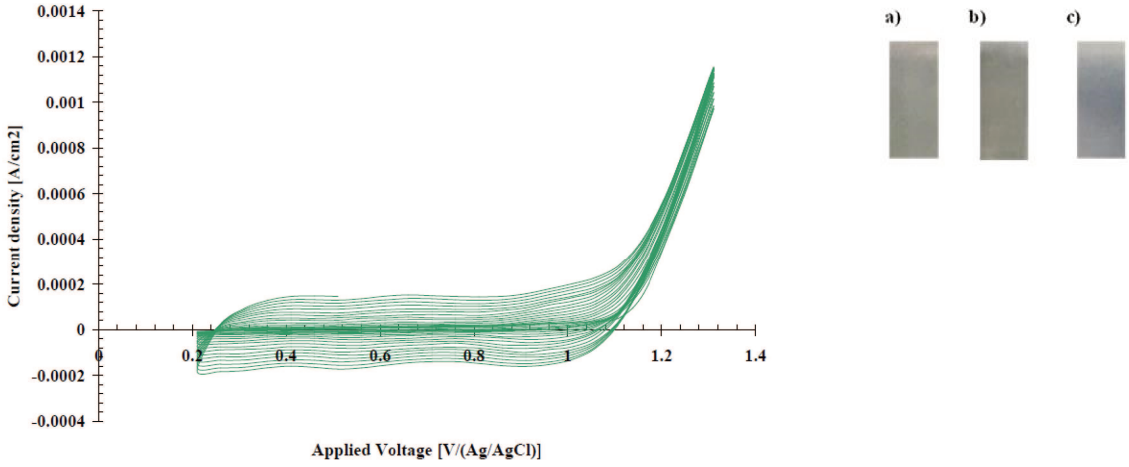

Figure 4.4. Cyclic voltammetry of a **copol[2].** Adapted from [1]. Polymeric films of (a) P(NDI2ODT4), b) P(EDOT) and c) co(NDI2ODT4-EDOT) on ITO/PET.

The first cycle of NDI2ODT4 CV presents an oxidation potential onset of +1.15 V that indicates the potential at which the monomer starts to be oxidized. The current reaches a peak value at +1.24 V. The oxidation onset lowered with the number of cycles suggesting that the previously formed oligomers are easier to oxidize than the monomer. The increase in the number of cycles is also accompanied by an increase in current indicating the film thickening on the electrode surface.

Cyclovoltammetry curve shapes differ when comparing the polymerization of NDI2ODT4 (Figure 4.2) or EDOT (Figure 4.3) to that of (NDI2ODT4)m-(EDOT)n copolymer (Figure

4.4). This result suggests successful copolymerizations and incorporation of both monomers. In particular, in the NDI2ODT4 system an oxidation onset at 1.17 V and an oxidation peak at 1.23 V were observed (potentials referred to Ag/AgCl 3.5 M), whereas in EDOT rich systems different curve shapes along with different open circuit voltages and no oxidation peaks are found.

Similarly to what previously was shown for NDI2ODT4-EDOT, it was necessary to investigate the electrochemical behavior of NDI2ODT4 and bis-Th2P-C_{60} monomers, in order to electropolymerize the new bis-fulleropyrrolidine(bis-Th2P-C_{60}) system with NDI2ODT4. In particular, the electrochemical behavior of monomers was analyzed by means of CV measurements obtained on GC electrode in C_6H_5Cl:CH_3CN (2:1 v:v) solutions containing 0.1M $TBAClO_4$ at monomers concentrations of $4 \cdot 10^{-4}$ M and reported in Figure 4.5.

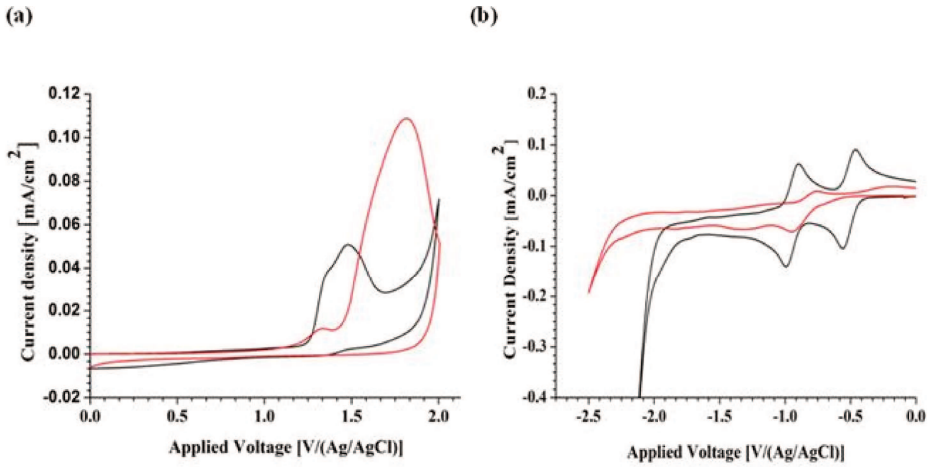

Figure 4.5. a) oxidation scan and b) reduction scan CV of NDI2ODT4 (black), bis-Th2P-C_{60} (red) respectively.

As shown in the Figure 4.5a, the oxidation scan was attributed to the oxidation of the polythiophene chains for both monomers. In the scan registered in the reduction potential range (Figure 4.5b), as far as NDI2ODT4 is concerned, the peaks correspond to the reduction of NDI units [3] while for bis-Th2P-C_{60} the four reduction reactions are typical of the fullerene C_{60} derivatives [4] respectively. Since the bis-Th2P-C_{60} is a mixture of bisadducts, the reduced CV has undefined and non-reversible C_{60} waves as opposed to monoadduct where the four reductions are well defined in C_{60} [5]. As can be seen from the Table 4.1, the small difference between the onset potential of the two monomers (1.2 eV

NDI2ODT4 and 1.1 eV bis-Th2P-C_{60}) suggests a high probability of copolymerization between them [2]. The electrochemical parameters are derived from the cyclovoltammetry in Figure 4.5 and are shown in Table 4.1.

Table 4.1: Electrochemical parameters derived from the cyclovoltammetry: GC working electrode; Ag/Ag+ reference electrode; Pt counter electrode; 0.1M $TBAClO_4$; scan rate: 200 mV/s ; concentrations:$1 \cdot 10^{-3}$ M.

monomers	E_{onset}	E^1_{ox}	E^2_{ox}	E^1_{red}	E^2_{red}	E^3_{red}	E^4_{red}
P(NDI2ODT4)	1.2	1.3	1.5	-0.5	-1	-	-
bis-Th2P-C_{60}	1.1	1.3	1.8	-0.9	-1.4	-1.8	-2.2

Furthermore, as evident from Figure 4.6a, cyclic voltammetry of the bis-Th2P-C_{60} in the oxidation potential range led to the formation of an irreversible peak at about +1.3 V and the strong suppression of the current indicating that the oxidation product passivated the electrode surface. Although no visible film was formed on the electrode, the oxidized monomers probably undergo the coupling with the formation of low soluble non-conducting bithiophene dimers which cover the electrode and passivate the surface. Therefore, cyclovoltammetry is not an optimal deposition technique for bis-Th2P-C_{60}.
Conversely, oxidation of NDI2ODT4 (Figure 4.5a) starts at more positive potentials that of bis-Th2P-C_{60}, at about 1.2 V vs.Ag/AgCl. Both, the loop formed in the cyclic voltammogram in the backward scan and appearance of a broad reduction wave were indicative for deposition of the polymer on the electrode by chronoamperometry in C_6H_5Cl-CH_3CN solvents, which is correlated with the findings on the optimal polymerization conditions for NDI2ODT4 deposited in CH_3CN-CH_2Cl_2 by cyclic voltammetry discussed above. In order to provide simultaneous oxidation of both monomers to form a copolymer, the galvanostatic technique is used, i.e. polarizing the ITO/PET substrates at a constant potential of 1.5 V vs Ag/AgCl for a time necessary for obtaining uniform film on the electrode. The chronoamperometric curves of deposition are shown in Figure 4.6. Obtained data were used to estimate the polymerization charge density (Q, mC/cm^2) by the integration of the corresponding chronoamperograms. It was possible to determine that electrodeposition charges of 1.23 mC, 1.54 mC, and 3 mC, were suitable for reproducible coverage of the working electrodes with thin films of P(NDI2ODT4), P(bis-Th2P-C_{60}) and co(NDI2ODT4- bis-Th2P-C_{60}) respectively (Figure 4.6b).

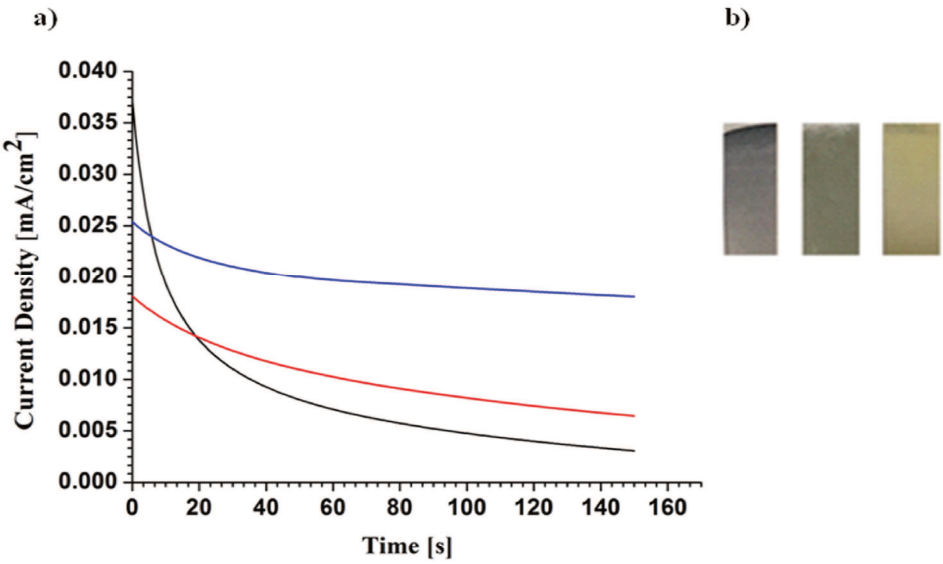

Figure 4.6. a) Deposition chronoamperometric curves: P(NDI2ODT4) (black), P(bis-Th2P-C_{60}) (red) and co(NDI2ODT4- bis-Th2P-C_{60}) (blue), b) Polymeric films on ITO/PET: grey, brown and yellow respectively.

As derived from the estimated electrodeposition charges and the chronoamperometric curves of polymer film deposition presented in Figure 4.6, the curve obtained for a copolymer is a sum of the polymerization curves of the two homopolymers.

Assuming that the polymerization follows the following equation:

$$M + E \longrightarrow P$$

where M is the monomer, E is the electrolyte and P is the polymer, then the kinetic equation can be formulated as equation 3.3:

$$Rp = d[W]/dt = k\,[E]^a[M]^b \qquad (3.3)$$

where Rp is the polymerization rate which represents the electrogenerated polymer weight, W, per unit time, per cm^2 of the electrode surface, and a and b are respectively the reaction orders with respect to the electrolyte and monomer, and k is the specific rate constant of the polymerization process. Since the electrolyte is in excess of the monomer concentration, the charge consumed and produced during the electropolymerization process depends on the monomer M, so that the produced charge Q should be proportional to the weight of the electrogenerated polymer: $Q = kW$ [5–8]. Thus, it is possible to approximate the ratio between charges deposited between the two homopolymers with the molar ratio of the two in the copolymer. The molar ratio corresponds to 4:5 P(NDI2ODT4)- P(bis-Th2P-C_{60}).

4.1.2. Thin films characterization

- XPS characterization

P(NDI2ODT4), P(EDOT) homopolymer and $(NDI2ODT4)_m$-$(EDOT)_n$ copolymer thin films were chemically characterized by XPS investigation (Figure 4.8) in order to experimentally confirm the formation of copolymer systems on ITO/PET substrates. Remarkably, XPS allows for the evaluation of the composition of the copolymers obtained by varying the molar ratio of P(NDI2ODT4) and P(EDOT) in the film.

Figure 4.7a reports the XPS C1s spectra of the different electropolymerized thin films, respectively a) P(NDI2ODT4); b) P(EDOT); c) **copol [2]**; d) **copol [1]** and e) **copol [3]**.

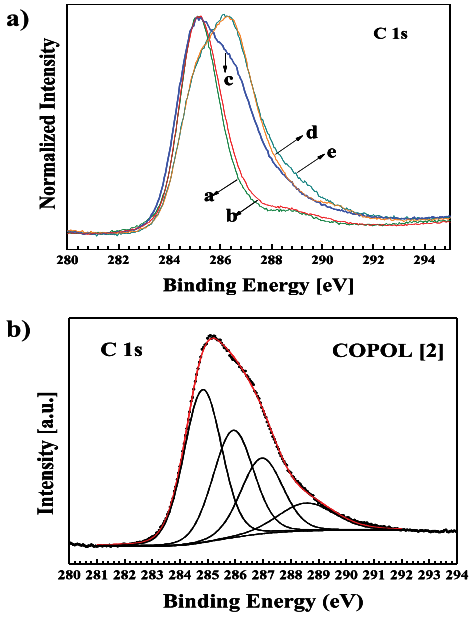

Figure 4.7.a) Normalized C1s XPS spectra of the electropolymerized thin films: a) P(NDI2ODT4); b) P(EDOT); c) **copol [2]**; d) **copol [1]** and e) **copol [3]**. b) XPS curve-fitting of the C 1s photoelectron spectrum of the **copol [2]** thin film. Adapted from[1].

The C1s peak shape of the **copol[1]** and **copol[3]** copolymers closely resemble those of predominant P(NDI2ODT4) and P(EDOT), respectively. The C1s peak of **copol[2]** copolymer appears different because it is located in-between the two homopolymers. In particular, the C 1s peak is a convolution of four main different components, as reported in Figure 4.8b.

In Table 4.2 XPS surface chemical quantitative analysis of the electropolymerized thin films is reported.

Table 4.2. XPS surface chemical quantitative analysis of the electropolymerized thin films. Elemental composition is expressed as an atomic percentage. Adapted from [1].

SAMPLE	C1s	O1s	N1s	S2p	In3d	Sn3d
P(NDI2ODT4)	70.5	18.4	2.0	3.1	5.3	0.7
COPOL [1]	81.9	11.0	1.9	4.7	0.4	-
COPOL [2]	67.3	23.4	1.4	7.1	0.7	-
COPOL [3]	68.6	23.8	0.8	6.5	0.3	-
P(EDOT)	58.4	33.4	-	7.8	0.4	-

By considering the surface C/S and N/S atomic percentage ratios (see Table 4.2), it is possible to evaluate the actual monomer incorporation in the $(NDI2ODT4)_m$-$(EDOT)_n$ copolymers as a function of the monomer concentration ratios employed for the electropolymerization (Scheme 4.1). Furthermore, In and Sn peaks were ascribed to the presence of ITO substrate, i.e. the working electrode onto which thin films were deposited. Remarkably, no XPS signal due to the supporting electrolyte (i.e. chloride peak) was observed.

The same XPS measurements were carried out on P(NDI2ODT4), P(bis-Th2P-C_{60}) and co(NDI2ODT4-bis-Th2P-C_{60}) thin films in order to assess the composition of polymeric systems on the ITO/PET substrates. In Table 4.3 atomic composition values derived from the XPS surface chemical quantitative analysis of the electropolymerized thin films are reported.

Table 4.3. XPS surface chemical quantitative analysis of the electropolymerized thin films. Elemental composition is expressed as at% (atomic percentage).

SAMPLE	C1s	O1s	N1s	S2p	Cl2p
P(NDI2ODT4)	83.3	10.8	2.1	3.7	0.1
P(bis-Th2P-C_{60})	80.7	13.6	1.7	2.4	1.5
co(P(NDI2ODT4)-bis-Th2P-C_{60})	85.3	7.6	2.5	4.1	-

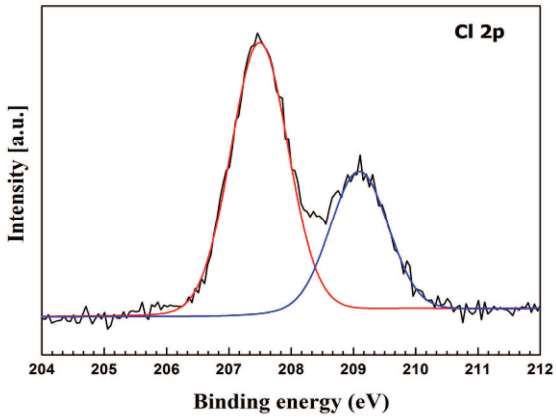

Figure 4.8. XPS curve-fitting of the Cl 2p photoelectron spectrum of the P(NDI2ODT4) electropolymerized from C_6H_5Cl:CH_3CN via chronoamperometry.

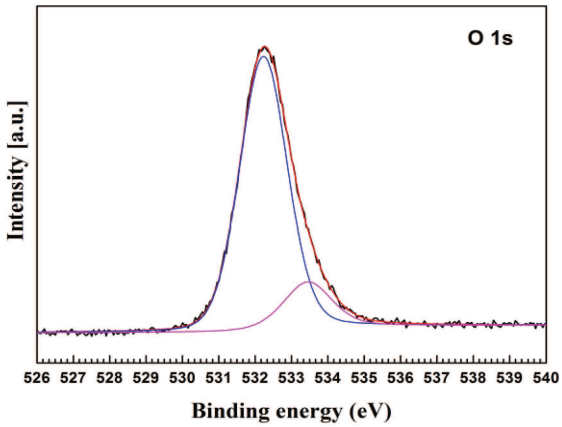

Figure 4.9. XPS curve-fitting of the O 1s photoelectron spectrum of the PNDI2ODT4 electropolymerized from C_6H_5Cl:CH_3CN via chronoamperometry.

It is worth noticing that both polymers, P(NDI2ODT4) (Fig. 4.8 and 4.9) and P(bis-Th2P-C_{60}), contain a single Cl species, (in Cl 2p spectra, a $2p_{3/2}$ / $2p_{1/2}$ doublet at 207.0 and 209.0 eV respectively), and two O species (O 1s spectra show two different species at 532.0 and 533.0 eV respectively). The presence of chlorine and oxygen in these samples can be attributed to the ClO_4^- counter-ion used during electrochemical copolymerization, which causes a strong excess of oxygen [9]. This could be tentatively ascribed to the electrochemical method for the synthesis of the polymer on the ITO, i.e. chronoamperometry, which imposes a certain voltage bias onto the working electrode, eventually determining residual charges due to the supporting electrolyte in the deposited material.

Moreover, In and Sn presence was not observed for NDI2ODT4-bis-Th2P-C_{60} films polymerized in mixture of CH_3CN-CH_6Cl_5-$TBAClO_4$, indicating a better surface coverage of ITO substrate (the working electrode on which thin films are deposited) with respect to NDI2ODT4-EDOT polymerization from CH_3CN-CH_2Cl_2-$LiClO_4$ mixture. The distribution of carbon species in as-deposited thin films is shown in Fig. 4.10 and expressed as peak area percentage in Table 4.4.

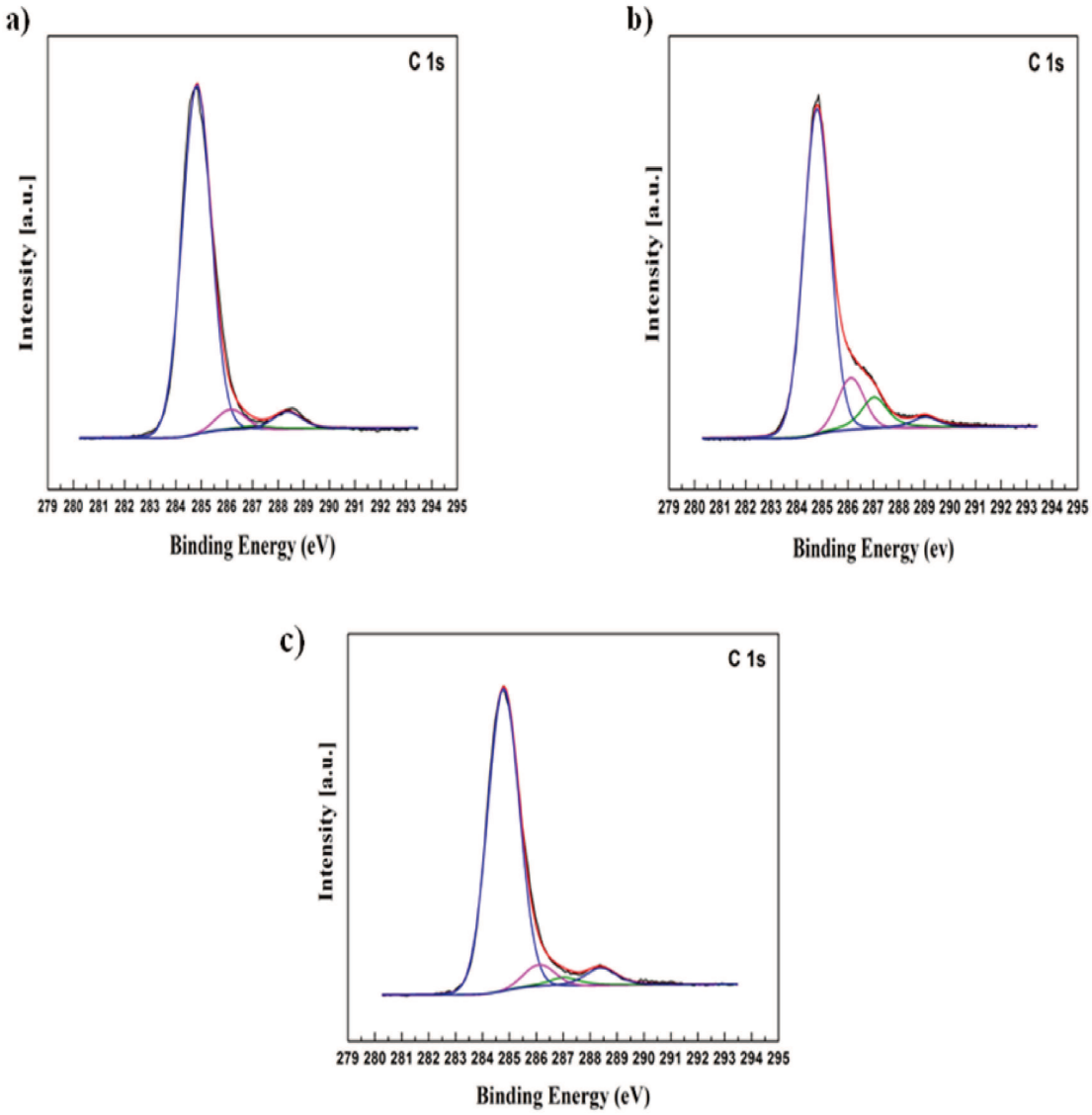

Figure 4.10. XPS curve-fitting of the C 1s photoelectron spectrum of the a) P((NDI2ODT4); b) P(bis-Th2P-C_{60}); c) co(NDI2ODT4-bis-Th2P-C_{60}) thin films respectively.

Table 4.4: Distribution of carbon species is expressed as peak area percentage of the electrodeposited polymer.

SAMPLE	C-C	C-S	C-N	C=O
Bending Energy(eV)	284.80	286.10	287.1	288.6
P(NDI2ODT4)	88.74	5.10	1.27	4.89
P(bis-Th2P-C_{60})	75.32	12.14	7.32	3.44
co(NDI2ODT4-bis-Th2P-C_{60})	84.61	6.06	3.31	6.03

It is possible to estimate the combination ratio of NDI2ODT4 and bis-Th2P-C_{60} in the copolymer by confronting the total transferred charge during the deposition.
Using two separate depositions of 150 s, with monomers in 10^{-4} M concentration with supporting electrolyte, $TBACLO_4$, 0.1 M, a 4:5 ratio was observed for P(NDI2ODT4):bis-Th2P-C_{60} combination ratio. Such a result is compatible with XPS findings.

- Electronic and optical proprieties

In order to investigate the nature of the electronic transitions in the systems which are of interest for this thesis, molecular models comprising NDI2ODT4-EDOT and s-NDI2ODT4-bis-Th2P-C_{60} molecular system were subjected to full geometry optimization and TDDFT calculations.
The computed molecular geometries are qualitatively similar to those known for analogous species, such as the P(NDI2OD-T*) series [10–12]: the NDI moiety and the bonded thiophene-derivative chain lie in planes tilted by approximately 50°; this strongly diminishes electron conjugation throughout the polymer chain. In particular, the transition at a lower energy in the investigated structures has a charge-transfer (CT) nature, with electron density migrating from the π-system of the EDOT chain to the π-system of NDI2ODT4. The HOMO and the LUMO are the molecular orbitals most largely involved in this CT transition, but in the larger systems several other quasi-degenerate orbitals can be observed with sensible weights.It is interesting to note that when the orbital conjugation in P(EDOT) is interrupted by NDI2ODT4 units, the CT transition shifts to higher wavelength (Fig. 4.11a).

In order to confirm the above, the optical properties of both homopolymers and copolymer have been investigated. In this regard, the UV-Vis absorption spectra of P(NDI2ODT4) and P(EDOT) homopolymers **copol[1]**, **copol[2]** and **copol[3]** were registered and reported in Figure 4.11b.

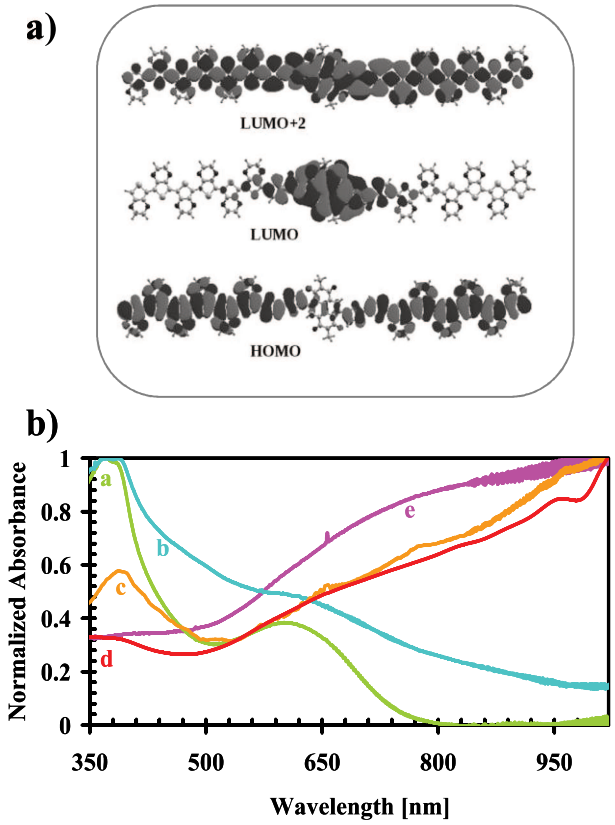

Figure 4.11. a) DFT computations of $(EDOT)_6$-P(NDI2ODT4-$(EDOT)_6$ showing selected MO topologies. b) Optical absorption spectra of: P(NDI2ODT4)(a), **copol [1]** (b), **copol [2]** (c), **copol [3]** (d) and P(EDOT) (e). Adapted from [1].

The UV-visible spectra of P(NDI2ODT4) show two transition bands: according to DFT characterization, the high energy band (350-450 nm) have been attributed to excited states more localized on thiophene units ($\pi \rightarrow \pi*$ transition), whereas the low energy band (550-800 nm) have been assigned to an intramolecular charge transfer transition[1]. By considering the P(NDI2ODT4) homopolymer and copol[2], it is clearly visible a red shift of the CT transition band as well as a spectral absorption up to the near IR region as an indication that by adding EDOT units to NDI2ODT4.

In order to investigate the effect caused by bis-Th2P-C_{60} in the polymer chain on optical properties of NDI2ODT4, UV-vis absorption spectra were recorded on thin films electrodeposited onto ITO/PET substrates (Figure 4.12).

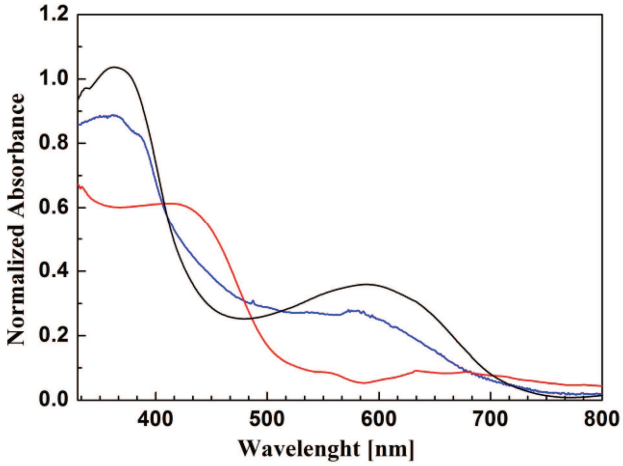

Figure 4.12. Comparison of absorption spectra of electrodeposited polymer films of P(bis-Th2P-C_{60}) red, P(NDI2ODT4) black and co(NDI2ODT4- bis-Th2P-C_{60}) blue on ITO/PET.

The spectrum showed in Figure 4.12 shows two transition bands a high-energy band 350-450 nm and band 550-800 nm features of the P(NDI2ODT4) system. The spectrum of P(bis-Th2P-C_{60}) shows a 430 nm band due to thiophenic conjugation in the polymer while the inclusion of bis-Th2P-C_{60} in the polymer chain of NDI2ODT4 caused a UV-vis shift of the transfer charge CT band of P(NDI2ODT4) to lower wavelengths [13].

Molecular models of NDI2ODT4-bis-Th2P-C_{60} molecular system were also subjected to geometry optimization and subsequent TDDFT calculations (Figure 4.13).

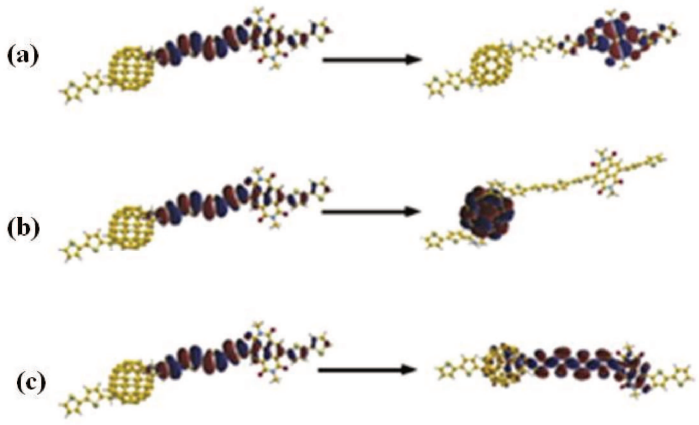

Figure 4.13. Electronic transitions between molecular orbitals HOMO and LUMO in the NDI2ODT4- bis-Th2P-C_{60} molecular system.

The DFT data show three transitions:

- 486nm: Transmission (CT) from thiophene chains to NDI macrocycle (a);
- 371nm: CT transition from thiophenic chain to fullerene(b);
- 366nm: transition π → π * localized on the thiophene chains combined with a CT transition from thiophene chain to fullerene (b+c).

HOMO is localized on thiophenic chains, LUMO in NDI macrocycle, LUMO+1 on fullerene, while LUMO +4 on thiophenic chains. The inclusion of bis-Th2P-C_{60} in the polymer of NDI2ODT4 causes a decrease in the angle between the two central moieties of the thiophene chain (160 degrees compared to 180 degrees in the P(NDI2ODT4)). This distortion decreases the HOMO energy (which in the copolymer has an antibonding character between the two central thiophenic groups) and consequently shift the CT transitions from the 501 nm calculated for P(NDI2ODT4) at 486 nm.

4.1.3. Modulation and control of optoelectronic properties

For the estimation of the optical contrast and response time, we applied square wave potentials (SWP) on homopolymers and copolymers thin films electrodeposited onto transparent ITO/PET electrodes (2.4 cm^2) and transmittance vs time curves recorded at suitable wavelengths. The best conditions (potential and λ_{max}) were identified by recording the absorption spectra of the films at different polarization potentials.

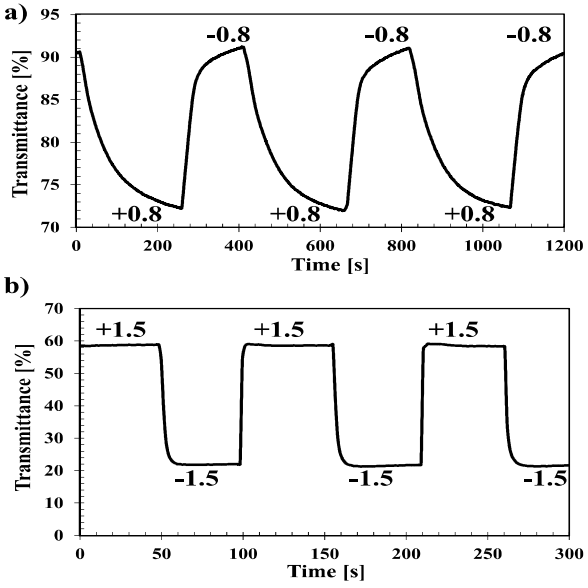

Figure 4.14. Transmittance vs time plots in CH_3CN (0.1 M $LiClO_4$) for a) P(NDI2ODT4) thin films at 900 nm and b) **copol[2]** thin films at 580 nm. Adapted from [1].

It has been seen that P(NDI2ODT4) polymer displays the highest ΔT of 19% between +0.8V and -0.8V and at 900 nm (Figure 4.15a). It appears green in the neutral and oxidized (+0.8V) state while brown in the reduced (-0.8V) state, respectively. By considering the electrochemical charge required for a complete switching and the optical density at 900 nm, it was possible to calculate a coloration efficiency of 302 cm^2C^{-1}. Another **copol[2]** exhibits an optical contrast up to 37% at 580 nm and response times of 13 (ox→red) and 15 (red→ox) seconds (Figure 4.15b) under a square wave potential between +1.5V and -1.5V (Table 4.5).

Table 4.5: Summary of the electrochemical and optical data for the different electropolymerized thin films. Adapted from [1].

POLYMER	Oxidation Onset[V]	λ_{max} [nm]	Eg,opt[eV]	Response time [sec]	ΔT [%]
P(NDI2ODT4)	**1.15**	**370**	**1.71**	**108 o→r 35 r→o**	**19**
Copol[1]	**1.15**	**370**	**1.50**	**50 o→r 20 r→o**	**20**
Copol[2]	**1.50**	**390**	**1.15**	**13 o→r 15 r→o**	**37**
Copol[3]	**1.50**	_	_	**10 o→r 13 r→o**	**30**
P(EDOT)	**0.95**	_	_	**12 o→r 10 r→o**	**34**

For these experiments, it is important to point out that in the case of thin films containing P(bis-Th2P-C_{60}), electrochromic properties are not found, as evident from the the absorption spectra (Figure 4.15) in which absorbance is plotted as function of the wavelength of the P(NDI2ODT4), P(bis-Th2P-C_{60}) and the co(NDI2ODT4)-bis-Th2P-C_{60}) by varying the cell voltage from + 0.8V to -2.0V, then subjecting the film to oxidation and reduction.

The optical properties of P(NDI2ODT4) are modified with the voltage applied to the polymeric film. It is possible to observe the maximum variation of absorption by passing from cathodic to anodic potentials at 430 and 900nm. In the case of P(bis-Th2P-C_{60}), a decrease in the peak intensity is observed. At -2V the peak at 430 nm disappears

altogether. This is due to the instability of the polymer as it is subjected to negative polarization stresses.

On the contrary, the copolymer shows a certain degree of variation of the absorption spectrum with the applied potential. Specifically, polarizing from the anode to the cathodic direction, a shift of peak absorption to lower energies is observed. This effect is called bathochromic effect. In addition, as cathodic potential increases, new bands such as 470 nm and the disappearance of others at 370 nm and 600 nm are noted, respectively.

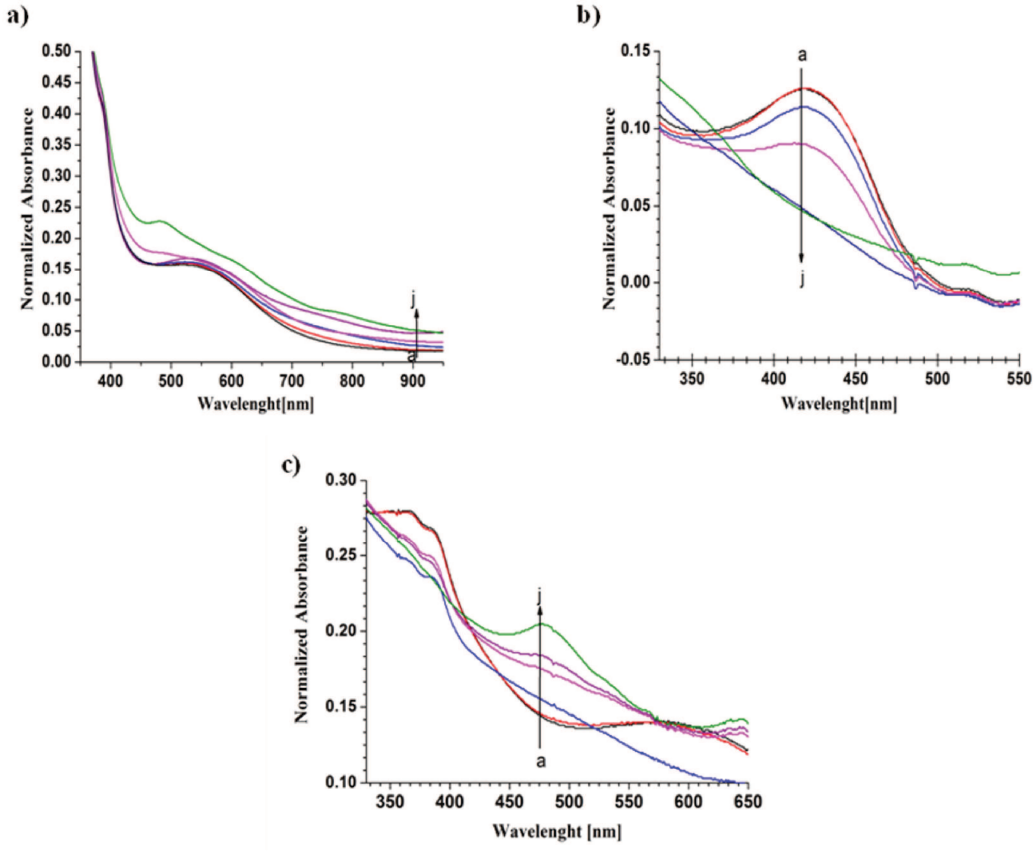

Figure 4.15. Absorption spectra of a) P(NDI2ODT4) at applied potentials (a) 0.8 V at (j) -0.8V vs Ag wire b) P(bis-Th2P-C_{60}) and c) *co*(NDI2ODT-bis-Th2P-C_{60}) at applied potentials (a) 2 V at j) -2V vs Ag wire.

The Transmission-time spectrum is registered a 900 nm applying an anode potential ±0.8V for 200 second and a cathodic potential for 200 sec on P(NDI2ODT4), while for copolymer a 430 nm and applying ±2V for 150 seconds, respectively (Figure 4.16).

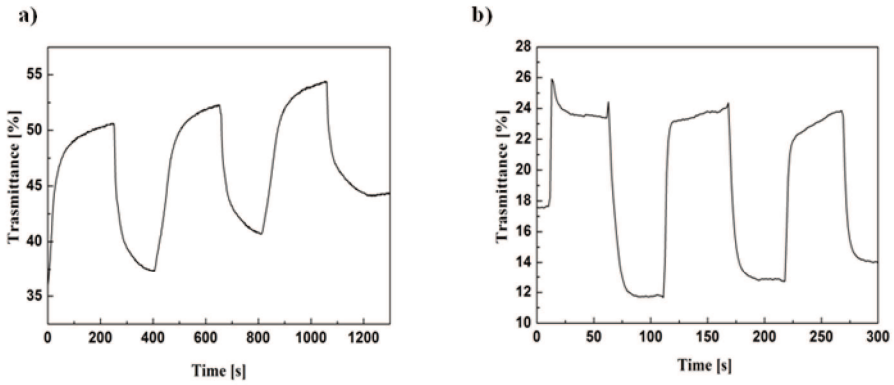

Figure 4.16. The transmission-time spectrum of the P(NDI2ODT4) recorded at 900 nm by applying an anode potential of 0.8V for 200 sec and a cathodic potential of -0.8V for 200sec a). The transmission-time spectrum of the *co*(NDI2ODT4- bis-Th2P-C_{60}) recorded at 470 nm by applying an anode potential of 2V for 150 sec and a cathodic potential of -2V for 150 sec.

As can be seen in Fig. 4.16, ΔT of P(NDI2ODT4) is 15%, compared to the previously demonstrated 20%. The variation of T vs time is also less stable, which is likely due to the fact that the polymer was electrodeposited under different experimental conditions, in a different electrolytic solution, finally causing variations chemical-physical properties of the film. The copolymer shows a variation of the transmittance with the potential applied due to a chromatic variation between the polymer in oxidized and reduced state (from brown to red).The copolymer displays a small optical contrast of 13% between +2V and -2V and at 470 nm (Figure 4.16b); remarkably, it displays high stability in the explored time and potential ranges. By copolymerization, the P(bis-Th2P-C_{60}) acquires novel optoelectronic properties which it would not present itself.

4.1.4. Electrochromic devices

The copolymers with the best electrochromic performances, i.e. of NDI2ODT4-EDOT systems, were employed to fabricate a solid-state electrochromic devices (ECD). In this regard, **copol[2]** and **copol[3]** electrodeposited onto ITO/PET electrodes were sandwiched with a second ITO/PET electrode using a (PMMA)-based gel electrolyte (Figure 4.17). Onto these devices, a square wave potential between ±1.5V was applied and the transmittance vs time plots were recorded by irradiating at 580 nm and 588 nm, respectively. **Copol[2]** (Figure 4.17b) and **copol[3]** based ECDs showed an optical contrasts of 22% and 29%, respectively. On the other side, the solid-state electrochromic devices (ECD) of NDI2ODT4-bis-Th2P-C_{60} copolymer systems showed an optical contrast of 6%.

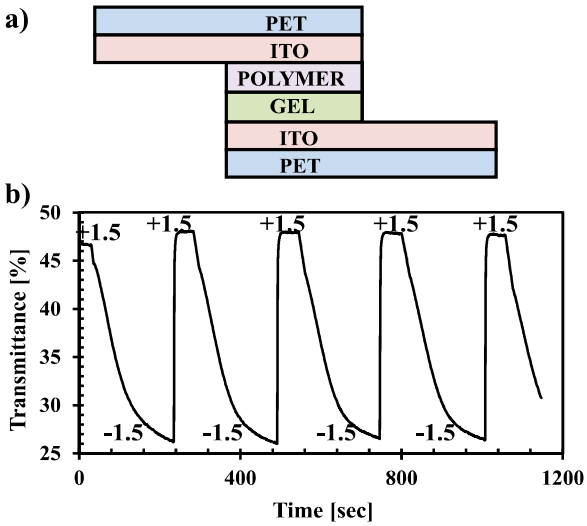

Figure 4.17. a) Solid state ECD configuration and b) transmittance vs time plots of a representative **copol[2]**-based ECD. Adapted from [1].

4.1.5. Polymer film Morphology and Charge Transport

The electrochromic parameters rely heavily on the film morphology[14]. It has been demonstrated that the electropolymerization conditions (e.g. solvents and/or support electrolytes, applied voltage) affect the morphological structure and consequently the electrochromic properties of the films. In particular, the solvent has a major influence on P(EDOT) film electrochromic properties[15].

In order to investigate the correlations between the optical properties and morphological features of electrodeposited films, their surface topography was characterized by AFM.

Figure 4.18 shows the AFM images of P(NDI2ODT4), *co*(NDI2ODT4-EDOT) and P(EDOT) films electrodeposited by cyclovoltammetry in an electrolytic solution containing CH_2Cl_2-CH_3CN (3: 2, v: v) and 0.01 M $LiClO_4$.

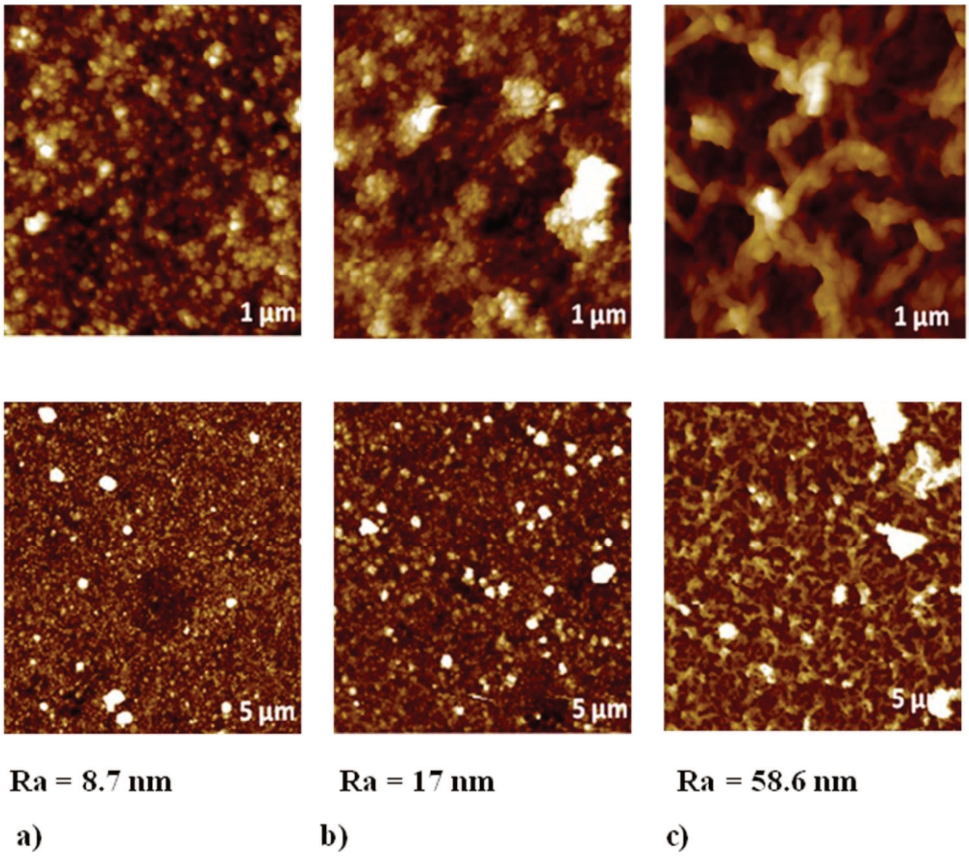

Figure 4.18: AFM morphology and corresponding surface roughness (Ra) values calculated from the images. a) P(NDI2ODT4); b) co(NDI2ODT4-EDOT) and c) P(EDOT), electrodeposited by cyclovoltammetry in an electrolytic solution containing CH_2Cl_2-CH_3CN (3: 2, v: v) and 0.01 M$LiClO_4$. The superimposed size in the bottom-right corner refers to the lateral dimension of the image.

AFM morphology images presented in Figure 4.18 show that both homopolymers and copolymer have different morphologies. In particular, the morphology of both P(NDI2ODT4) and *co*(NDI2ODT4-EDOT) is characterized by round grains and amorphous aggregates, while the P(EDOT) film exhibits well-defined and structured fibers. The surface roughness of the electrodeposited polymers was also found to be different, e.g. the surface of *co*(NDI2ODT4-EDOT) is characterized by higher values of Ra = 17 nm than P(NDI2ODT4) Ra = 8.7 nm, and greater size for the grains. Observed white particles of different sizes with sharp structure represent the salt remaining on the polymer surface even after several washings with the solvent mixture used for electrodepositing the films.

Thin film samples of P(NDI2ODT4), *co*(NDI2ODT4-bis-Th2P-C_{60}) and P(bis-th2P-C_{60}) were electrodeposited by chronoamperometry at 1.5V in an electrolytic solution containing C_6H_5Cl:CH_3CN and 0.1 M $TBAClO_4$ and AFM morphological images are shown in Figure 4.19.

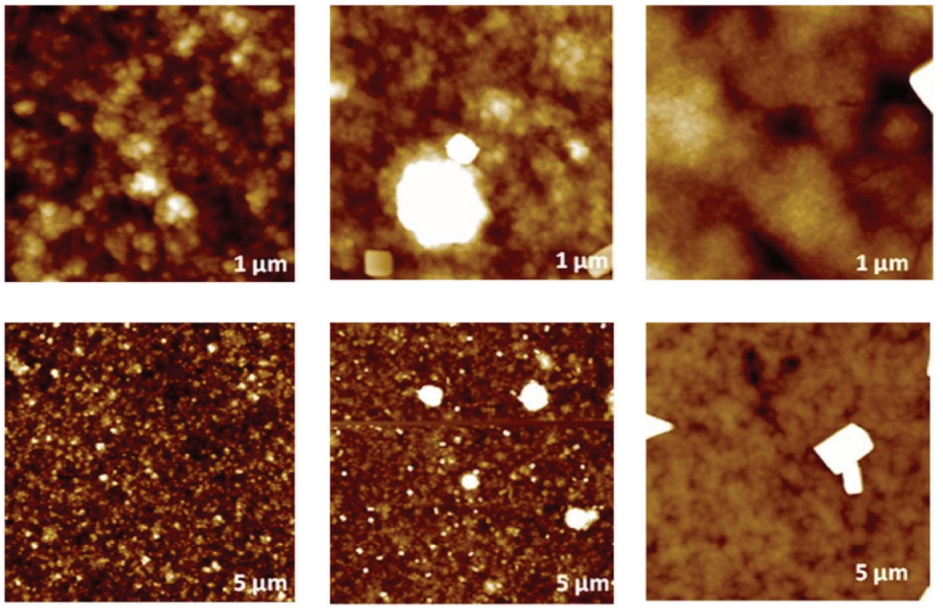

Figure 4.19: AFM morphology images and corresponding Ra calculated from the images with 5µm of a) P(NDI2ODT4), b) *co*(NDI2ODT4-bis-Th2P-C_{60}) and c) P(bis-th2P-C_{60}) respectively, electrodeposited by chronoamperometry at 1.5V in an electrolytic solution containing C_6H_5Cl: CH_3CN 0.1 M $TBAC1O_4$.

AFM analysis in Figure 4.19 also shows the inclusion of bis-th2P-C_{60} into P(NDI2ODT4) triggers a different morphology in the resultant polymer film.

The topographies of P(bis-th2P-C_{60}) was characterized by larger aggregates with higher R = 20.6 nm values, while the topography of P(NDI2ODT4) and co(NDI2ODT4-bis-Th2P-C_{60}) were characterized by smaller aggregates and a lower roughness (Ra = 9.5 nm and Ra = 11.6 nm respectively).

To note, the surface of co(P(NDI2ODT4)-EDOT) bis characterized with the higher values roughness (Ra = 17 nm) with respect to the one of the co(P(NDI2ODT4)-bis-Th2P-C_{60}) (Ra = 11.6 nm). Such a difference in the roughness might affect the electrochromic properties of the polymers. In fact, co(P(NDI2ODT4)-EDOT) as it can be seen from the paragraph 4.1.4. exhibits higher optical contrast with respect to the co(P(NDI2ODT4)-bis-Th2P-C_{60}). This can probably be attributed in addition to the different performance of the two materials to the higher roughness of the surface which in turn facilitates the ions diffusion in the electrolyte media towards the polymer film and, thus, increases the optical contrast[16,17].

Given the excellent optoelectronic properties of the co(NDI2ODT4-EDOT) system, it is interesting to investigate the effect on morphology by EDOT incorporation even by SEM. For this purpose, SEM images have been acquired on P(NDI2ODT4), P(EDOT) and *co*(NDI2ODT4-EDOT) respectively. Results of the investigation are shown in Figure 4.20.

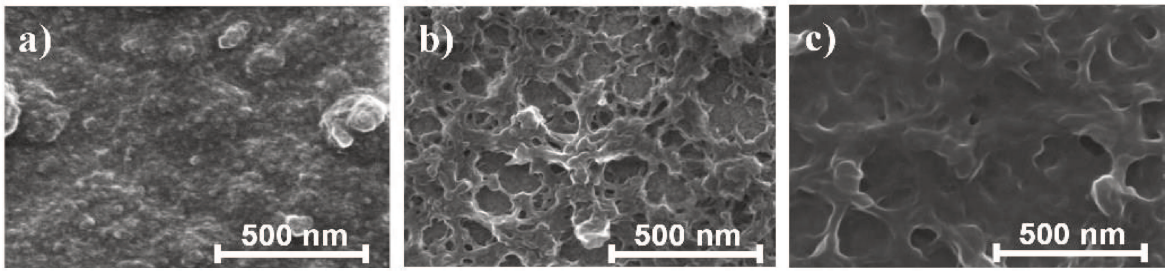

Figure 4.20. SEM images of a) P(NDI2ODT4), b) *co*(NDI2ODT4-EDOT) and c) P(EDOT). Adapted from [1]

Figure 4.20b shows that the morphology of *co*(NDI2ODT4-EDOT) is different from that shown for homopolymers (Figures 4.20a-c) due to the inclusion of EDOT units in the polymer chain. The surfaces of all studied films are rough with particle grain of different size. In particular, *co*(NDI2ODT4-EDOT) film is mainly porous with a globular structure particles having a size in the 10-40 nm range, whereas P(NDI2ODT4) film surface is more compact with particle grain size of 8-20 nm.

As for a number of applications, it may be desirable to achieve smoother film surfaces. To achieve this, a smooth surface was obtained by thermal annealing of the *co*(NDI2ODT4-EDOT) thin films at 160 °C for 40 minutes (Figure 4.21).

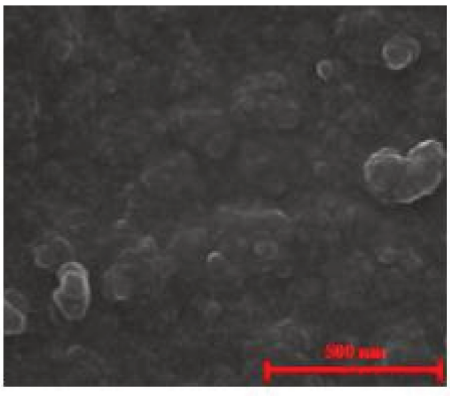

Figure 4.21. *co*(NDI2ODT4-EDOT)morphology after the thermal annealing at 160 °C for 40 minutes. Adapted from [1]

After the thermal annealing of the copolymer, as can be seen in Figure 4.22, the surface of the *co*(PNDI2ODT4-EDOT) changes considerably, resulting less rough. These results suggest that the homogeneity and increased packing/alignment of polymer chains may be favorable for performance enhancement in electrochromic polymers. This is due to the presence of distinct boundaries in the polymer that causes decreased inter- and intra-chain connectivity that may hinder the charge migration along the conjugated backbone and hopping across polymer chains surfaces[18].

In order to investigate the electrical properties of electrodeposited polymers including material conductivity and charge transport, the electrical measurements have been on electrodeposited polymeric films. Figure 4.22 shows the measured IV curves of the investigated structures in the -0.2 + 0.2V bias range.

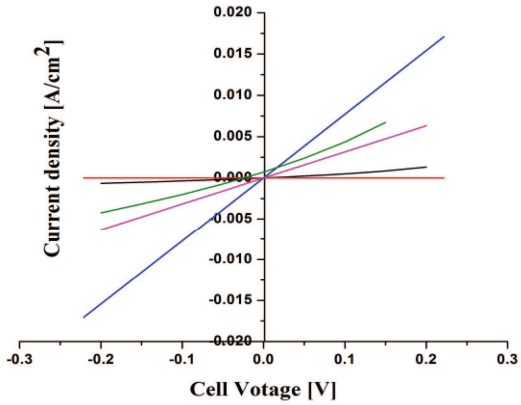

Figure 4.22. Current density-voltage in the -0.2+0.2V bias range plots for P(NDI2ODT4) black, **copol[2]** red, P(EDOT) blue, P(bis-Th2P-C_{60}) magenta and *co*(PNDI2ODT4-bis-Th2P-C_{60}) green.

As shown in Figure 4.22 both the P(EDOT) and the P(bis-Th2P-C_{60}) exhibit an ohmic behavior, where the P(EDOT) was characterized by a higher conductivity value ($3*10^{-6}$ S/cm) than that of P(bis-Th2P-C_{60}) ($5*10^{-7}$ S/cm).

Conversely, P(NDI2ODT4) and copolymers do not exhibit ohmic behavior probably due to the energy barrier formation at the polymer/electrode interface. It is interesting to note that copolymers result in a decrease of the conductivity, especially in **copol[2]**, while having less effect in *co*(NDI2ODT4-bis-Th2P-C_{60}) which conductivity approaches P(bis-Th2P-C_{60}).

Figure 4.23 shows the measured I-V curves of the investigated structures in the -1.5- +1.5 V bias range.

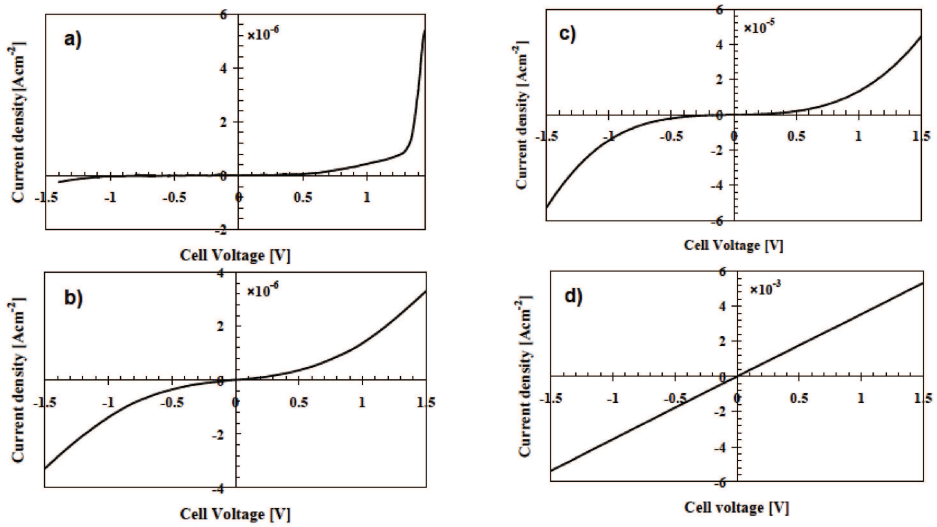

Figure 4.23.Current density-voltage plots for a) P(NDI2ODT4), b) **copol[1]** , c) **copol[2]** and d) P(EDOT). Adapted from [1]

In Figure 4.23 are shown the I-V curves measured at higher bias voltage range. We note the I-V curves of the copolymers and that of the P(NDI2ODT4) show a marked non-linear shape, whereas the electrodeposited P(EDOT) preserves an ohmic behavior. Both, **copol[1]** and **copol[2]** at higher bias potential shows I-V curves obeying to an $I=KV^2$ law, which is typical of the space charge limited current (SCLC) regime. From the Equation 3.4[19]:

$$J_{SCL} = \frac{9}{8}\varepsilon_0\,\varepsilon_r\,\mu\frac{V^2}{d^3} \qquad (3.4)$$

which governs the transport in a space-charge limited current regime, (where JSCL= space charge limited current; V= voltage; d=thickness, μ=charge carriers mobility, ε_0= permittivity in vacuum, ε_r= relative static permittivity), the carrier mobility values of **copol[1]** and **copol[2]** were found to be 2.5×10^{-7} $cm^2/V\cdot s$ and 1.7×10^{-6} $cm^2/V\cdot s$, respectively, using SCLC measurements. These results suggest that by increasing the EDOT moiety content, the copolymers exhibit higher carrier mobilities in agreement with the greater content of the electron-rich EDOT.

4.2 Push-pull copolymers in organic solar cells (OSCs)

In order to realize photovoltaics cells based on P(NDI2ODT4), P(bis-Th2P-C_{60}) and *co*(NDI2ODT4-bis-Th2P-C_{60}) systems, electronic transfer studies were carried out with P3HT.Polymeric systems were electrodeposited on ITO/PET or P(EDOT): PSS-dop/ITO /PET by chronoamperometry, as shown in the previous section.
Subsequently, organic solar cell devices fabricated by this approach are based on PHJ whit P3HT and the electrodeposited polymer. Accordingly, the resulting OSCs devices were realized following two different architectures:

-PET/ITO/electrodeposited polymer/P3HT/Al
-PET/ITO/ P(EDOT): PSS-i-PrOH /electrodeposited polymer/ P3HT/Al

4.2.1. (NDI2ODT4-bis-Th2P-C_{60})/P3HT PHJ OSCs

In order to confirm the charge transfer between electrodeposited films and P3HT, the fluorescence intensity is recorded on pure P3HT and compared to that recorded on the planar heterojunction. (Figure 4.24). As can be seen in Figure 4.24, PHJ causes a fluorescence quenching of P3HT. This is due to electronic transfer between the polymers and the P3HT. P(bis-Th2P-C_{60}) has a higher electronic transfer with P3HT than P(NDI2ODT4) while, the *co*(NDI2ODT4-bis-Th2P-C_{60}).

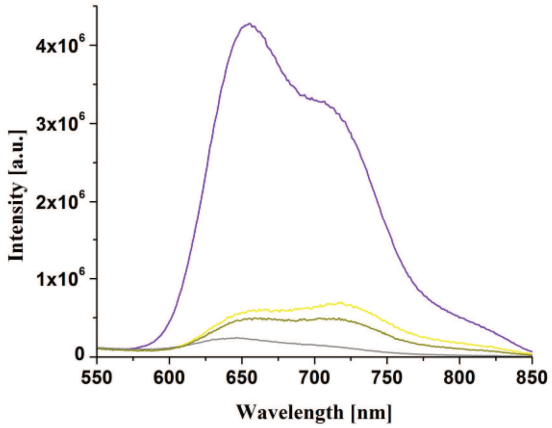

Figure 4.24. a) Comparison of fluorescence spectra of P3HT (black) and PHJs whit electrodeposited polymers, P(NDI2ODT4) grey, *co*(NDI2ODT4-bis-Th2P-C_{60}) brown and P(bis-Th2P-C_{60}) yellow respectively.

It is interesting to note that both homopolymers and *co*(NDI2ODT4-bis-Th2P-C_{60}) lead to significant fluorescence quenching of P3HT despite the restricted D/A interface of a PHJ structure. For this reason, they are promising for the realization of planar heterogeneous solar cells with P3HT by acting as electron-acceptor materials.

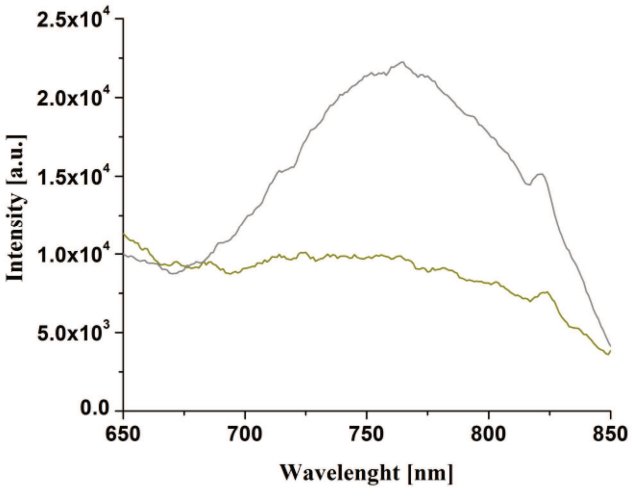

Figure 4.25. The fluorescence spectrum of P(NDI2ODT4) gray and *co*(P(NDI2ODT4)-bis-Th2P-C_{60}) brown at 600 nm excitation lambda.

Furthermore, from fluorescence experiments carried out at the excitation lambda of 600 nm onto films on P(NDI2ODT4) and *co*(NDI2ODT4-bis-Th2P-C_{60}) (Figure 4.25), it was possible to observe that the copolymer has significantly lower fluorescence intensity since inclusion of bis-Th2P-C_{60} units determines an internal charge transfer, from P(NDI2ODT4) to C_{60}, in accordance to the concept that C_{60} makes *co*(NDI2ODT4-bis-Th2P-C_{60}) a push-pull system. These observations are also confirmed by the DFT data discussed above in 4.1.2.

A crucial role in the efficiency of solar cells is played by the architecture of the device. The first cell was made according to this PET/ITO/electrodeposited polymer/P3HT/Al architecture, where the first layer was realized by a thin film of the acceptor system electrodeposited on ITO/PET (anode) followed by a second layer formed by the polymeric P3HT donor system on which the aluminium electrode (cathode) was deposited by thermal evaporation (Figure 4.26).

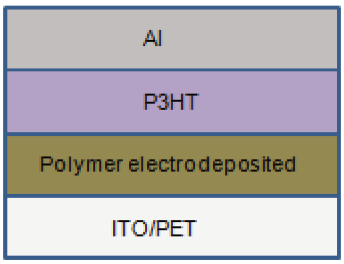

Figure 4.26. Schematic representation of the PET/ITO/ electrodeposited polymer/P3HT/ Al solar cell device.

The photovoltaic parameters PET/ITO/ electrodeposited polymer/P3HT/Al of the device are reported in Table 4.6. As shown in Table 4.6, the parameter values are very low, and the co(NDI2ODT4-bis-Th2P-C_{60}) does not lead to significant results. The main problem stems from the architecture of the device. In fact, in this configuration, in which the ITO should act as an anode (i.e. hole extractor), the acceptor polymer (which receives electrons) is in contact with the anode itself. The P3HT, acting as a donor (hence carrying holes), is in contact with the cathode (which should instead receive electrons).

Table 4.6: Photovoltaic properties of the PET/ITO/ electrodeposited polymer/P3HT/ Al device, in which different electrodeposited polymers were investigated as acceptor systems.

SAMPLE	Voc(V)	Jsc(mA/cm^2)	FF	µ(%)
P(bis-Th2P-C_{60})	0.15	0.02	0.24	0.0007
P(NDI2ODT4)	0.10	0.01	0.56	0.0003
co(NDI2ODT4-bis-Th2P-C_{60})	-	-	-	-

Given these results, it was necessary to realize the inverted architecture of the device by introducing an electron transport layer in the previously shown device architecture. For this reason, polymer systems are electrodeposited onto films at a different thickness on P(EDOT): PSS-PrOH at a different thickness on ITO/PET to realize devices according to a so-called inverse structure in which the P(EDOT):PSS layer represents the ETL instead of HTL(hole transfer layer).

In fact, it is known from a previous report that Isopropanol-treated P(EDOT):PSS was applied as a new ETL in P3HT:PCBM bulk heterojunction polymer solar cell (BHJ-PSC) devices for the first time, revealing the electron transport property of IPA-treated P(EDOT):PSS in sharp contrast to the well-known hole transport property of the untreated P(EDOT):PSS [20].

Therefore, the second cell was made according to this architecture PET/ITO/P(EDOT):PSS-i-PrOH/electrodeposited polymer/P3HT/Al architecture reported in Figure 4.27.

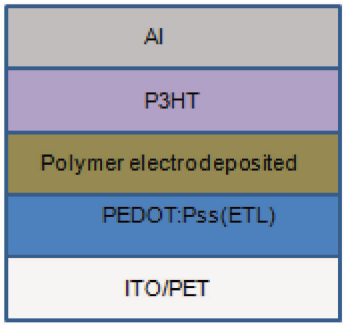

Figure 4.27. Schematic representation of the device: PET/ITO/P(EDOT):PSS-dop/electrodeposited polymer/P3HT/Al.

Since the thickness of the polymeric film influences the performance of a solar cell, PET/ITO/P(EDOT):PSS-i-PrOH /electrodeposited polymer/ P3HT/Al device are prepared and characterized by varying the thickness of the polymeric films. Thanks to the electrochemical approach that allows having control over the deposited layer of the polymer[2], it was possible to prepare different thickness polymers by varying the deposition time of the polymer on the working electrode. The evaluation of the thickness of electrodeposited polymer films on P(EDOT):PSS-i-PrOH was carried out by AFM. For AFM characterization, a vertical incision was made on each sample using a pin. Under the microscope, the engraving appears as a groove, easily identifiable so that it was possible to obtain the profile in the border area between the groove and the edge.

The photovoltaic parameters of the ITO/P(EDOT):PSS-i-PrOH/electrodeposited polymer/ P3HT/Al with P(NDI2ODT4), P(bis-Th2P-C_{60}) and copolymer at different thicknesses (measured by AFM) are reported in Tables 4.7-4.9 respectively.

Table 4.7: Photovoltaic properties of the OSCs prepared with P(NDI2ODT4).

Thickness(nm)	Voc(V)	Jsc(mA/cm^2)	FF	η(%)
10	0.93	0.00623	0.23	0.0013
20	0.93	0.00519	0.23	0.0011
30	0.86	0.00499	0.20	0.0008

Table 4.8: Photovoltaic properties of the OSCsprepared with P(Bis-Th2P-C_{60}).

Thickness (nm)	Voc(V)	Jsc(mA/cm^2)	FF	η (%)
10	0.71	0.015	0.28	0.003
20	0.72	0.0097	0.24	0.0017
30	0.71	0.0055	0.23	0.0009

Table 4.9: Photovoltaic properties of the OSCs prepared with *co*(NDI2ODT4-bis-Th2P-C_{60}).

Thickness (nm)	Voc(V)	Jsc(mA/cm^2)	FF	η (%)
10	0.85	0.00324	0.22	0.0009
20	0.85	0.00322	0.22	0.0006
30	0.80	0.00329	0.20	0.0005

As shown from the Tables (4.7-4.9), it was possible to get complete information about the parameters for all the investigated systems. It is surprising to note that V_{oc} values are quite high compared to electrodeposited systems and most polymers in the literature for photovoltaic applications [21]. The highest obtained V_{oc} value (0.93V) is the one obtained for P(NDI2ODT4) system. Again, *co*(NDI2ODT4-bis-Th2P-C_{60}) exhibits intermediate properties with respect to homopolymers.

It is also very important to note that the thickness affects the photovoltaic properties of the OSCs in all three systems. In fact, it was possible to obtain best performances by using polymer film thicknesses of 10nm. This can be explained because the OSCs has a planar architecture. Then, the smaller the thickness, the higher is the probability that the charges reach the electrodes. On the other hand, if it is too thin, absorption is significantly decreased and then, it becomes important to find the right compromise between charging and absorption of radiation.

It is worth noting that *co*(NDI2ODT4-bis-Th2P-C_{60}) permits to obtain stable J_{sc} current values at the investigated film thickness. This can be explained by the fact that C_{60} makes co(NDI2ODT4-bis-Th2P-C_{60}) a push-pull system, in which P(bis-Th2P-C_{60}) determines an internal charge transfer, from P(NDI2ODT4) to C_{60}. These observations are also confirmed by the fluorescence quenching experiments and DFT data.

In conclusion, P(NDI2ODT4), P(bis-Th2P-C_{60}), *co*(NDI2ODT4-bis-Th2P-C_{60}) are good acceptor with P3HT in PHJ-based OSCs. However, the photovoltaic properties of the OSCs, are overall not very good. This is due in part to the material interfaces involved in

the planar configuration but, it is also important to remark the molecular distortion in the *co*(NDI2ODT4-bis-Th2P-C_{60}) which, finally, is not optimal for optoelectronics and also photovoltaics applications.

This is detrimental to the optoelectronics and photovoltaics applications. In this regard, Th4P-C_{60} monoadducts constitute an ideal solution. On the hand, their synthesis leads to a quite good yield (51%) in comparison to bis-Th2P-C_{60} (22%) and, remarkably, a high stereo selectivity towards the trans isomer (see 3.2-3.3). Furthermore, the optimization in the design of the molecular structures of the Th4P-C6o copolymers systems by single-step synthesis allows for fine control of the morphology of OSCs by improving the components miscibility.

4.2.2. Electrochemical characterization of Th4P-C_{60} copolymer additives

For the purpose of their electronics application, it is important to analyze the electrochemical behavior of the Th4P-C_{60} copolymers systems. The electrochemical behavior of copolymers **5a-c** was investigated by means of CV measurements in o-DCB-CH_3CN (4:1v/v), 0.1 M $TBAClO_4$ at scan rate of 200 mV/s (Figure 4.28).

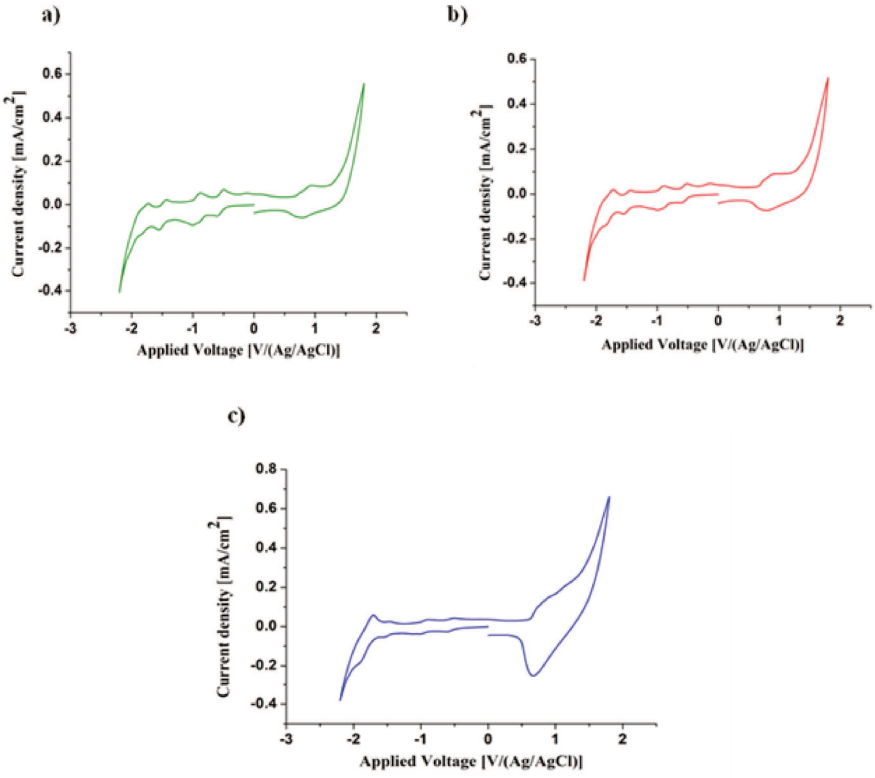

Figure 4.28. Cyclic voltammograms of copolymers **5a-c**.

The oxidation and reduction scan of the cyclic voltammograms are dominated by an

oxidation attributed to the polythiophene chains and by four reduction reactions typical of the fullerene C_{60} derivatives respectively, observed for all studied compounds[4]. From oxidation and reduction cyclovoltammetry of copolymers **5a** to **5c**, the oxidation and reduction potential decreases respectively due to the increasing polythiophene chain length (Table 4.10). Furthermore, as thiophenic chains increase, there is a decrease in the onset oxidation potential, this consequently results in an increase of HOMO energy levels passing from copolymer **5a** to **5c**. The values of the calculated optical parameters of the compounds are reported in Table 4.10.

Table 4.10: Electrochemical parameters of the copolymers **5a-c**.

compound	E_{onset}	E^1_{ox}	E^1_{red}	E^2_{red}	E^3_{red}	E^4_{red}
5a	**0.66**	**0.94**	**-0.59**	**-1.00**	**-1.56**	**-1.84**
5b	**0.63**	**0.90**	**-0.57**	**-0.97**	**-1,53**	**-1.82**
5c	**0.58**	**0.87**	**-0.55**	**-0.94**	**-1.51**	**-1.80**

4.2.3. Th4P-C_{60} copolymers as push-pull systems

In order to see if the copolymers behave as p-n types against P3HT and PCBM, the HOMO-LUMO levels were obtained and compared to those of the P3HT PCBM which are already known in the literature. Electrochemical and optical techniques were employed to determine the HOMO and LUMO levels of the films. Oxidation and reduction in conjugated polymers correspond to doping and de-doping, or to the removal of electrons from the HOMO and the addition of electrons to the LUMO respectively, as shown in Figure 4.29.

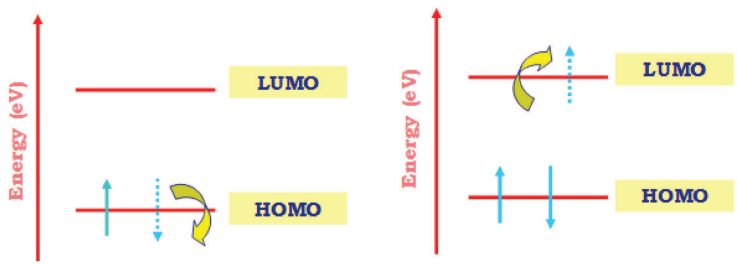

Figure 4.29. Representation of the doping and de-doping process in conjugated polymer systems.

The CV is, in fact, a method for calculating the ionization potential that approximates sufficiently the HOMO level of the material from the vacuum level and the electronic

affinity, through the initial values of oxidation and reduction. Thus, the onset potential of oxidation represents the potential at which hole injection begins at the HOMO level, the onset reduction represents the energy required to reduce the polymeric film.

The HOMO level was calculated from onset oxidation potential [$E_{onset,ox}$],[5] according to the Equation (3.5):

$$E_{HOMO}=-(E_{[onset,ox\ vs\ NHE]} + 4.5) \qquad (3.5)$$

where is $E_{[onset,ox\ vs\ NHE]}$ the potential for oxidation of the copolymer vs Ag/AgCl compared to the normal hydrogen electrode (NHE), while 4.5eV to be equivalent to 0.0 V vs. NHE.

The LUMO level was obtained from Equation 3.6:

$$LUMO = LUMO + E_g^{opt} \qquad (3.6)$$

Absorption spectra acquired on deposited compounds by drop casting on ITO/PET (Figure 4.30) were used for evaluation of the optical band gaps (E_g^{opt}) of the compounds, according to the procedure applied for indirect band gap semiconductor. The value of band gap, in electron volt, was calculated by absorption spectrum fitting (ASF) method, in particular by parameter λ_g from the following Equation (3.7):

$$E_g=1239.83/\lambda_g \qquad (3.7)$$

where the parameter was λ_g extrapolating the linear of the $(Abs(\lambda)/\lambda)^{1/m}$ vs. $1/\lambda$ curve at $(Abs/\lambda)^{1/m}=0$ [22].

The optical parameters of copolymers are reported in table 4.11.

Table 4.11: Electrochemical and optical parameters of copolymers **5a-c**.

compounds	HOMO(eV)	λ_g (nm)	E_g^{opt}(eV)	LUMO(eV)
5a	**-5.37**	**690**	**1.80**	**-3.57**
5b	**-5.34**	**705**	**1.75**	**-3.59**
5c	**-5.29**	**696**	**1.77**	**-3.52**

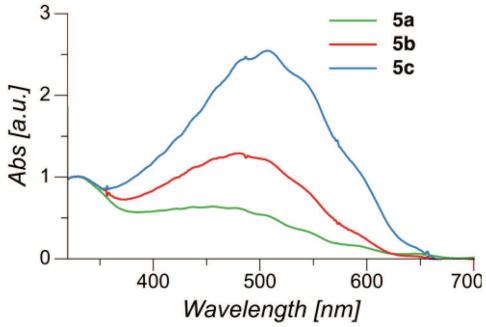

Figure 4.30. UV-Vis spectra of the copolymers **5a-c**.

The HOMO LUMO levels and the low band gap of the investigated copolymers correspond to the values obtained for the similar molecules in the literature [23]. In order to evaluate the behavior of copolymers in an organic photovoltaic device with P3HT-PCBM, HOMO and LUMO energy levels were compared to those of P3HT and PCBM, which are already known in the literature (Figure 4.31).

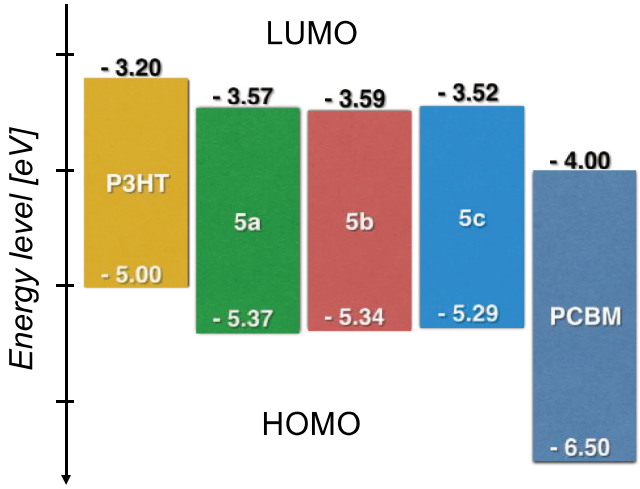

Figure 4.31: The energy level scheme of the material illustrating the HOMO-LUMO levels of the copolymers respect at those of P3HT and PCBM.

The Figure 4.27 shows the schematic diagram representing calculated HOMO and LUMO energy level of copolymers **5a-c**, compared with those of PCBM and P3HT.

The HOMO and LUMO levels of the copolymers are positioned between the energy level of P3HT and PCBM, in this way should improve the charge transfer process [24]. It is possible to see a slight increase in the HOMO energy level with increasing the content of thienyl units; this phenomenon has already been observed in the literature [25,26].

Current-voltage measurements have been performed on bi-component OSCs, in which the copolymers have been employed as n-type or p-type systems (Tables 4.12-4.14).

Table 4.12: Photovoltaic properties of the OSCs with copolymer **5a**.

	Voc (V)	Jsc (mA/cm^2)	FF	η (%)
Single layer5a	**0.48**	**0.58**	**0.23**	**0.06**
P3HT:5a (n-type)	**0.45**	**0.39**	**0.38**	**0.07**
5a:PCBM	**0.64**	**0.78**	**0.26**	**0.13**

Table 4.13: Photovoltaic properties of the OSCs with copolymer **5b**.

	Voc (V)	Jsc (mA/cm^2)	FF	η (%)
Single layer 5b	**0.52**	**0.79**	**0.21**	**0.11**
P3HT:5b(n-type)	**0.40**	**0.24**	**0.41**	**0.04**
5b-PCBM(p-type)	**0.73**	**1.07**	**0.25**	**0.19**

Table 4.14: Photovoltaic properties of the OSCs with copolymer **5c**.

	Voc (V)	Jsc (mA/Cm2)	FF	η (%)
Single layer 5c	**0.68**	**0.11**	**0.24**	**0.02**
P3HT:5c(n-type)	**0.55**	**0.05**	**0.41**	**0.01**
5c:PCBM(p-type)	**0.80**	**2.72**	**0.31**	**0.67**

In order to evaluate their electrical properties, copolymers were tested initially as single layer OSCs and then by coupling them with PCBM or P3HT. In particular, single layer OSCs without P3HT and PCBM have been realized and tested. Importantly, these copolymers can be considered as "push-pull" systems with electron acceptor moieties (fullerene units) directly linked to donor polymer (polythiophenic chains). Subsequently, it was possible to show that copolymers can act as p-type is coupled with PCBM and as n-type if coupled with P3HT. Given the predominance of the polythiophenic units compared to the fullerene units, the copolymers show better photovoltaic parameters by acting as donor systems (p-type). For the same reason, the copolymer **5c** with longer polythiophenic chains exhibits better values of J_{sc} (2.72 mA cm^{-2}), V_{oc} (0.80 V) and PCE (0.67 %) when coupled with PCBM.

4.2.4. Th4P-C_{60} in thin films of P3HT:PCBM BHJs

The design of copolymers **5a-c** is of fundamental importance for finely controlling the morphology in OSCs because they are able to improve the P3HT:PCBM miscibility. In particular, the copolymers **5a-c** have been investigated as compatibilizers for photovoltaic thin films of P3HT:PCBM BHJ.

It was possible to understand that the regioregularity of the polythiophenic chains affects the packing and consequently the π-π stacking of P3HT in a thin film. In this regard, from XRD spectra of thin films, it is possible to conclude that the addition of a little amount of **5b**-additive (2 wt.%) in P3HT thin films is able to modify its structure so that the

diffraction signal from the (100) plane completely disappear (Figure 4.32). Interestingly, after thermal annealing at 110 °C for 5 min, both P3HT thin films with and without copolymers show a diffraction signal at 2θ = 5.5°.

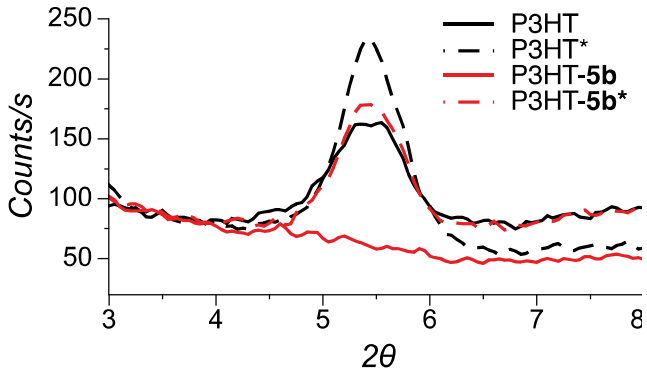

Figure 4.32. X-ray diffraction of structure P3HT films with and without of copolymer **5b**, before (solid lines) and after thermal annealing (dashed lines).

The annealed P3HT thin film produced a more intense diffraction signal as compared to that processed with the copolymers, suggesting a decreased crystallinity of P3HT, in this way it is possible to reduce phase separation of donor and acceptor, leading to thinner interpenetrating networks of the blend layers [27].

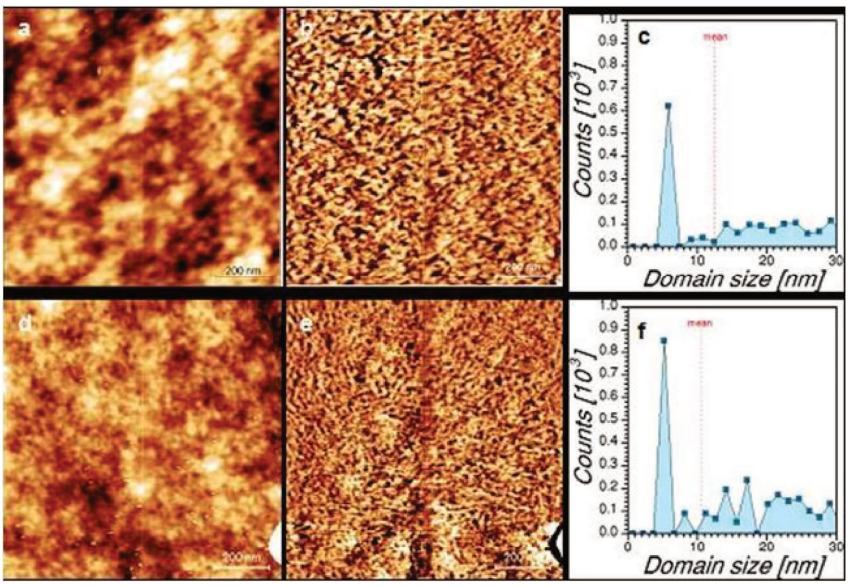

Figure 4.33. AFM analysis of the thin film of BHJ deposited without (upper row) and with (lower row) 5b copolymer (2 wt.%), after annealing at 110°C for 5 minutes: a, d) morphology; b, e) phase-lag images; c, f) P3HT domain size distributions.

AFM analysis of annealed samples (Figure 4.33) is able to confirm the hypothesis that the insertion of the additive is able to induce a different morphology and a meaningful alteration in the domain size in the nanometric structures of the investigated materials. For instance, in Figure 4.33a and 4.33d, the surface morphology of BHJs without and with copolymer **5b** (2 wt.%) are reported. These samples are characterized by globular and superimposed aggregates that assemble with size visibly smaller for the BHJ with the copolymer. Indeed, BHJ without copolymer **5b** in Figure 4.33a has an RMS surface roughness of 0.86 nm whereas BHJ with the copolymer shows a halved value of only 0.43 nm. This grain size difference appears still more evident in the phase-lag images (Figure 4.33b and 4.33e), where P3HT and PCBM domains give respectively bright and dark contrast. The size distributions for the P3HT domains is extracted for BHJ without and with the copolymer by statistical analysis (Figure 4.33c and 4.33f). The size distribution for the BHJ without copolymer extends over 30 nm and has a mean value of 12.5 nm. On the other side, BHJ with copolymer **5b** displays a distribution with a mean value of 10.6 nm.

In order to investigate the effect of the copolymers addition into the P3HT:PCBM BHJ active layer photoluminescence (PL) measurements were performed (Figure 4.34).

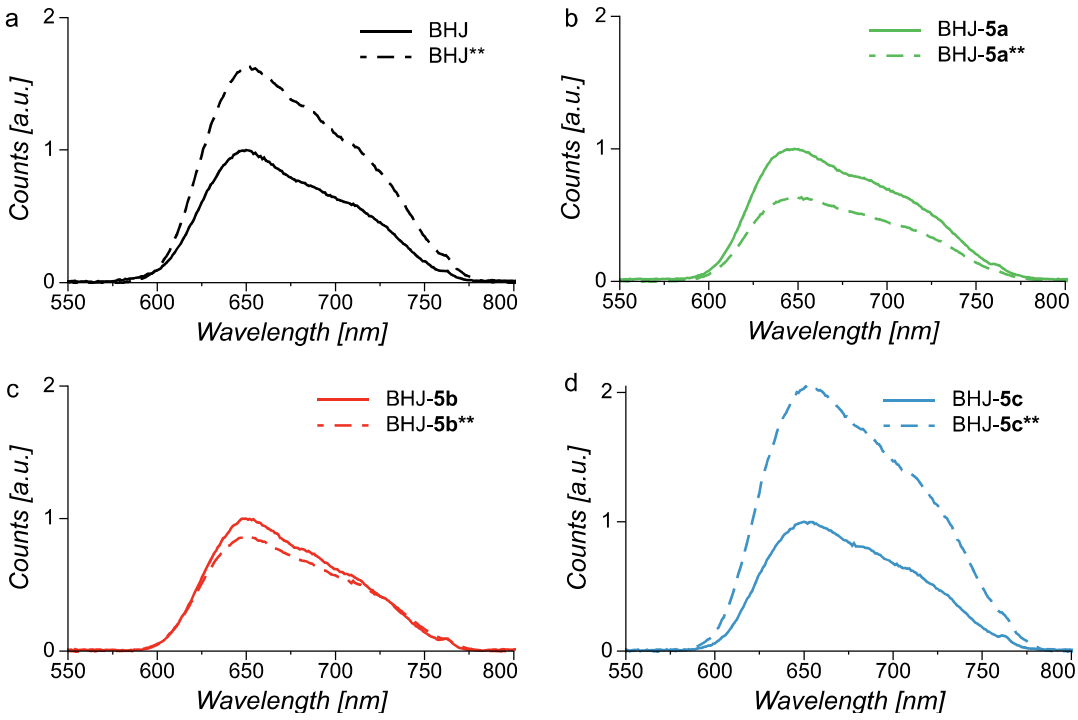

Figure 4.34. Fluorescence spectra of pristine BHJ (a) and BHJs with copolymers 5a (b), 5b (c) and 5c (d) before and after thermal annealing at 120 °C for 10'.

As expected, it is possible to observe a significant PL quenching due to efficient charge transfer from the donor P3HT to the acceptor PCBM, which is a consequence of a good mixing between these materials. Accordingly, thermal annealing (120 °C, 10 min.) determines an increase in the PL intensity of pristine BHJs because phase separation leads to the formation of P3HT domains larger than the exciton diffusion length [28,29]. Similarly to pristine BHJ, the addition of **5c** to BHJ determines a strong increase of PL intensity after thermal annealing. This observation is in agreement with a picture in which the phase separation relates to the length of polythiophenic chains into the copolymer. On the contrary, BHJs with **5a** and **5b** show a further improvement of PL quenching even after prolonged thermal annealing. This result suggests that these copolymers are able to limit the phase separation process.

In fact, the shorter chain of copolymers **5a-5b** gives high PL intensity under annealing in accordance with the formation of a large number of small domains which are suitable for charge separation processes, i.e. with a size comparable to the exciton diffusion length (Figure 4.35). Indeed, considering the length of the repetitive units of copolymers **5a-c**, the polythiophenic chains can be estimated to be about 6 nm, 9 nm, and 16 nm, respectively. Interestingly, the exciton diffusion length in regioregular P3HT thin films is about 6 - 10 nm [30,31] and the exciton dissociation appears to be more efficient for the BHJ with the copolymers (**5a**, **5b**) with the polythiophenic chains in that length range. This result well agrees with the above AFM features showing P3HT domains of about 10 nm obtained by adding the copolymer **5b**.

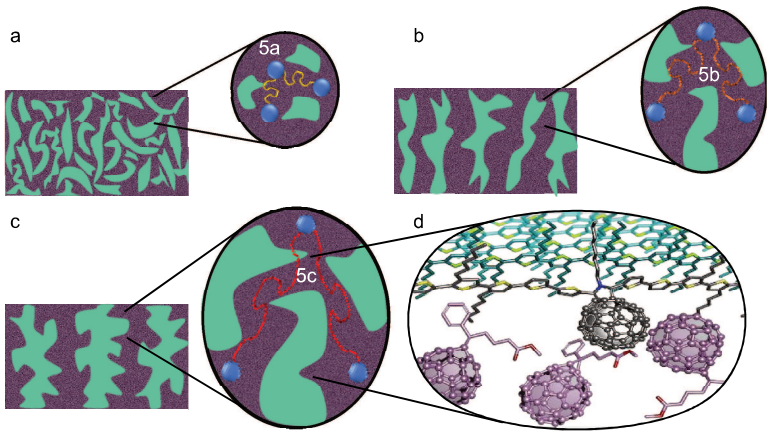

Figure 4.35. Schematic representation of the effect of three copolymers on the domain size distribution in BHJ.

4.2.5. Effect of the copolymers on the performances of P3HT:PCBM BHJ

In order to investigate the effect of copolymers in P3HT:PCBM BHJ solar cells current density-voltage (J-V) curves of the OSCs with and without copolymers **5a-c** were acquired (Figure 4.36). The corresponding photovoltaic performance data summarized in Table 4.15.

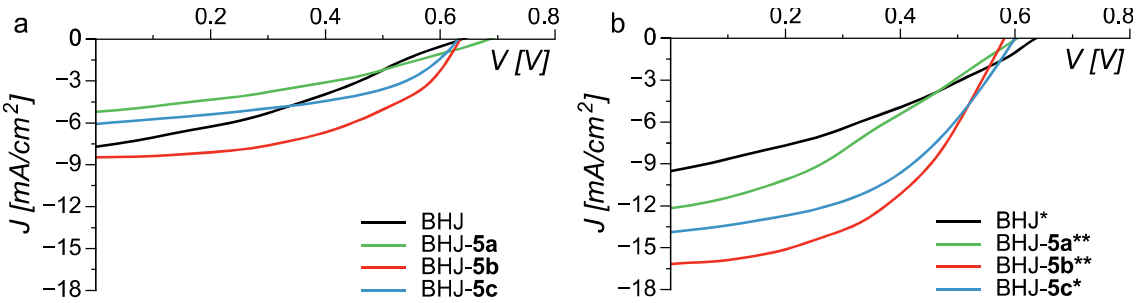

Figure 4.36. Current density−voltage (J−V) characteristics of BHJ solar cells without and with copolymers **5a-c** before (left) and after thermal annealing (right).

Table 4.15. Photovoltaic properties of the BHJ OSCs.

OSCs	Voc (V)	Jsc (mA/cm2)	FF	Η (%)
BHJ	0.63	7.71	0.34	1.63
BHJ*	0.62	9.52	0.33	1.97
BHJ**	0.55	6.81	0.22	0.82
BHJ-5a	0.68	5.22	0.35	1.24
BHJ-5a*	0.61	10.30	0.33	2.07
BHJ-5a**	0.60	12.17	0.33	2.40
BHJ-5b	0.63	8.47	0.45	2.38
BHJ-5b*	0.60	14.67	0.45	3.92
BHJ-5b**	0.59	16.15	0.47	4.46
BHJ-5c	0.63	6.07	0.46	1.83
BHJ-5c*	0.60	13.90	0.46	3.84
BHJ-5c**	0.60	9.03	0.25	1.36

a)Annealed devices are marked by asterisks: * 110 °C for 5’; ** 120 °C for 10’

Table 4.15: Photovoltaic parameters of the copolymers **5a** in BHJ devices.

BHJ	Wt.%	Voc (V)	Jsc (mA/cm2)	FF	η (%)
5a	15	0.60	4.31	0.24	0.63
	5	0.60	4.47	0.26	0.70
	2	0.60	12.17	0.35	2.40
5b	15	0.58	4.95	0.21	0.59
	5	0.58	12.73	0.17	1.22
	2	0.59	16.15	0.47	4.46
5c	15	0.59	4.05	0.23	0.55
	5	0.59	8.31	0.24	1.17
	2	0.60	13.90	0.46	3.84

Photovoltaic properties of the OSCs were investigated by introducing varying amounts (2%, 5%, and 15%) of copolymers **5a-c** and by performing annealing at two different conditions: 110 °C for 5' or 120 °C for 10'. Details about the effect of the different amount of the copolymers are reported in tables 4.15.

- OSCs without annealing

Before annealing, the OSC without additive exhibits a PCE of 1.63% with Jsc of 7.71 mA cm^{-2}, Voc of 0.63 V, and FF of 0.34. In the presence of **5a**, PCE value decreases to 1.24 % due to a decrement of Jsc (5.22 mA cm^{-2}). This confirms that shorter polythiophene chains induce the formation of a large number of small domains resulting in a charge transfer with limited percolation channels for the charge carriers within the BHJ producing a reduced charge collection to the electrodes.

Instead, OSCs with **5b** and **5c** show improved performances, compared to a device without additives, with PCE values increased from 1.63 % to 2.38 % and 1.83 % respectively.

The lower value obtained with **5c** than that with **5b** can be ascribed to the decrease of Jsc (6.07 mA cm^{-2}), thus confirming the hypothesis that longer polythiophenic chains lead to a phase separation with domains significantly exceeding the exciton diffusion length. Despite this, the PCE value of device with 5cis greater than that without copolymers, thanks to the higher FF (0.46) probably due to the domain size more suitable for charge transport and thus the decreased recombination probability. Instead, the domain size obtained with 5 blikely ensures an appropriate balance between exciton dissociation and

charge percolation to the electrodes. Indeed, in this case, both Jsc and FF show an increase from 7.71 mA cm^{-2} and 0.34 to 8.47 mA cm^{-2} and 0.45 respectively, showing the best performance among all different devices.

- OSCs with110 °C for 5' annealing

Thermal annealing (5', 110 °C) leads to a more pronounced difference in performances between OSCs with and without copolymer additives.
In particular, the device without copolymers shows an increased Jsc from 7.71 mA cm-2 to 9.52 mA cm^{-2} resulting in a PCE of 1.97 %. OSC with 5a exhibits an increase from 1.24 % to 2.07 % due to the remarkable improvement of Jsc, almost doubled compared to the reference device, i.e. the device before annealing (from 5.22 to 10.30 mA cm-2). Indeed, OSCs with **5b** and **5c** show Jsc values significantly increased from 8.47 and 6.07 mA cm^{-2} to 14.67 and 13.90 mA cm^{-2}, respectively.

- OSCs with 120 °C for 10' annealing

The last thermal annealing (10', 120 °C) process permits to further investigate copolymers effects on the performance of the OSCs. In absence of copolymers, OSCs show worse performances compared to that annealed at 110 °C (PCE of 0.82 %). Similarly, the PCE value of the device with **5c** decreases from 3.84 % to 1.36 %. On the contrary, thermal annealing further improves PCE in presence of 5a and 5b, respectively to values of 2.40 % and 4.46 %, respectively.
The optimal percentage to improve the performance of OSCs was equal to 2 wt.% of copolymers. Finally, the best performance (4.46 %) was obtained by adding 2 wt.% of **5b** after annealing the OSCs at 120 °C for 10'.The designed copolymers act as efficient morphological compatibilizers in BHJs and can effectively stabilize the morphology of BHJ and improve the stability of devices not only by limiting the phase separation between donor and acceptor materials but also by modulating the domains size.
It is interesting to note that better PCE in P3HT:PCBM BHJ OCSs was obtained when the additive introduced decreased the crystallinity of P3HT and thus increased the miscibility of the D/A blend layer. Such an effect was already demonstrated by Park et al who

suggested that reduced crystallinity of active layer ensures good miscibility of D and A materials and therefore results in optimized separation of the nanophase [27].

The fine-tuning of donor/acceptor interfaces structures by this set of new compatibilizers studied inhere permits to achieve an OSCs on ITO/PET substrates with optimal photovoltaic parameters. Conversely, literature data suggest low increments of efficiency caused by the additives in P3HT:PCBM BHJ OSCs on ITO/glass, mainly due to the nature of the copolymer units as the presence of bulky insulating blocks hinders the exciton transport to the D/A interface, resulting in an increase of the series resistance and deteriorating the charge carrier transport in the device [32,33].

4.3. Push-pull copolymers for flexible electrochemical non-enzimatic sensor

The Th4P-C_{60} monomer can finally be employed as a suitable molecular system to be combined with hemin by chronoamperometric electrochemical synthesis on ITO/PET substrates for specific sensing of H_2O_2. This fulleropyrrolidine thiophene-hemin system is to be considered an ideal system for non-enzymatic-based electrochemical sensors.

4.3.1. Electrodeposition of Th4P-C_{60}-hemin

Herein, we studied the systems based on Th4P-C_{60} monomer electropolymerized with hemin porphyrin in order to realize a non-enzymatic flexible electrochemical biosensor. The deposition of homopolymers and dyad of fulleropyrrolidine **3**-hemin on ITO/PET was carried out by galvanic techniques by applying a potential of 1.5V for 150 seconds. The electrolytic solution consisted of a homogeneous mixture of CH_2Cl_2, 0.1M of $TBAClO_4$, the concentration of the two monomers of $4 \cdot 10^{-4}$ M and $8 \cdot 10^{-4}$ M porphyrin respectively. The chronoamperometric curves of deposition are shown in Figure 4.37.

After passing an oxidation charge of 7.3mC, 0.5mC and 7.7mC, the electrodes were covered with P(Th4P-C_{60}), P(hemin) and co(Th4P-C_{60}-hemin) system. Thin films on the electrode were relatively minimal due to the low starting concentration.

The electrocatalytic ability of the dyad films was evaluated from CV response in 0.1 M KCl with and without the presence of H_2O_2 and compared to those of homopolymers of fulleropyrrolidine **3** and hemin respectively.

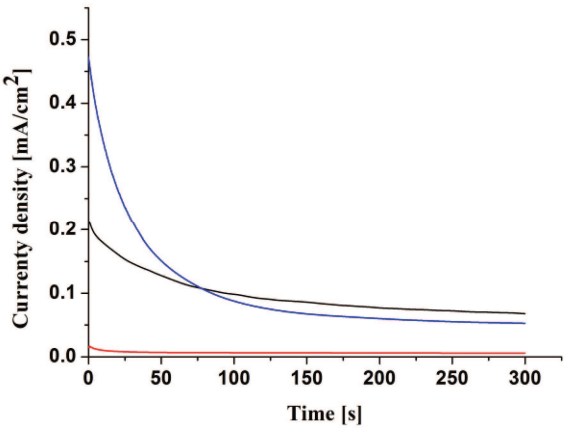

Figure 4.37: Chronoamperometric deposition curves of Th4P-C_{60} (black), hemin (red) and Th4P-C_{60}-hemin system (blue) respectively.

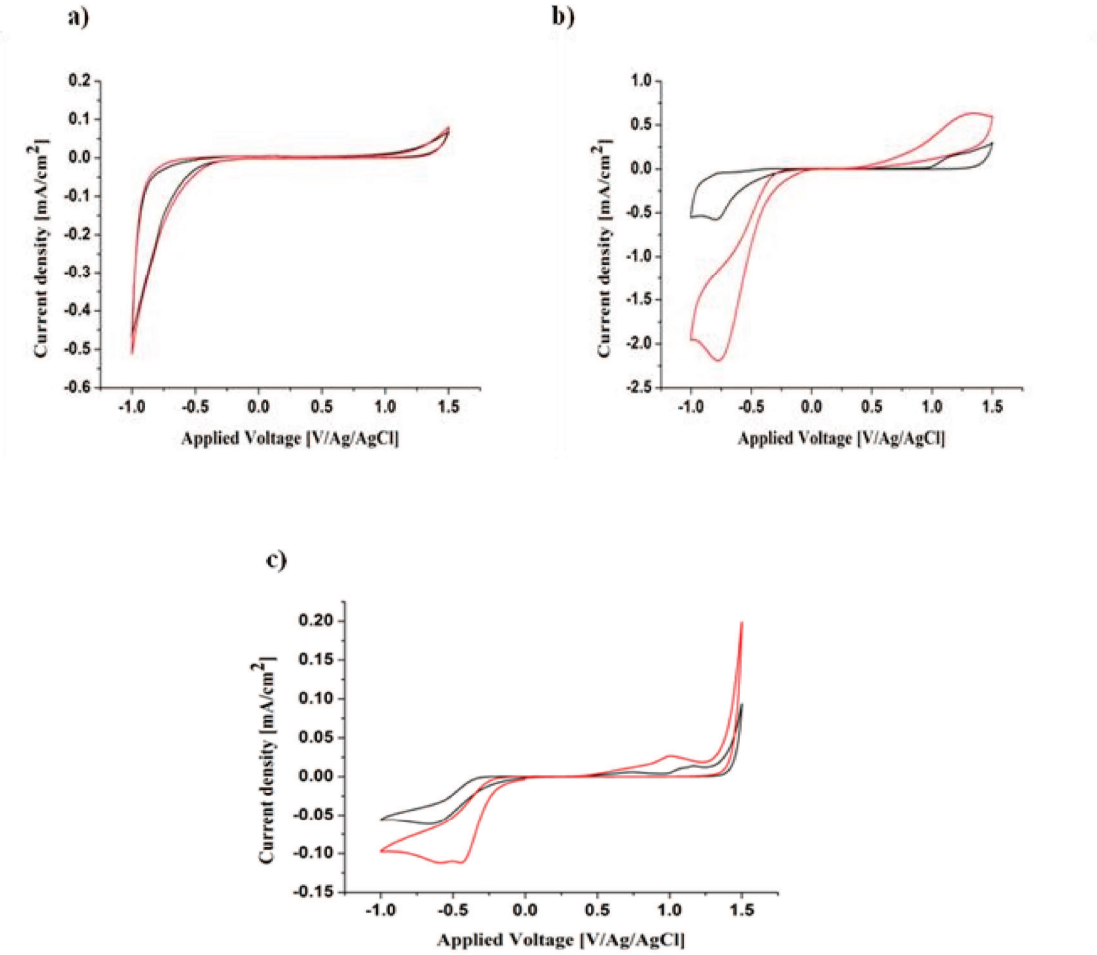

Figure 4.38. CVs of a) P(Th4P-C_{60}), b) P(hemin) and c) co(Th4P-C_{60}-hemin) in 0.1 M KCl aqueous solution before (black) and after (red) the addition of 1µl H_2O_2 respectively.

The electrochemical potential window was chosen based on the response range of the ITO / PET substrate, since potentials below -1.3V reduce the substrate, and, hence, affecting the reduction electrochemistry of the systems studied. Figure 4.38 shows the oxidation and reduction scan of the systems before and after the addition of 1 µl of hydrogen peroxide.

As can be seen from Figure 4.38 a, the CV in both oxidation and reduction of P(Th4P-C_{60}) does not exhibit any peak, it should exhibit the four fullerene reduction waves, pointing at low polymer concentration on the electrode even if you form a uniform yellow film but with a low thickness on the electrode. However, it is noteworthy that after the addition of H_2O_2 the CV does not change, suggesting no electrochemical efficacy towards the presence of the analyte. As for polyhemin, it Figure 4.38b shows that a peak at 0.9V is apparent in oxidation region, while in a reduction range a peak at -0.6V was also observed.

After the addition of H_2O_2, the current of both peaks increases. It is noteworthy that the displacement of the peak in the oxidation scan of the copolymer (Figure 4.34c) from 0.9V to 1V was observed upon addition of the analyte. Moreover, it is evident that dyad of fulleropyrrolidine3 and hemin (Figure 4.38c) exhibits much larger current responses towards the analytes than polyhemin (Figure 4.38b) and poly fullerene (Figure 4.38a), respectively.

4.3.2. Electroanalytical performance PET/ITO/ Th4P-C_{60}-hemin/H_2O_2

Electroanalytical performance in the presence of H_2O_2 was scrutinized at a fixed potential of 1.1 V, previously determined by CV. The chronoamperometric response of P(Th4P-C_{60}) (Figure 4.39a) was in line with CV response findings and confirmed that upon the addition of H_2O_2 no variation in current values was observed. However, clear and defined step-like current change response was visible upon the addition of the analyte in the range 1-28 mM (Figure 4.39b). On the contrary, in case of polyhemin (Figure 4.39c) upon the addition of H_2O_2 fast response was observed in the concentration range up to 7mM, while the following additions led to the increase of response time to ca. 400 sec to achieve the plateau values of current, due to low quantity of active porphyrin deposited onto the surface of the electrode due to low concentration used during the synthesis. Sensitivity and limit of detection (LOD) are the key parameters used to evaluate the sensing performances. Sensitivity per unit area was computed from the slope of the straight line obtained by plotting the current increases vs. glucose, lactate or drug concentration.The corresponding calibration curve for dyad response is presented in Figure 4.35 d, suggesting that system showed the sensibility values at 0.067 μA/(mM*cm^2), R^2=0.9946 with LOD ca. 1 mM.

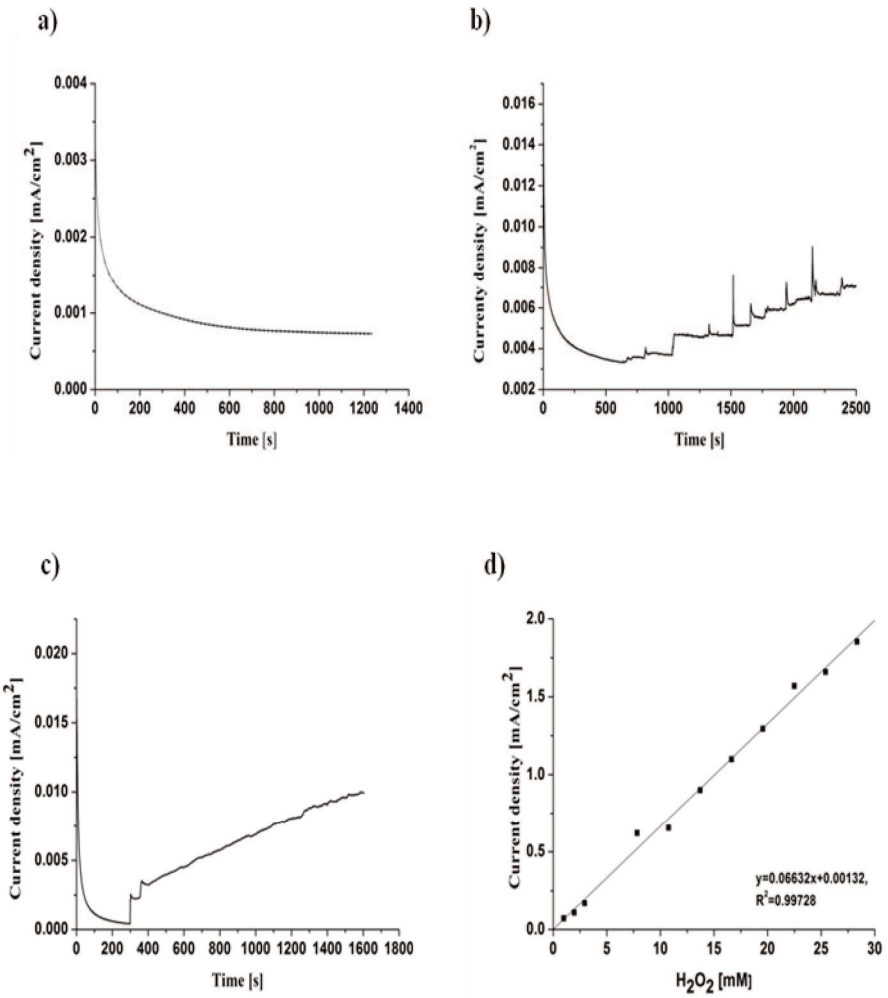

Figure 4.39. a-c) Chronoamperometric response to the addition of various volumes of 9.8 MH_2O_2 in 0.1M KCl aqueous solution for a) P(Th4P-C_{60}), b) co(Th4P-C_{60}-hemin), c) P(hemin), d) calibration curve, corresponding to the response of the co(Th4P-C_{60}-hemin) to the H_2O_2.

References

[1] V. Figà, C. Chiappara, F. Ferrante, M. P. Casaletto, F. Principato, S. Cataldo, Z. Chen, H. Usta, A. Facchetti, B. Pignataro, *J. Mater. Chem. C* **2015**, *3*, 5985.

[2] F. Alakhras, *Artic. J. Braz. Chem. Soc* **2016**, *27*, 941.

[3] E. Ahmed, G. Ren, F. S. Kim, E. C. Hollenbeck, S. A. Jenekhe, *Chem. Mater.* **2011**, *23*, 4563.

[4] D. Dubois, K. M. Kadish, S. Flanagan, L. J. Wilson, *J. Am. Chem. Soc.* **1991**, *113*, 7773.

[5] J. L. A. I.Villarreal, E.Morales, T.F.Otero, *Synth. Met.* **2001**, *123*, 487.

[6] W. A. B. Shymaa S. Medany, Khaled M. Ismail, *Synth. Met.* **2004**, *142*, 93.

[7] K. M. Ismail, *Electrochim. Acta* **2007**, *52*, 3883.

[8] C.Rüssel and W.Janicke, *J. Electroanal. Chem. Interfacial Electrochem.* **1986**, *199*, 139.

[9] S. A. Spanninga, D. C. Martin, Z. Chen, *J. Phys. Chem. C.* **2010**, *114*, 14998.

[10] X. Guo, M. D. Watson, *Org. Lett.* **2008**, *10*, 5333.

[11] M. M. Durban, P. D. Kazarinoff, C. K. Luscombe, *Macromolecules* **2010**, *43*, 6348.

[12] R. Steyrleuthner, M. Schubert, I. Howard, B. Klaumünzer, K. Schilling, Z. Chen, P. Saalfrank, F. Laquai, A. Facchetti, D. Neher, *J. Am. Chem. Soc.* **2012**, *134*, 18303.

[13] G. A. Sotzing, C. A. Thomas, J. R. Reynolds, P. J. Steel, *Macromolecules* **1998**, 31, 3750.

[14] J. H. Huang, C. Y. Hsu, C. W. Hu, C. W. Chu, K. C. Ho, *ACS Appl. Mater. Interfaces* **2010**, *2*, 351.

[15] E. Poverenov, M. Li, A. Bitler, M. Bendikov, *Chem. Mater.* **2010**, *22*, 4019.

[16] S. A. Sapp, G. A. Sotzing, J. R. Reynolds, *Chem. Mater.* **1998**, *10*, 2101.

[17] P. M. Beaujuge, J. R. Reynolds, *Chem. Rev.* **2010**, *110*, 268.

[18] W. T. Neo, Z. Shi, C. M. Cho, S. J. Chua, J. Xu, *Chempluschem* **2015**, *80*, 1298.

[19] R. Steyrleuthner, M. Schubert, F. Jaiser, J. C. Blakesley, Z. Chen, A. Facchetti, D. Neher, *Adv. Mater.* **2010**, *22*, 2799.

[20] W. Zhang, X. Bi, X. Zhao, Z. Zhao, J. Zhu, S. Dai, Y. Lu, S. Yang, *Organic Electronics*, **2014**, 15, 3445.

[21] E. Nasybulin, J. Feinstein, M. Cox, I. Kymissis, K. Levon, *Polymer*, **2011**, 52, 3627.

[22] N. Ghobadi, R. Moradian, *Int. Nano Lett.* **2013**, *3*, 47.

[23] K. M. Kaunisto, N. K. Subbaiyan, C. B. K.C., V. I. Chukharev, H. M. Hakola, T. K. Vuorinen, V. M. Manninen, N. V. Tkachenko, H. J. Lemmetyinen, F. D'Souza,

Synth. Met. **2014**, *195*, 193.

[24] B. Qi, J. Wang, *Phys. Chem. Chem. Phys.* **2013**, *15*, 8972.

[25] *Curr. Appl. Phys.* **2010**, *10*, S206.

[26] S. H. Ko, H. Pan, C. P. Grigoropoulos, C. K. Luscombe, J. M. J. Fréchet, D. Poulikakos, *Appl. Phys. Lett.* **2007**, *90*, 141103.

[27] J. H. Park, J.-I. Park, D. H. Kim, J.-H. Kim, J. S. Kim, J. H. Lee, M. Sim, S. Y. Lee, K. Cho, *J. Mater. Chem.* **2010**, *20*, 5860.

[28] S. Cataldo, C. Sartorio, F. Giannazzo, A. Scandurra, B. Pignataro, *Nanoscale* **2014**, *6*, 3566.

[29] E. F. Palermo, S. B. Darling, A. J. McNeil, *J. Mater. Chem. C* **2014**, *2*, 3401.

[30] S. Swaraj, C. Wang, H. Yan, B. Watts, J. Lüning, C. R. McNeill, H. Ade, *Nano Lett.* **2010**, *10*, 2863.

[31] P. E. Shaw, A. Ruseckas, I. D. W. Samuel, *Adv. Mater.* **2008**, *20*, 3516.

[32] C. Yang, J. K. Lee, A. J. Heeger, F. Wudl, *J. Mater. Chem.* **2009**, *19*, 5416.

[33] M. Raïssi, H. Erothu, E. Ibarboure, H. Cramail, L. Vignau, E. Cloutet, R. C. Hiorns, *J. Mater. Chem. A* **2015**, *3*, 18207.

5. Conclusion

In this thesis, different push-pull copolymers made of alternated donor-acceptor units have been conveniently synthesized by electrochemical and/or chemical methods, while different solution approaches have been employed to realize plastic thin film electronic devices.

As a first push-pull system, copolymers made of the acceptor (A) NDI2ODT4 and donor (D) EDOT units have been electrodeposited and novel electrochromic devices have been realized on PET/ITO flexible substrates. Remarkably these copolymers showed the possibility to modulate different fundamental properties of the thin films including band gap, optical absorption, carriers mobility, surface hydrophilicity and film morphology by varying the donor-acceptor ratio. As to the specific electrochromic behavior, a wide optical absorption range up to the near IR region and a high coloration efficiency has been observed together with tuned response time and optical contrast.

Also starting from the study of novel bis-Th2P-C_{60} monomers and polymers, copolymeric thin films of D NDI2ODT4 and A bis-Th2P-C_{60} have been prepared by anodic oxidation on ITO/PET electrodes. In this case, the presence of pendant fullerene moieties causes the distortion of the main polymeric chain leading to a shift of the charge transfer band to lower wavelengths. Accordingly, the electrochromic properties of NDI2ODT4- bis-Th2P-C_{60} copolymers show intermediate performance with respect to the NDI2ODT4 and bis-Th2P-C_{60} homopolymers.

The same copolymers have been used in planar heterojunction devices together with P3HT leading toa good fluorescence quenching as an indication that these materials are promising also for devices based on charge-transfer phenomena. The combination of different D-A moieties and the employment of different D-A ratios leads also in this case to a modulation of the optoelectronic properties giving interesting information on the molecular design of double cable systems.

More interestingly, the combination of D and A moieties in functional copolymers has been exploited for the improvement of the morphology of thin film bulk heterojunctions (BHJs) made of similar D and A molecular systems.

Indeed, the small percentages of novel fulleropirrolidine(A)-thiophene(D) copolymers acted as segregation modulators in P3HT/PCBM BHJs allowing to improve the state-of-the-art power conversion efficiency of plastic P3HT/PCBM OSCs.

Finally, preliminary results on the application of fulleropirrolidine(A)-thiophene(D) based systems electrochemically co-deposited with hemin molecules shows an interesting

synergic effect with respect to the recognition of H_2O_2 in plastic electrochemical sensors. This gives interesting perspectives for the application of properly designed D-A copolymers and/or co-deposited systems for the recognition of drugs.

Acknowledgements

First of all, I would like to thank my supervisor Prof. Bruno Giuseppe Pignataro to whom I owe considerable gratitude for his guidance and encouragement helped me in all the time of the research and writing up this thesis.

I would like to thank Prof. Antonio Facchetti of Northwestern University for the synthesis and characterization of naphtalenediimidethiophene systems used in this work. I would like to express my appreciation to Prof. Francesco Giacalone and Dr. Vincenzo Campisciano from the University of Palermo chemical synthesis and characterization of fullerene-based monomers and polymers used in this work and useful discussions during the data elaboration. I would like to thank Dr. Michelangelo Scopelliti for XPS measurements. I would like to mention Dr. Yana Aleeva for guidance and discussion in electrochemical experiments and preparation of sensing systems. I would like to thank Ing. Fabio Principato for electrical measurements and useful discussions during the data elaboration. Furthermore, I would like to Dr. Camillo Sartorio for the assistance in electron transfer measurements and fluorescence measurements, preparation of photovoltaic devices and for the fundamental help he gave me during the thesis writing. I would like to express my gratitude to Dr. Sebastiano Cataldo for AFM measurements. I would like to express my gratitude to Dr. Francesco Ferrante for computational data. And last, but not the least I would like to thank Giuseppe Arrabito for his continuous help during Ph.D. and Licia Cavalieri for moral support during the years of Ph.D. and nice time spent together during conferences and scientific meetings.